



TAMPEREEN TEKNILLINEN YLIOPISTO
TAMPERE UNIVERSITY OF TECHNOLOGY

ANDRII PAZYNYCH
A STUDY OF THE HARMONIC CONTENT OF DISTRIBUTION
POWER GRIDS WITH DISTRIBUTED PV SYSTEMS
Master of Science Thesis

Examiner: Enrique Acha
The examiner and the topic were
approved in the Faculty of Computing
and Electrical Engineering
Council meeting on 05.03.2014

ABSTRACT

TAMPERE UNIVERSITY OF TECHNOLOGY

Master's Degree Programme in Electrical Engineering

PAZYNYCH, ANDRII: A study of the harmonic content of distribution power grids with distributed PV systems

Master of Science Thesis, 76 pages, 20 Appendices

June 2014

Major: Smart Grids

Examiner: Dr. Prof. Enrique Acha

Keywords: Photovoltaic, DC-DC Converter, DC-AC Inverter, Total Harmonic Distortion, Interharmonics, Distribution Grids, Distributed Energy Resources

A photovoltaic system transforms solar radiation into electrical energy using so-called PV panels. A key component of this system is the power electronics subsystem which enables maximum power extraction from the available solar irradiation, as well as connection to the AC power grid. However, the current and voltage waveforms at the point of common coupling (PCC) with the power grid contain a degree of harmonic distortion which, in some instances, may surpass that recommended by existing standards. The presence of high harmonic distortion in an electrical installation significantly decreases power quality and the renewable energy sources' power electronics carries the potential to yield high harmonic distortion.

This thesis reports on an investigation of some of the factors that impact adversely the quality of the current and voltage waveforms in an electrical power distribution network with distributed photovoltaic systems. These factors include irradiance levels, imperfect conditions of the filtering system, resonant conditions, load imbalances and selection of the inverter's switching frequency. To quantify current and voltage harmonic injections, a two-stage model of a photovoltaic array was designed in Simulink in order to show the impact of a single photovoltaic system. The basic PV system model is then applied to a model of an electrical power distribution grid, with several distributed PV units.

The study indicates that irradiance is the primary factor influencing THD and that at low PV power outputs, harmonic emissions may exceed the recommended harmonic distortion limits, particularly when resonant conditions exist at the output of connection of the PV plant. Different MPP control methods employed in the DC-DC conversion stage were also investigated and it is observed that they do not seem to have much impact on THD. This applies in the absence of partial shading, an issue which was not considered as part of this research project. As expected, the use of well-designed filters is the key to keeping harmonics emissions low. Nevertheless, perfect filtering does not exist in actual installations and the study also investigates the impact of imperfect filtering parameters and filter branch failure, on the voltage and current waveforms at PCC.

PREFACE

This Master of Science thesis was written at the Department of Electrical Energy Engineering at the Tampere University of Technology. The supervisor of the thesis was Professor Enrique Acha.

I would like to thank my supervisor Enrique Acha for his valuable observations and feedback during the progress of the research work. In addition I would like to thank Xavier del Toro Garcia and Luis Castro Gonzalez for their technical advice and useful discussions. I would also like to thank my friends and family for all their support.

TABLE OF CONTENTS

Abstract	ii
Preface.....	iii
Abbreviations and notations	vi
1. Introduction.....	1
1.1. Integration of PV power systems	3
1.2. Harmonic effects	4
1.2.1. Impact on the power grid.....	4
1.2.2. Harmonic limitations.....	6
1.2.3. Research on harmonic generation due to PV installations	7
1.3. Objectives of the thesis	9
1.4. Main contributions.....	9
1.5. Publication.....	10
2. Photovoltaic power systems	11
2.1. Introduction	11
2.2. Photovoltaic power plants	11
2.2.1. Solar cells	11
2.2.2. Solar modules and generators.....	14
2.3. Factors influencing the performance of a PV array.....	17
2.4. Modelling of photovoltaic generators in Simulink.....	18
2.4.1. Mathematical model.....	18
2.4.2. Physical model.....	19
2.4.3. Modelling based on experimental data	20
2.5. Summary	21
3. DC-DC converters.....	22
3.1. Introduction to basic DC-DC converters	22
3.2. Operation principles.....	22
3.2.1. Pulse width modulation.....	22
3.2.2. Conduction modes	23
3.3. Buck.....	24
3.4. Boost	25
3.5. Buck-Boost.....	26
3.6. Steady-state analysis	27
3.7. Modelling of DC-DC converters in Matlab/Simulink	28
3.8. Summary	30
4. MPPT techniques	31
4.1. Introduction	31
4.2. The perturb and observe method	32
4.3. The incremental conductance plus integral regulator method	34
4.4. General problems related to local MPP techniques.....	36
4.5. Summary	37

5.	Basic DC-AC inverters.....	38
5.1.	Grid connected renewable energy systems	38
5.2.	Fundamentals of switched-mode inverters	39
5.3.	Selection of the switching frequency and the frequency modulation ratio..	40
5.4.	Typical inverter topologies	41
5.5.	Control of a grid-connected inverter.....	43
5.6.	Filter design considerations.....	45
5.6.1.	Calculation of base values	45
5.6.2.	Filter design rules and restrictions	45
5.6.3.	Filter design calculation	47
5.7.	Summary	49
6.	Simulation results.....	50
6.1.	Distribution network model	50
6.2.	Simulation results of a single PV array	51
6.2.1.	Analysis of the Powergui FFT tool.....	55
6.2.2.	Effect of irradiance levels on the THD	56
6.2.3.	Impact of the operating conditions of LCL filters	57
6.2.4.	Impact of the open-circuit conditions of LCL filters	59
6.2.5.	Impact of the loading type and load unbalance on the THD.....	61
6.2.6.	Impact of resonance conditions on the THD.....	62
6.3.	Harmonic emissions caused by multiple PVGs in the network	65
6.4.	Summary	68
7.	Conclusions.....	69
7.1.	Suggestions for future research	70
	References	72
	Appendix A: Data for the power distribution system	77
	Appendix B: Data of PV panels	78
	Appendix C: Harmonic spectrum at different sides of the DC-DC converter	79
	Appendix D: Harmonic assessment of electric power distribution grids with distributed pv systems	82

ABBREVIATIONS AND NOTATIONS

NOTATION

A	Diode ideality factor
D	Duty cycle ratio
f_s	Switching frequency
f_1	Fundamental frequency
I_o	Diode saturation current
I_{o1}	Dark saturation current due to recombination in the quasi neutral region
I_{o2}	Dark saturation current due to recombination in the depletion region
I_{ph}	Photocurrent
I_{sc}	Short-circuit current
I'_{sc}	Short-circuit current in case of no parasitic elements
k	Boltzmann constant
m_a	Amplitude modulation ratio
m_f	Frequency modulation ratio
t_{off}	Turn-off time
t_{on}	Turn-on time
T_s	Switching time
$V_{control}$	Peak amplitude of the control signal in a PWM controlled inverter
V_{tri}	Amplitude of the triangular signal in a PWM controlled inverter
V_{oc}	Open circuit voltage
V_t	Thermal voltage

ABBREVIATIONS

AC	Alternating Current
BCM	Boundary Conduction Mode
Btu	British Thermal Unit
CCM	Continuous Conduction Mode
CSI	Current Source Inverter
DC	Direct Current
DCM	Discontinuous Conduction Mode
IEEE	Institute of Electrical and Electronics Engineers

I-V	Current-Voltage
MPP	Maximum Power Point
NPC	Neutral-Point-Clamped Inverter
PCC	Point of Common Coupling
PLL	Phase-Locked Loop
PV	Photovoltaic
PVG	Photovoltaic Generator
P-V	Power-Voltage
PWM	Pulse Width Modulation
RMS	Root Mean Square
STC	Standard Test Conditions
THD	Total Harmonic Distortion
VSI	Voltage Source Inverter
VSC	Voltage Source Converter

1. INTRODUCTION

Electricity production is one of the key factors that define the economic development of a country. It is not difficult to argue the direct correlation between these two factors: the wealthier the people are, the more spending power they have; with a large proportion of this going into acquiring consumer electronic equipment and other electricity driven commodity products. Therefore, all countries are constantly in need of increasing power generation due to increasing standard of living and population growth. *Figure 1.1* shows the world primary energy consumption in quadrillion Btu for the last 30 years [1].

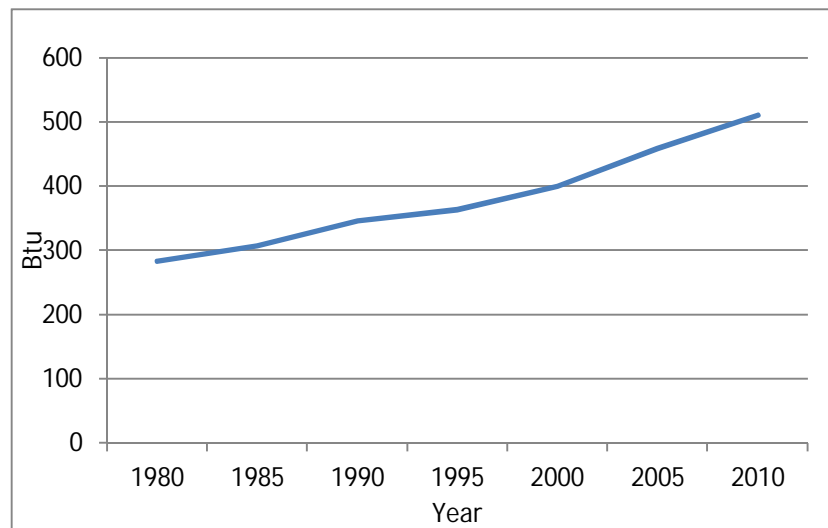


Figure 1.1. World energy consumption.

According to data compiled by the U.S Energy Information Administration, for the last half a century energy consumption has increased exponentially, with the ensuing need for more power generation [1]. However due to environmental concerns, building new generation units is becoming harder. For instance, the EU Commission's 20/20/20 target for climate change mitigation sets three cornerstone objectives to be achieved by 2020 [2]:

- Reduce the greenhouse effect by 20%
- Increase the share of renewable energy generation to 20%
- Improve the performance index of energy facilities by 20%

The push is for the integration of renewable sources of energy into the power grid. Renewable, clean energy is available in the form of wind, solar, geothermal, hydropower,

biomass, osmotic energy, hydrogen based fuel cells, tide, wave and ocean currents. Non-renewable energy, currently being promoted by some governments as clean energy, such as uranium ore and carbon-based, organically derived fuel including coal, petroleum, and natural gas are shown in *Figure 1.2*.

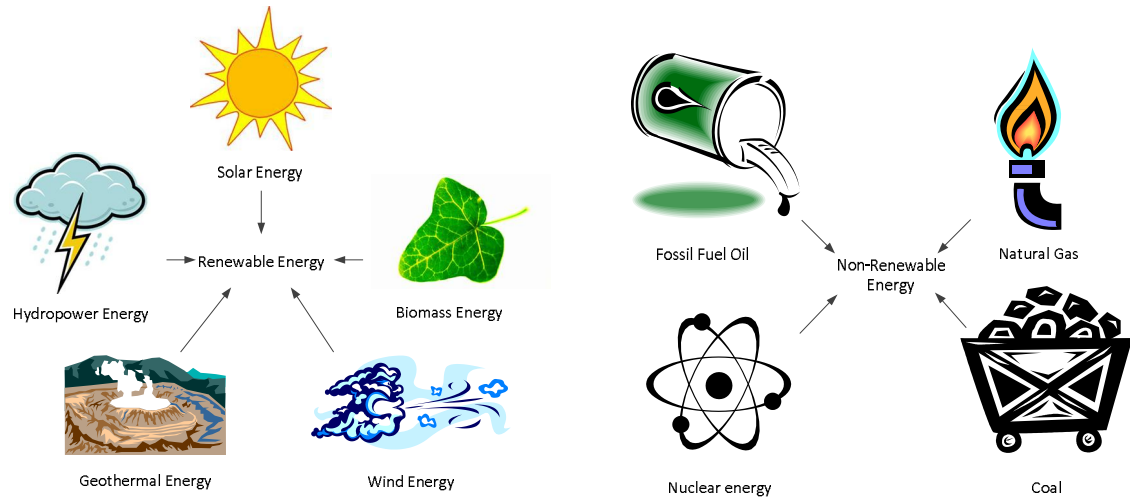


Figure 1.2. Types of energy resources.

During the period 2001-2011 the world's total renewable energy production grew from 2862,4 TWh to 4475,5 TWh, which corresponds to 4,5% annual growth [3]. One of the most prominent and fastest spreading technologies is the photovoltaic. According to the information gathered by the Observ'ER the annual growth rates of PV systems was 52,2% for the period of 2001-2011.

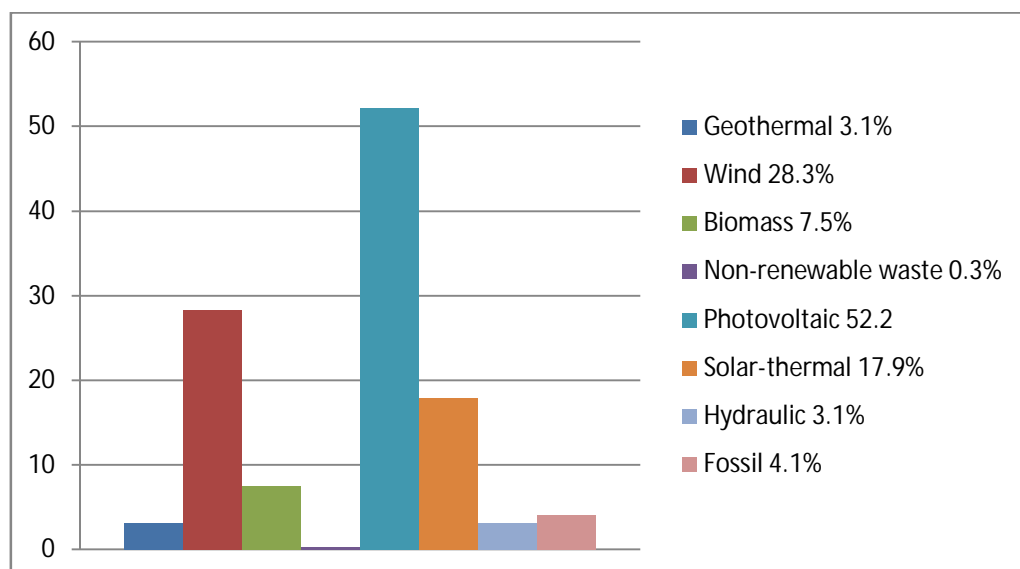


Figure 1.3. Annual growth rates of production by source [adapted from 4].

Valkealahti et. al. 2006 indicates that worldwide forecasting of PV electricity generation gives a figure of around 6000 GW by 2040 [5].

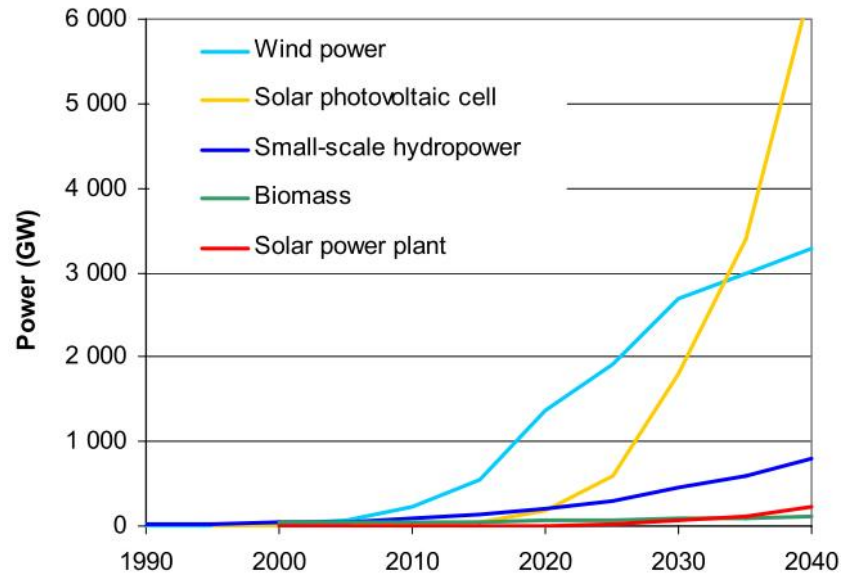


Figure 1.4. Worldwide estimates of renewable energy production [5].

These figures make the photovoltaic technology one of the fastest growing means of electrical energy production. Nevertheless, owing to the novelty and the complexity of the technology in its grid-connected fashion, there is a great deal of research being carried out on the integration of photovoltaic power systems into the grid.

1.1. Integration of PV power systems

Power electronics is the cornerstone of photovoltaic integration into the power grid. Power converters are required to connect a photovoltaic energy system to the AC power grid. There are two main approaches of how to do that: using a single stage or using a two-stage topology. In the former only the DC to AC is used, whereas in the latter, a DC to DC and a DC to AC converters are used. The two stage technique enables maximum power extraction for a given amount of solar irradiance and it is the preferred method and, therefore, it is the one implemented in this thesis.

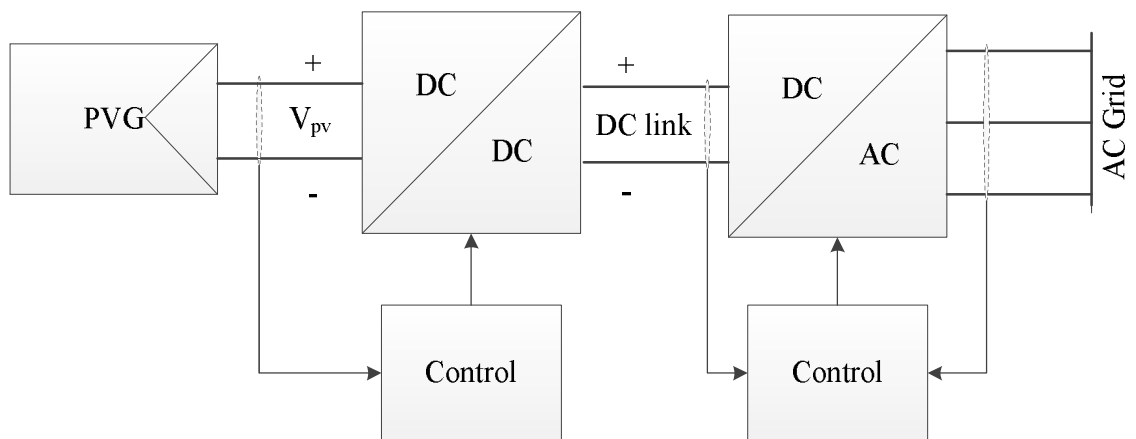


Figure 1.5. Double stage PV system.

The schematic diagram shown in *Figure 1.5* makes reference to the controllers of the power electronics converters, where advanced control algorithms are required for correct operation. In addition, the converters themselves are complex structures comprising an arrangement of advanced semiconductor valves. Only two decades ago, photovoltaic systems were finding it difficult to make commercial inroads due to the high cost of components and low performance indexes. However, PV installations were still being used as sources of electrical energy where no other options were available, such as in space stations. However, nowadays, due to much improved economies of scale, advancements in material science, power electronic converters and overall technological progress, the use of photovoltaic systems is growing exponentially. It should be remarked that power electronics converters are an essential part of any grid-connected photovoltaic system, helping the PV system to maximize power production. However, their use has associated drawbacks which require an in-depth investigation. One such issue is the subject of this thesis, namely, the current and voltage harmonic distortion that they incur and the ensuing interaction with the power grid.

1.2. Harmonic effects

1.2.1. Impact on the power grid

According to IEEE, harmonic is a sinusoidal component of a periodic waveform with a frequency that is an integral multiple of the fundamental frequency [6]. This term is especially known to musicians in the form of overtones. In simple words, a harmonic is a kind of “impurity” or “noise” which prevents a signal from being purely sinusoidal. A harmonic has a mathematical representation. According to Fourier theory, any periodic waveform can be decomposed into an infinite number of sinusoidal waveforms that are harmonics of a fundamental frequency [7]. When these individual waveforms are added up they reproduce the original waveform. The Fourier series of a signal may be represented by the following set of formulas:

$$f(t) = \frac{a_0}{2} + \sum_{n=1}^{\infty} a_n \cos(n\omega t) + b_n \sin(n\omega t) \quad (1.1)$$

$$a_n = \frac{2}{T} \int_{t-T}^t f(t) \cos(n\omega t) dt \quad (1.2)$$

$$b_n = \frac{2}{T} \int_{t-T}^t f(t) \sin(n\omega t) dt \quad (1.3)$$

$$T = \frac{1}{f_1} \quad (1.4)$$

where T is the length of the time-domain function $f(t)$, n determines the rank of the harmonic and f_1 is the fundamental frequency.

A popular term used in power engineering to assess the harmonic distortion of the system is THD or the total harmonic distortion. THD can characterize distortion in both current and voltage and can be computed in the following manner:

$$THD = \frac{\sqrt{I_{RMS}^2 - I_{RMS(1)}^2}}{I_{RMS(1)}} \cdot 100\% \quad (1.5)$$

$$THD = \frac{\sqrt{V_{RMS}^2 - V_{RMS(1)}^2}}{V_{RMS(1)}} \cdot 100\% \quad (1.6)$$

where V_{RMS} is the sum of all harmonic components of voltage, including the fundamental, I_{RMS} is the sum of all harmonic components of current, including the fundamental, $V_{RMS(1)}$ is the fundamental component of voltage waveform and $I_{RMS(1)}$ is the fundamental component of current waveform. The existence of harmonics in power grids is caused by either non-linear components or linear, time-variant components. Examples of such loads are DC-DC converters, inverters, rectifiers, switch-mode power supplies, electric arc furnaces, AC and DC motor drives, static VAR compensators, saturated iron cores, fluorescent lamps and other domestic appliances.

Rectifiers are typical sources of harmonic currents with a relatively constant content, regardless of the impedances presented by the system. These harmonics, termed characteristic harmonics, are defined by the pulse number of the rectifier, as presented below:

$$h = kq \pm 1 \quad (1.7)$$

where h is the harmonic number, k is a positive integer and q is the number of pulses of the converter [7]. For example a twelve-pulse rectifier will have harmonic currents at 11th, 13th, 23rd, 25th, etc.

It is worth mentioning that loads which are not pulsating synchronously with the fundamental frequency, such as induction motors, cycloconverters, static frequency converters and arc furnaces, may be sources of interharmonics [8]. Interharmonics are frequencies that are not integral harmonics of the fundamental frequency [9]. They are usually presented as discrete frequencies or as a wide-band spectrum. The IEEE 519 standards do not provide general information of the phenomena. However, due to the increasing complexity of power electronics systems, more precise technical specifications, measurement methods and limitations will be included in the IEEE standards in the near future [8].

The presence of harmonics does not necessarily mean that electrical equipment will not operate or that consumers will not be able to use electricity but, nevertheless, they do have some detrimental effect on the overall equipment and system performance. The effect of harmonics can be divided into four categories [6]:

- effect on the power system
- effect on the consumer load
- effect on the communication circuits
- effect on the revenue bills

Perhaps one of the most negative influences that harmonic current might have on the power system is the overheating of equipment, which results in additional power losses and premature ageing of equipment. Transformers, capacitors, generators and motors are particularly susceptible to the thermal loss-of-life. Another noticeable effects of harmonics are the risk of interference in measuring and control equipment, false tripping of protective equipment and thyristor firing errors in power electronics converters. In addition, harmonic currents might induce noise in nearby communication lines.

A fact to take into account is the presence of resonance conditions in the power circuit which significantly amplifies the negative effects of harmonics. Resonances in power circuits can be of two types: series resonances and parallel resonances. A series resonance occurs in situations where the inductance and capacitance are connected in series. In such cases the series resonance represents a low impedance path for harmonic currents at the natural frequency and results in a high voltage distortion between the capacitance and the inductance. Parallel resonances occur when the frequency of the parallel combination of the inductor and the capacitor is equal or close to the harmonic frequency. Such a phenomenon stimulates reinforcement of the harmonic current flowing between the capacitor banks and the inductor which results in damage to the capacitor fuse or overheating of the transformer [10].

High order harmonic currents may cause the destruction of fuses in capacitor banks, resulting in reactive power capability loss. Harmonic voltages cause equipment insulation stress. If the voltage across a capacitor bank is altered due to harmonics, it can cause corona effect, which can result in capacitor failure [11].

As discussed previously, the presence of harmonics cause incorrect readings on meters, which may alter electricity billing. Harmonic voltage distortion is the cause of errors in kilowatt-hour metering, whereas harmonic currents increase the fundamental current, leading to an increase in kilowatt-hour consumption [12], [13].

Other negative effects of harmonic currents are lower power factors in the system, generator overheating, equipment malfunctions, high circulating currents in neutral wires and risk of fire in distribution cables [14].

1.2.2. Harmonic limitations

Owing to the adverse effect that harmonics have on the operation of electrical installations, the subject is an important element in electrical energy systems; it is an active topic of electrical energy engineering research. Special guidelines for utilities have been prepared and compiled in IEEE 519 standard [6]. Table 1.1 illustrates total voltage harmonic distortion limits presented in the guidelines.

Table 1.1. Voltage Distortion Limits from IEEE 519 [6].

Bus Voltage at Point of Common Coupling	Individual Voltage Distortion (%)	Total Voltage Distortion THD (%)
Below 69 kV	3	5
69 kV to 137.9 kV	1.5	2.5
138 kV and above	1	1.5
<i>Note:</i> High voltage systems can exceed the limit up to 2%, if the source of harmonics is a high voltage DC terminal.		

The figures presented in *Table 1.1* show the acceptable level of voltage distortion at the point of common coupling. These limitations are valid for durations of more than one hour, whereas for shorter periods of time, such as start-up or unusual conditions, the THD limit may increase by 50%. Current harmonic distortion limits are more specific, depending on such factors as the type of investigated component and the combined total voltage harmonic distortion. For instance, in IEEE 929 it is stated that the current total harmonic distortion in photovoltaic systems should be less than 5% [15]. However, each individual harmonic must be within the limits presented in *Table 1.2*.

Table 1.2. Current Distortion Limits from IEEE 929 [16].

Odd Harmonics	Distortion Limit
3 rd -9 th	<4.0%
11 th -15 th	<2.0%
17 th -21 st	<1.5%
23 rd -33 rd	<0.6%
Above the 33 rd	<0.3%

1.2.3. Research on harmonic generation due to PV installations

As discussed in Section 1.1, in order to connect a photovoltaic system to the AC grid, the power produced by the PV installation requires changing from DC to AC, an action which results in voltage and current harmonic distortion. The presence of high harmonic levels in the power grid is undesirable owing to its detrimental effects, such as those discussed in Section 1.2.2. Hence, it is of great importance to assess the harmonics injection caused by PV installations. This is an ongoing area of timely research and it has not yet been investigated in an exhaustive manner due to the relative novelty of the PV technology when connected to the power grid. However, some researchers have already presented their findings regarding the factors influencing the current and voltage harmonic generation of PV units, some of which are reviewed below.

Zhao and Liu [17] investigated the impact of environmental factors and PWM control methods on the current harmonic injection at the point of common coupling produced by one photovoltaic unit and two photovoltaic units. The main finding of the

study is that the irradiance is the primary factor influencing the level of current harmonic distortion, especially THD, which deteriorates at low irradiance levels. Similar results are observed in this thesis. The second finding is that different PWM control methods have different impact on the harmonic level. The third finding is that two photovoltaic systems may yield less current harmonic distortion at the point of common coupling, than a single one. However, the analysis of multiple PV generators presented in the thesis shows, to some extent, different findings. In this case, the THD in the system with multiple PVGs tend to increase by a small margin, as the harmonic generation is affected by loading and the network of underground cables.

The research conducted by Benhabib, Myrzik and Duarte [18] suggests that the presence of additional non-linear loads, particularly RC-type loads, in low-voltage networks, may result in an increased THD. The tests conducted in this thesis show that RLC-type loads have the potential to significantly increase THD.

Rawa, Thomas and Sumner [19] investigated possible aspects of modelling simplifications in Simulink. For such a purpose, two models were tested: one model with full PV cell model, the power converter and the inverter; in the second model the PV module and the DC-DC converter are substituted by a simple voltage source. The aim of the research was to show that in normal operating conditions, the PV cell and the DC-DC converter do not play any significant role in harmonics injection. In this thesis, a further experiment relating to DC-DC converters is conducted; it shows that different MPPT control methods of DC-DC converters do not significantly impact THD.

The investigation presented in [20] shows the advantage of using LCL filters over single inductance filters in terms of minimizing current harmonic distortion. According to the findings reported in this paper, this is due to the third-order, low-pass filter characteristics of LCL filters. The findings presented in this thesis also show the advantages of using LCL filters, gives the method used in the LCL filter design and the selection of damping resistors for the resonance suppression.

The research conducted in [21] concludes that the harmonics produced by PV installations depend on the actual operating conditions and that the lower the PV power output, the higher the harmonics level emitted. The same conclusion is reached by Ortega, Hernandez and Garcia [22], namely that at low power outputs the harmonic current emissions would exceed the recommended maximum levels set in the IEEE 929 standard. Similar conclusion may be derived from the findings of this thesis, concerning low irradiance levels.

The impact of different operation modes on the current harmonic is presented in [23]. The emphasis of the work is on assessing different control methods, namely, proportional resonant controller, multi-resonant controllers, repetitive current and their corresponding combination. It is concluded that different control methods have different impact on current harmonic emission with proportional resonant plus repetitive current control method achieving the lowest distortion.

1.3. Objectives of the thesis

The main goals of the research presented in this thesis are listed below:

- To design a simulation platform in the Simulink simulation environment for a power distribution system which is suitable for assessing the integration of distributed PV generation units.
- To carry out comprehensive harmonics analyses for the distributed system under different controls and operating regimes, including imperfect and yet realistic filtering system conditions.

The thesis is structured in the following manner: the introductory chapter outlines the importance of using renewable energy in general and PV in particular. It touches on the technological concepts behind the PV technology and some of its problems, such as current and voltage harmonic injections. The second chapter provides an overview of photovoltaic power systems. This is followed by an introduction to DC-DC converters and modelling principles within the Simulink environment. The fourth chapter is devoted to the maximum power point tracking algorithms and their implementation models. Chapter five deals with VSC and grid-connected PV systems. The last chapter presents the power distribution system used in this work and the associated simulation results.

1.4. Main contributions

The results and analysis presented in this thesis relate to research carried out on the impact of environmental and operational conditions on PVGs, in their ability to produce periodic, non-sinusoidal voltage and current waveforms at PCC. In particular, the impact of irradiance, imperfect conditions of the filtering system, loading imbalances, selection of inverter switching frequency, the presence of resonance conditions and the choice of MPPT controller; were all comprehensively investigated.

The research casts additional light into the heretofore, little researched problem of the interharmonics produced by PVGs. It provides information of which are the main environmental and operational factors responsible for the generation of interharmonics and identifies where is the missing link in explaining fully the existence of such spurious frequencies.

The research demonstrates that the use of a well-design filtering system is of paramount importance to maintaining the operational integrity of the PV plant under a wide range of non-ideal but credible operating and environmental conditions, except in cases when the AC equivalent circuit at PCC exhibits an excitable resonance.

The impact of distributed PVGs was assessed using the model of a realistic power distribution system comprising a network of underground cables. Although the distribution power network did not show any obvious resonant problem but, even in cases of

standard environmental conditions and realistic *LCL* filter deterioration, some of the harmonic terms around the switching frequency surpass the limits given by the IEEE 929 standard. In addition, it was observed that the THD levels were larger than the THD levels observed in the case of one PVG.

1.5. Publication

The following journal paper has been written on the basis of the outcomes reported in this MSc thesis: “Harmonic assessment of electric power distribution grids with distributed PV systems”. On 2nd June 2014 it was submitted with a view to publication in The Scientific World Journal. It is inserted in this thesis in appendix D.

2. PHOTOVOLTAIC POWER SYSTEMS

2.1. Introduction

Photovoltaic is a technology that allows direct conversion of solar irradiation into electrical energy. This chapter provides an overview of a typical photovoltaic power system. The following section discusses the main components of a solar array as well as the more popular approaches used to develop mathematical models for photovoltaic panels. This is followed by an analysis of the factors that influence the operation of photovoltaic systems. Finally, different approaches to the modelling of a photovoltaic array in Simulink are provided.

2.2. Photovoltaic power plants

2.2.1. Solar cells

Solar cells are the basic building blocks of a photovoltaic system. A solar, or photovoltaic cell, is purpose-built semiconductor diode that allows conversion of photon energy into electrical DC electricity by invoking the photovoltaic effect. *Figure 2.1* shows the main parts and operations of a solar cell.

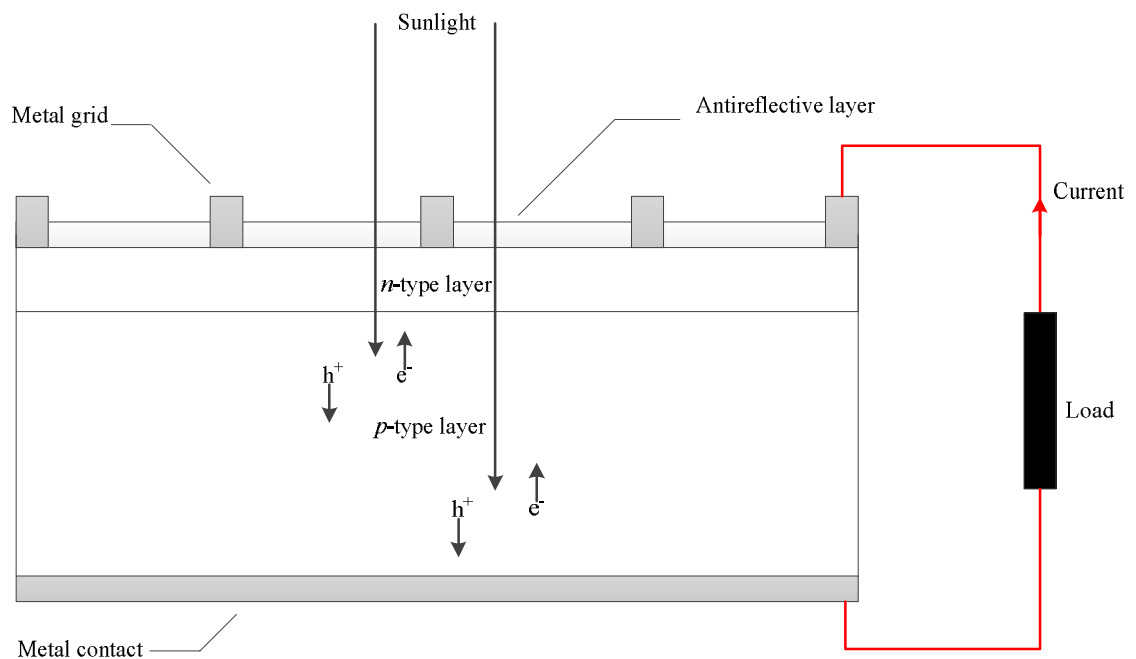


Figure 2.1. Construction of a typical photovoltaic cell [adapted from 24].

In general photovoltaic cells are made up of two different types of semiconducting materials with different electric characteristics; where positive and negative charges are formed on the opposite sides of the material interface, thus creating an electric field. When photons of solar irradiation are absorbed in the semiconductor material, electrons and holes are released to the conduction and valence band. The existence of the electric field makes it possible for electrons and holes to move to opposite sides of the material interface. Eventually, DC current can be made to flow by connecting the photovoltaic cells to an electric circuit.

The electrical characteristics of a photovoltaic cell under different operating conditions may be represented by means of an I-V curve. The current-voltage characteristic of photovoltaic is non-linear, and it is vital to understand its properties in order to model a cell. The I-V curve of a standard solar cell is presented in *Figure 2.2*, where I_{sc} is the short-circuit current, V_{oc} is the open circuit voltage, MPP is the maximum power point, I_{mpp} is the maximum current and V_{mpp} is the maximum voltage.

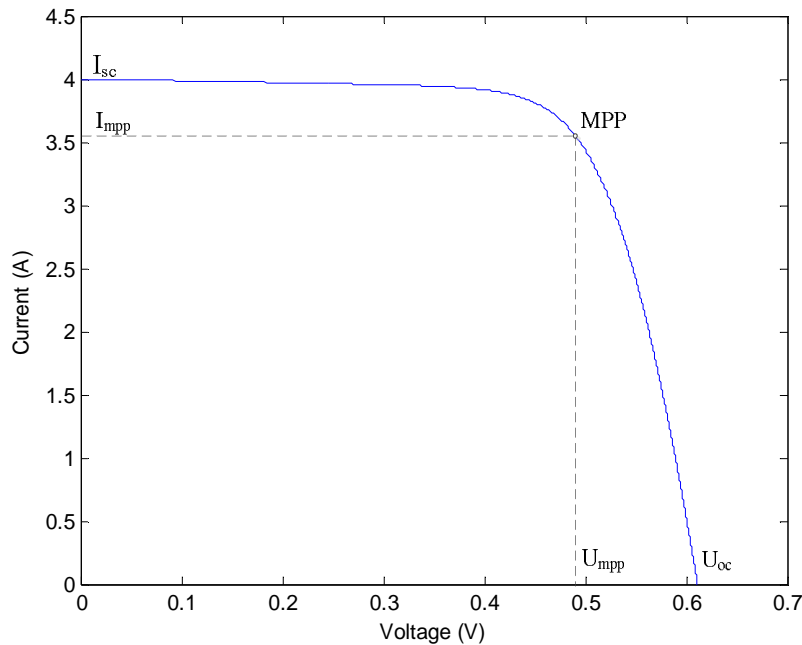


Figure 2.2. I-V curve of a photovoltaic cell.

The equation for the DC current produced by a photovoltaic cell can be derived from the minority carrier diffusion equation. The I-V characteristic of a photovoltaic cell is:

$$I = I_{sc} - I_{o1} \left(\exp^{\frac{qV}{kT}} - 1 \right) - I_{o2} \left(\exp^{\frac{qV}{2kT}} - 1 \right) \quad (2.1)$$

where I_{sc} is the short-circuit current, I_{o1} is the dark saturation current due to recombination in the quasi neutral regions, I_{o2} is the dark saturation current due to recombination in the depletion region, T is the temperature, k is the Boltzmann constant and q is the electron charge. By analysing this equation from an electrical circuit perspective, it gives an equivalent model of a cell, which is presented in *Figure 2.3*.

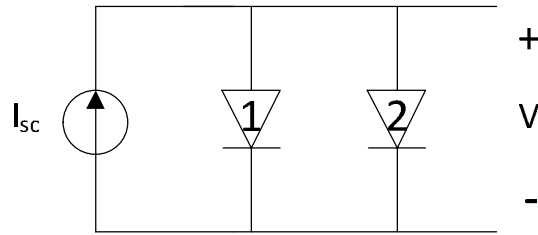


Figure 2.3. Simple solar cell circuit model.

A basic PV cell circuit model consists of an ideal current source and two diodes, representing, respectively, the dark saturation currents due to recombination in the quasi neutral and the depletion regions. The width of the depletion region is relatively small compared to the quasi-neutral region, and is usually neglected when modelling the cell. Therefore, the equation for the total current produced by a PV cell can be rewritten as:

$$I = I_{sc} - I_o \left(\exp^{\frac{qV}{AkT}} - 1 \right) \quad (2.2)$$

where I_o is the diode saturation current and A is the ideality factor. Due to this simplification, the circuit model of a photovoltaic cell transforms into equivalent one-diode model, as seen in *Figure 2.4*.

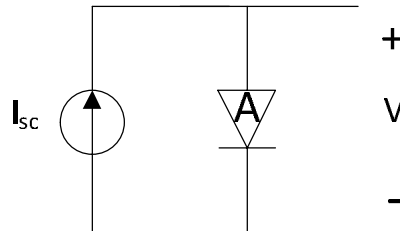


Figure 2.4. Solar cell circuit diagram for one-diode model.

For such a circuit the open circuit voltage can be written down as follows, giving an I-V characteristic:

$$V_{oc} = \frac{AkT}{q} \ln \left(\frac{I_{sc} + I_o}{I_o} \right) \quad (2.3)$$

The actual photovoltaic cell also has parasitic elements, namely parasitic shunt and series resistance. The main origin of the parasitic series resistance is the metal contacts and the transverse flow of current. The reason behind the parasitic shunt resistance is the p-n junction and impurities near the junction. Incorporating these parasitic elements into the equivalent circuit model provides certain changes to the I-V characteristic equation:

$$I = I'_{sc} - I_o \left(\exp \frac{q(V+IR_s)}{AkT} - 1 \right) - \frac{V+IR_s}{R_{sh}} \quad (2.4)$$

where I'_{sc} is the short-circuit current in case of no parasitic elements, R_{sh} is the parasitic shunt resistance and R_s is the parasitic series resistance.

Parasitic elements have a particular effect on the performance of the PV cell. A higher value of series resistance and a smaller value of shunt resistance will decrease the overall performance of a photovoltaic cell. The equivalent one-diode circuit diagram with parasitic resistances is shown in *Figure 2.5*.

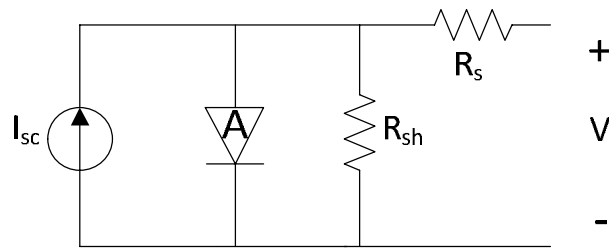


Figure 2.5. PV-cell equivalent diagram for one-diode model with parasitic elements.

2.2.2. Solar modules and generators

An individual solar cell generates a comparatively small voltage. For instance a typical solar cell with a surface area 100 cm^2 has voltage in the order of 600 mV and produces approximately 2-3 W. Therefore, solar cells are modelled in a number of series – parallel connections in order to achieve suitable voltage power outputs (*Figure 2.6*). A number of connected solar cells, usually in series, is called a solar module.

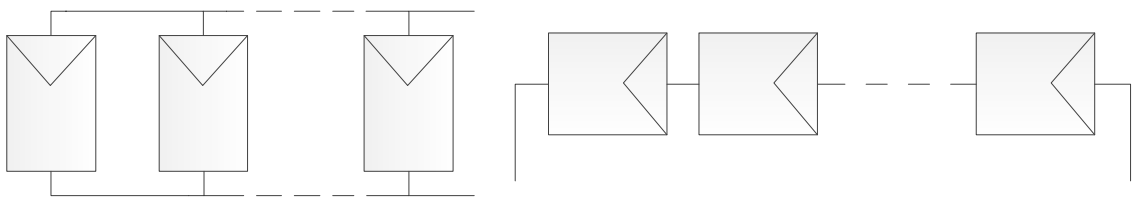


Figure 2.6. Parallel and series combination of solar modules.

Cells are connected in series in order to increase the voltage rating. Parallel connection of cells results in the higher current output. The effect of a series connection of solar cells on the I-V diagram is illustrated in *Figure 2.7*.

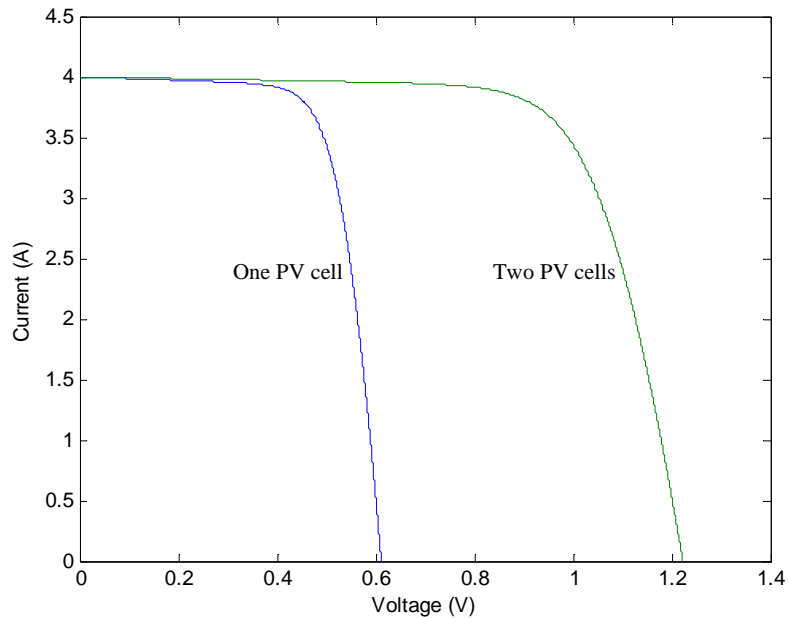


Figure 2.7. Series combination of solar cells.

The effect of parallel connections of solar cells on I-V diagram is illustrated in *Figure 2.8*.

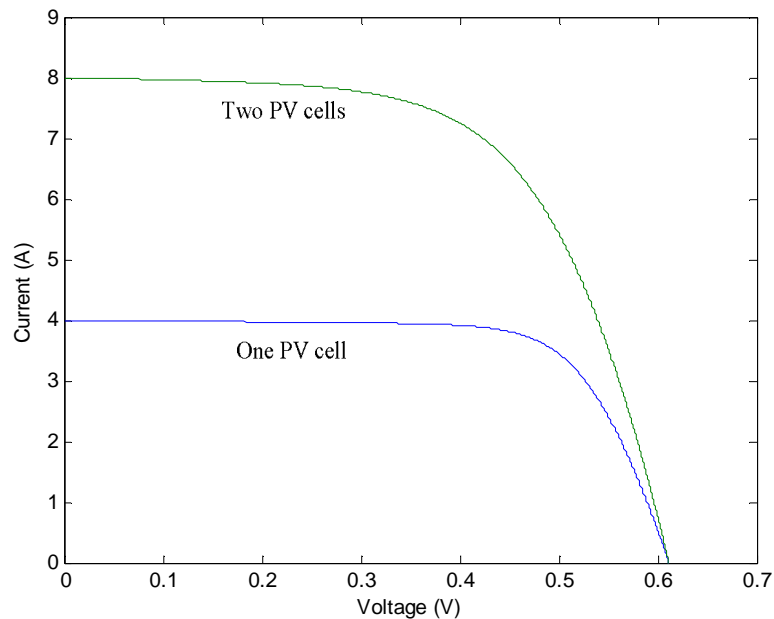


Figure 2.8. Parallel combination of solar cells.

When modelling solar modules it is normal to assume that photovoltaic cells have similar electrical characteristics, but problems will arise when cells start to operate under non-uniform conditions. For instance, partial shading is quite a common problem. Basically when a cell is shaded its power output decreases. In series connection, where only one cell is shaded, it may become reverse-biased and start to diffuse energy, resulting in damage to the cell. In order to prevent such failures, a bypass diode is implemented. *Figure 2.9* illustrates a typical photovoltaic module arrangement, consisting of 54

solar cells, 3 strings of 18 cells connected in parallel, where a bypass diode is connected in parallel with a string of solar cells. In case of partial shading, the PV current will not flow through the shaded region, thus preventing the failure.

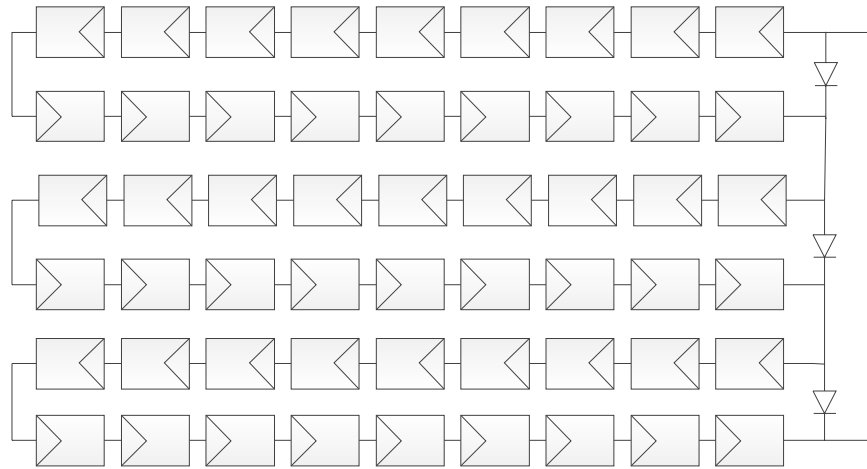


Figure 2.9. Implementation of bypass diode in a solar module.

The photovoltaic array is a structure consisting of a number of connected solar modules mounted on the same unit in order to provide specified electrical output characteristics required for a certain application. Basically, it is the same logic as with series and parallel connections of solar cells: series connection of the modules increases the voltage rating, parallel connection of the modules increases the current rating. *Figure 2.10* shows a typical “series-parallel” connection of a PV array. A typical way is to design an array with sufficient number of series strings in order to meet the voltage requirements and then add parallel strings to increase the power rating.

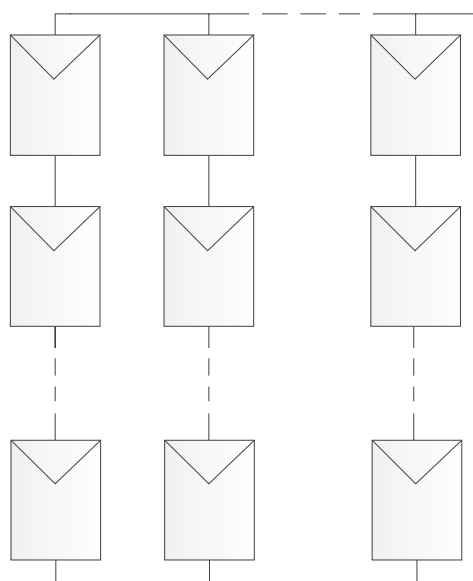


Figure 2.10. Typical solar array with “series-parallel” connection of modules.

2.3. Factors influencing the performance of a PV array

There are two main ambient factors affecting the performance of a photovoltaic cell: temperature and solar radiation on the surface of the cell. Both factors are described briefly in the following section below.

The effect of irradiance on the short-circuit current is almost linear; an increase in irradiance increases the short circuit current and vice-verse. This dependency can be seen in *Figure 2.11*.

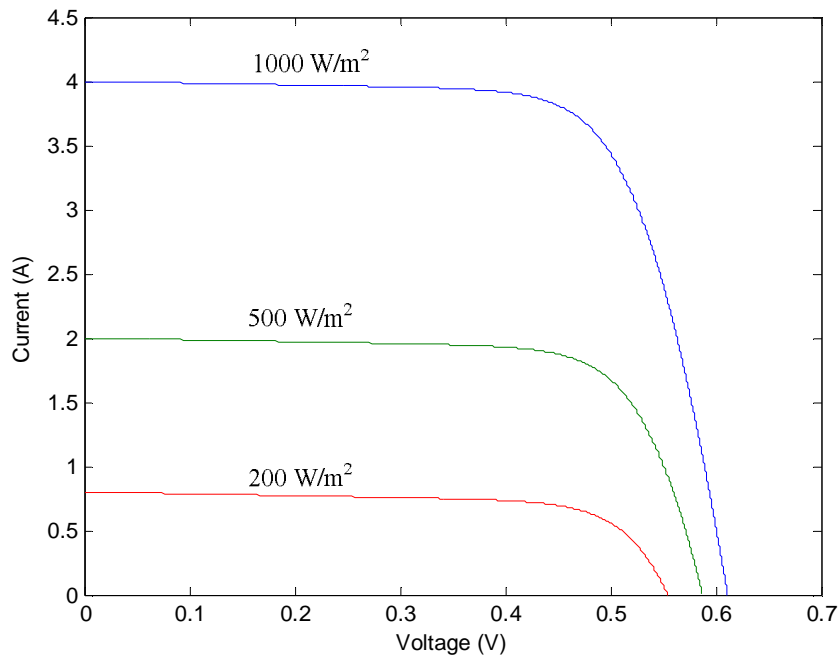


Figure 2.11. Influence of irradiance on the I-V characteristic.

According to equation (2.5), the open circuit voltage of photovoltaic cell depends logarithmically on the PV short-circuit current and therefore on irradiance.

$$V_{oc} = \frac{AkT}{q} \ln \left(\frac{I_{sc} + I_o}{I_o} \right) \quad (2.5)$$

With increasing temperature the short-circuit current increases slightly due to the narrowing of the band gap but the open-circuit voltage decreases more significantly, thus decreasing the overall performance of the cell. The effect of temperature on the I-V curve of solar cell is shown in *Figure 2.12*.

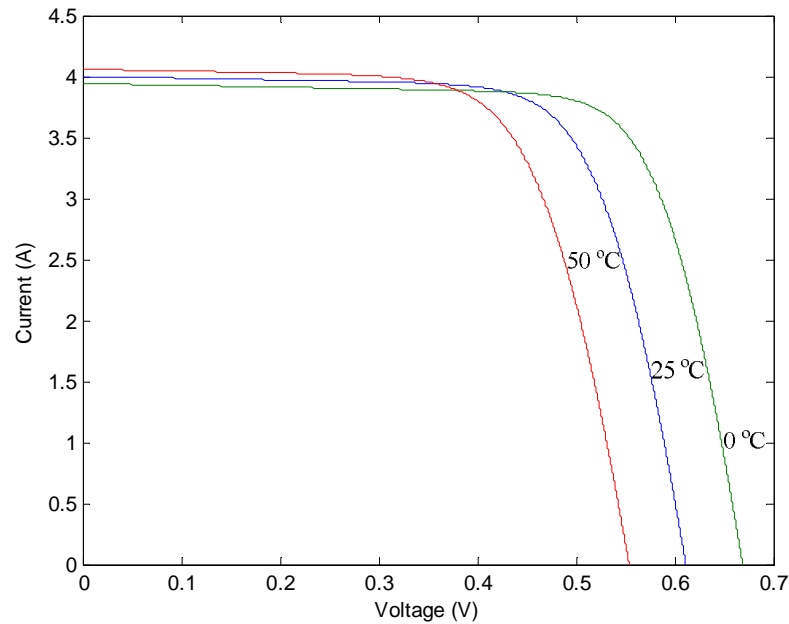


Figure 2.12. Influence of temperature on the I-V characteristic.

2.4. Modelling of photovoltaic generators in Simulink

As discussed in the previous sections, from the electrical circuit point of view, a photovoltaic cell can be modelled as a parallel connection of a current source and a diode, where the current source is responsible for photocurrent and the diode represents diode saturation current. In addition, a real photovoltaic cell would also have losses due to the p-n junction and metal contacts. These losses can be represented with the help of series and shunt resistances. Such an equivalent model is also suitable for representing a photovoltaic array with a versatile configuration of series and parallel connections.

Matlab and Simulink have many ways of modelling devices or components and modelling complex systems. This section outlines three different approaches of varying degree of complexity for modelling a photovoltaic system in Matlab/Simulink. First a simple mathematical model is provided. This is followed by the use of advanced component libraries to design a cell. Then, a more sophisticated approach based on experimental data is provided. For the interested reader, the following reference [25] is recommended, which has been used as foundation for photovoltaic cell model implemented in this thesis.

2.4.1. Mathematical model

The mathematical model, shown in this section is based on a Simulink implementation of a single diode photovoltaic module. Using the fundamental mathematical blocks from the Simulink library, it is straight-forward task to build the algebraic relationship. The set of equations used for the modelling of the cell are:

$$I = I_{ph} - I_o \left(\exp \frac{(V+IR_s)}{AV_t} - 1 \right) - \frac{V+IR_s}{R_{sh}} \quad (2.6)$$

$$V_t = \frac{kT}{q} \quad (2.7)$$

where I_{ph} is the photocurrent and V_t is the thermal voltage. The Simulink implementation of the mathematical model is presented in *Figure 2.13*.

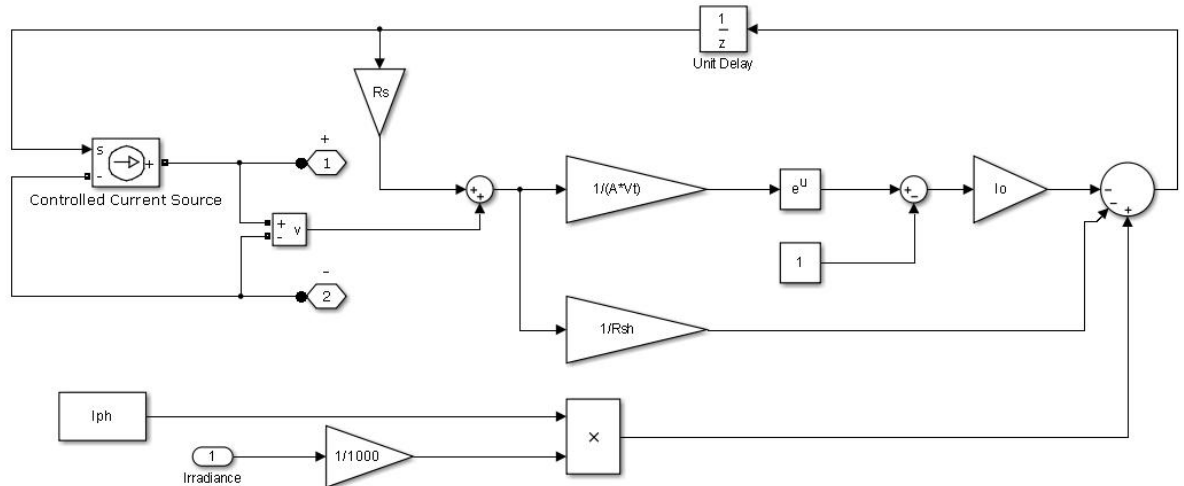


Figure 2.13. Mathematical model of a solar cell in Simulink.

This model of a photovoltaic cell can be used to model a photovoltaic array. The only change required is to scale up parameters. It is important to note that this is a simplified model, which does not take into account changes in ambient temperature. Therefore, some of the parameters were adjusted to fit the standard test conditions. However, as discussed in the previous chapter, changes in the ambient temperature are not so crucial to the performance of the photovoltaic cell. Furthermore, in real-life situations, changes in temperature exhibit a slow dynamics. On the contrary, changes in irradiance are vast in scale and can happen many times during a short interval.

2.4.2. Physical model

Simulink has advanced libraries including a tool called Simscape. Simscape is the basis for physical modelling techniques. Simscape has electrical components making it possible to model any electrical circuit. So it gives the opportunity to construct an equivalent model. Such functionality gives the advantage of being able to avoid mathematical equations when retrieving a mathematical algorithm, is problematic. *Figure 2.14* shows an equivalent, one-diode circuit of a photovoltaic cell implemented with the help of Simscape. The physical model corresponds directly to equation shown in (2.6).

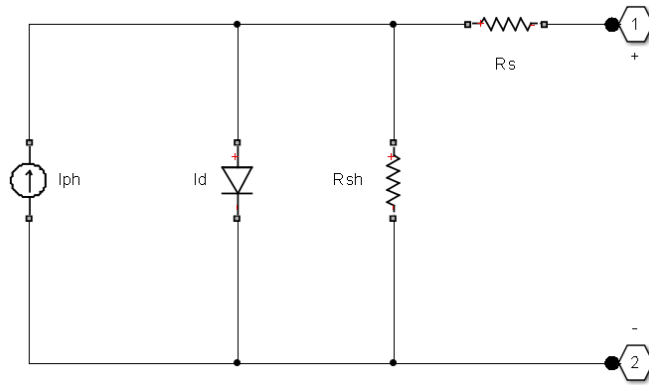


Figure 2.14. Physical model of a solar cell in Simulink.

A physical model may also be obtained with the use of an advanced component library, such as SimElectronics. The sources library of SimElectronics has the implemented model of a photovoltaic cell. It is a very detailed model of a solar cell, enabling the implementation of a single-diode or an eight parameter model, which is a double-diode model. In addition, it gives the opportunity to include the temperature behaviour of a device and to model temperature effects. It provides a model for microlevel analysis with very detailed simulation results.

2.4.3. Modelling based on experimental data

Matlab is a very flexible modelling and calculation platform, it provides the opportunity to design models based on the measured experimental data. One possible approach is to use the curve-fitting toolbox that facilitates the generation of mathematical models of the excitation-response kind. It is valuable solution when the actual solar panel is available and real data can be used. The data should include the behaviour of the photovoltaic module under different test conditions. The surface-fitting tool, which is a supplement to the curve fitting toolbox, allows creating a surface which aligns the loaded I-V curves in a mathematically reasonable form and generates Matlab code based on it. The generated code will correspond to the performance of the experimental photovoltaic panel. The code can be used to build an equivalent mathematical model, which later on can be used as a function for Lookup Table block. The main function of the Lookup Table block is to match the input variables to output values by interpolating previously defined data. The Simulink implementation of this concept is illustrated in *Figure 2.15*. In such a model the value of irradiance and the value of voltage determine the output current produced by the photovoltaic module.

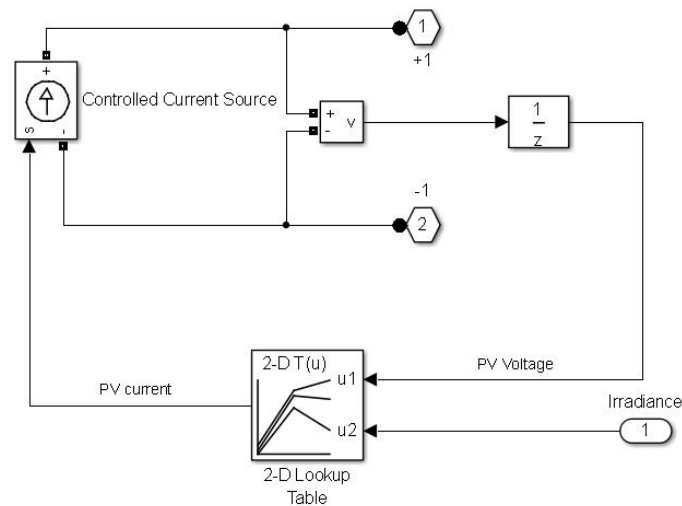


Figure 2.15. Model of a solar cell using experimental data.

Matlab provides other design instruments for setting up experimental driven model, such as the system identification toolbox which provides tools for constructing dynamic models and transfer functions. Another tool is the neural network toolbox, which is used for predictive modelling. It is extremely useful for modelling complex non-linear systems. For the interested reader in experimental driven models the following source [26] is recommended.

2.5. Summary

This chapter provided an overview of photovoltaic generators and introduced some basic approaches of PV cell modelling in the Matlab/Simulink environment. The mathematical model of the PV cell to be used in this research is the one presented in Section 2.4.1. The main reason for the selection of the simplest PV model is that the research interest in this thesis does not lie on the analysis of the performance the PV cell itself but rather on investigating the impact of the PVG at the point of connection with the power grid. The concern is more with the external performance of the PV cell rather than with its internal working mechanism. The model of one PV cell is used for modelling PV generators by simple scaling of the corresponding parameters. Such a model does not take into account changes in ambient temperature. However, it was concluded that temperature changes do not have significant effect on the current-voltage characteristic. PV partial shading is an issue of great importance in harmonic generation and it remains an outstanding issue of research to look at way of adapting the simple PV cell model to be able to represent conditions of partial shading.

3. DC-DC CONVERTERS

3.1. Introduction to basic DC-DC converters

Switched-mode DC-DC converters are widely used in regulated DC power supplies, renewable energy systems and motor drive applications. In general the main purpose of DC-DC converters is to keep the output voltage at a specified level, whereas in PV applications power electronics is also used to enable MPPT control. This will be discussed in chapter 4.

This chapter outlines the fundamentals of DC to DC switched mode converters, analysing the following converter topologies: buck, boost and buck-boost. The modelling of DC-DC converters in Matlab/Simulink is also addressed in this chapter.

3.2. Operation principles

3.2.1. Pulse width modulation

One or more power semiconductor devices, suitably coordinated, enables effective regulation of the output voltage. In most power electronics analyses such devices are assumed to be ideal switches to simplify modelling matters. According to Mohan et. al (2003) all modern power semiconductor devices can be grouped into three main categories [27]:

1. *Diodes*. The natural operation of the electrical circuit is responsible for the on and off states of the semiconductor valves.
2. *Thyristors*. The device is turned on with the help of control signals but, the turn off state is the result of the natural operation of the power circuit.
3. *Controllable switches*. The on and off states are controlled by control signals.

The last category involves a wide range of semiconductor devices such as bipolar junction transistors (BJT), metal-oxide-semiconductor field effect transistors (MOSFET), gate-turn-off thyristors (GTO), insulated gate bipolar transistors (IGBT) and MOS-controlled thyristors (MCT) [27].

One popular option to achieve output voltage regulation is by switching at a constant frequency using the so-called Pulse Width Modulation (PWM) control; PWM operates in such a way that the control signal is generated by comparing a reference voltage with a repetitive saw tooth waveform, as shown in *Figure 3.1*. The main aim of the control signal is to adjust the on and off time of the switch.

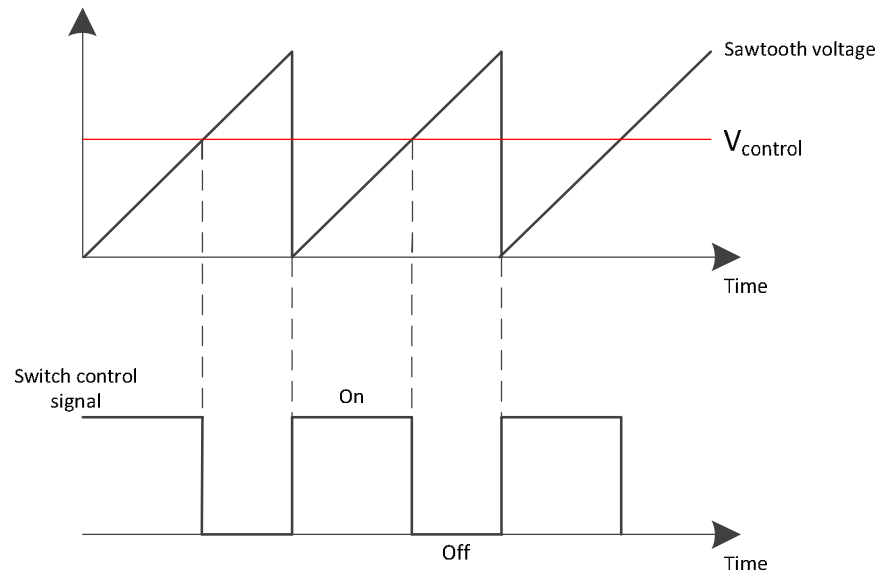


Figure 3.1. Pulse width modulation.

The reference voltage signal is produced either by comparing the desired value with the actual value or by amplifying the error. When the reference voltage signal is higher than the sawtooth waveform, the switch turns on. The opposite action would cause a switch to turn off. The duty cycle ratio of the converter and switching time given by (3.1) and (3.2), with f_s being the switching frequency.

$$D = \frac{t_{on}}{T_s} \quad (3.1)$$

$$T_s = \frac{1}{f_s} \quad (3.2)$$

3.2.2. Conduction modes

There are three main modes of converters' operation, namely: continuous conduction mode (CCM), discontinuous conduction mode (DCM) and boundary conduction mode (BCM). These modes have to do with the behaviour of the inductor current throughout the switching cycle, as depicted in *Figure 3.2*.

If the converter is operating in continuous inductor current mode then it means that the inductor current is all the time greater than zero. In discontinuous conduction mode the inductor current is zero during one part of the cycle, whereas in boundary mode the inductor current reaches zero at the end of the cycle. Also, in boundary mode the average inductor current would be half of the peak current. In this chapter only CCM mode will be discussed because the converter design used in PV application utilizes mostly the principle of CCM.

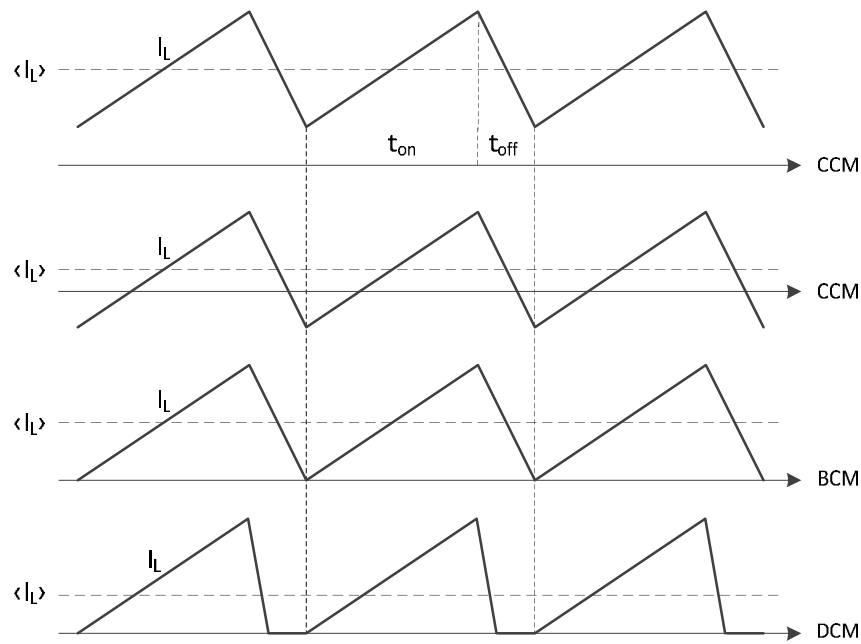


Figure 3.2. Conduction modes of a switched-mode converter.

3.3. Buck

The Buck converter is a step-down power converter which decreases an input voltage to the desired value at the output. *Figure 3.3* presents the basic circuit of the buck converter.

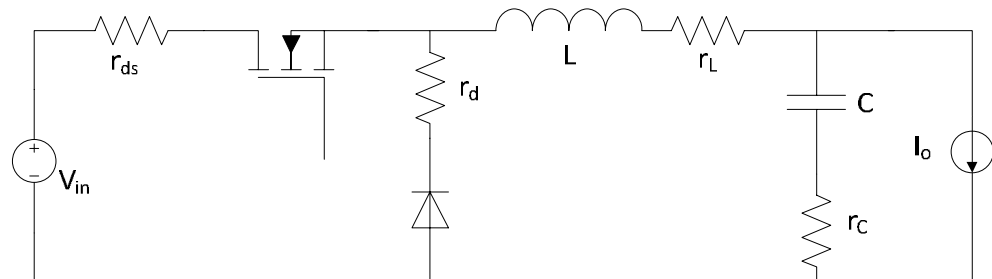


Figure 3.3. Circuit representation of a buck converter.

During CCM operation there are mainly two states. The first one is when the switch is closed and the diode is reverse biased. The second one is when the switch is opened and the diode is forward biased. Both of these sub-circuits are presented in *Figure 3.4*.

During the time when the switch is on, the input energy is supplied to the inductor and load, thus charging the inductor. During the off time period, when the switch is opened and there is no supply from the input, the inductor current cannot drop instantly to zero because of the energy stored in it during the on time; therefore the inductor current flows through the diode.

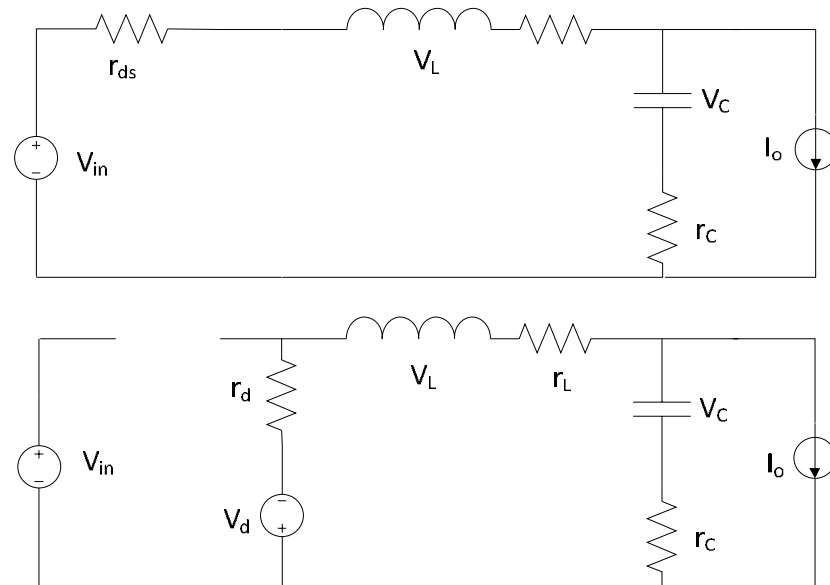


Figure 3.4. On and off sub-circuits of a buck converter.

3.4. Boost

The main task of a step-up boost converter, as its name suggests, is to increase the output voltage to the required level. A typical circuit diagram of a boost converter is presented in *Figure 3.5*.

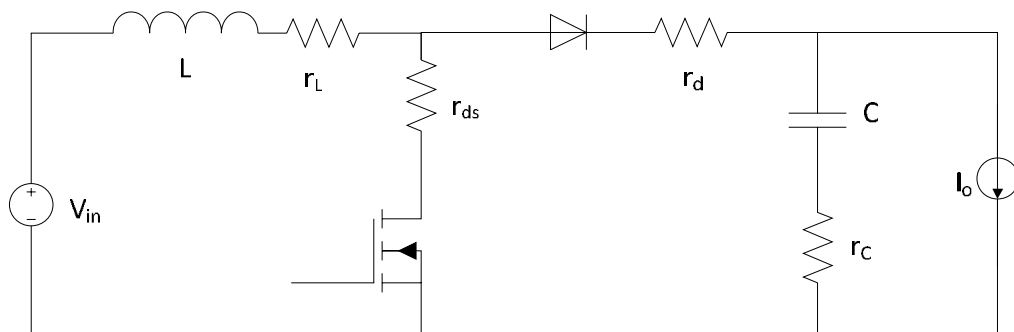


Figure 3.5. Circuit representation of a boost converter.

As in the previous case, there are two operation stages. The first one is when the switch is closed and the diode is reverse biased. In this case the output becomes isolated and there is no supply of power. During this stage the inductor is being charged throughout the time when the switch is closed. During the second stage, when the switch is off, the power from the input as well as that that was stored in the inductor is supplied to the load, thus increasing the output voltage. The on and off-state sub-circuits are presented in *Figure 3.6*.

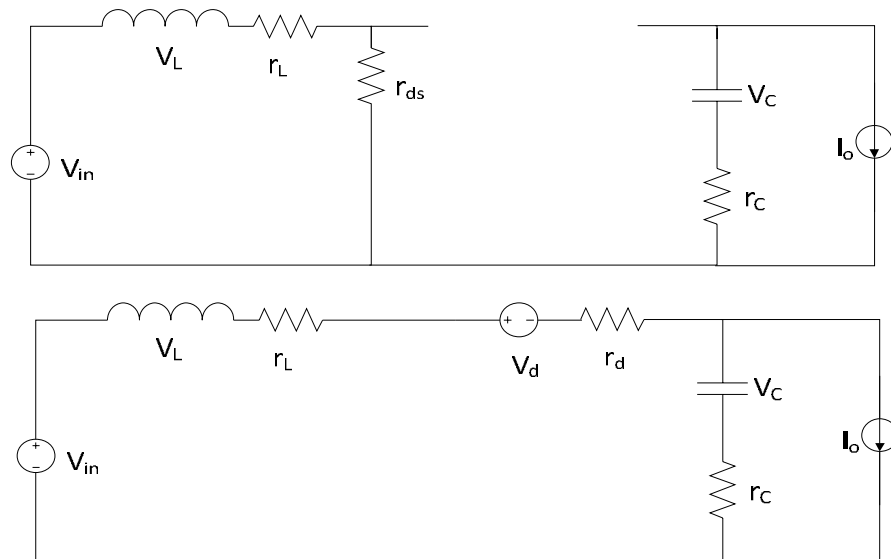


Figure 3.6. On and off sub-circuits of a boost converter.

3.5. Buck-Boost

The buck-boost converter may be seen to comprise the cascaded connection of a DC-DC buck and boost converters. Hence, the buck-boost converter possesses properties of both step-up and step-down converters. Another property of the buck-boost converter is the inverting function, which means that the output voltage has the opposite polarity of the input. The schematic diagram of the converter is presented in *Figure 3.7*.

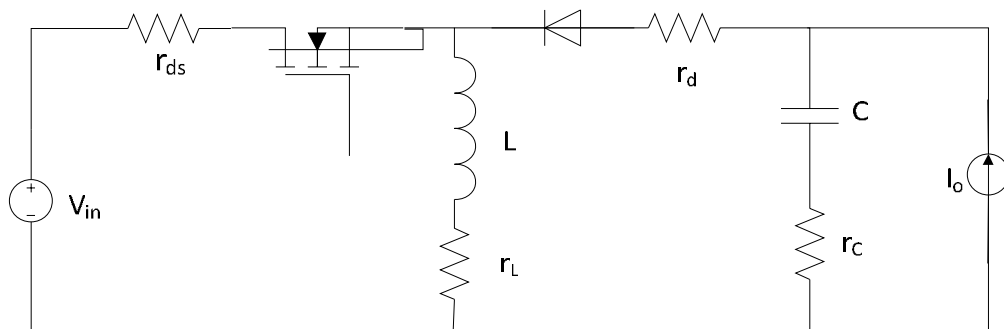


Figure 3.7. Circuit representation of a buck-boost converter.

The basic operational principal of the converter is relatively simple. During the on-state, when the diode is reverse biased, the input source supplies power to the inductor, which results in accumulating energy, whereas the load consumes the capacitor power. During the off-state, when the switch opens, the inductor acts as an energy source and supplies power to the load and capacitor. The circuit diagram for the on and off-state of a buck-boost converter is shown in *Figure 3.8*.

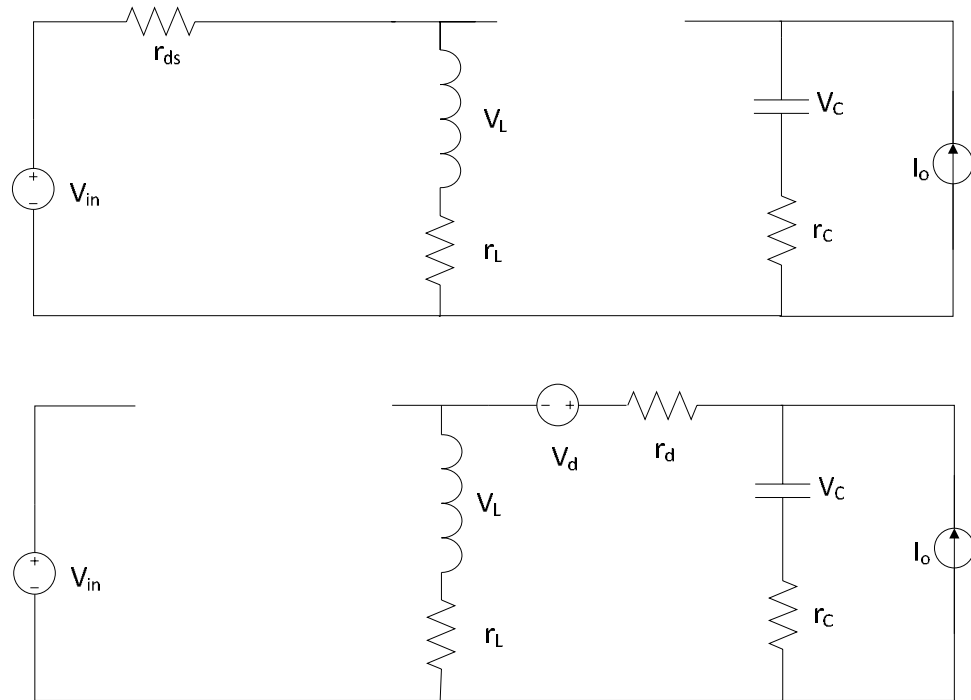


Figure 3.8. On and off sub-circuits of a buck-boost converter.

3.6. Steady-state analysis

As previously discussed one of the essential functions of a DC-DC switched mode converter is to either increase or decrease the voltage at the output terminals. The input-to-output relationship can be computed by applying volt-sec and amp-sec balance to the on and off time subcircuit structures of the converter. Volt-sec balance means that the average voltage across the inductor would be zero. Such computation yields the input-to-output conversion ratio $M(D)$. Amp-sec balance means that the average capacitor current would be zero. This yields the ratio of the inductor current to the output current. The following example shows how to carry out the steady-state analysis to the boost converter.

Table 3.1. Example of steady-state analysis applied to a boost converter.

On-time equations	Off-time equations
$V_L = V_{in} - (r_L + r_{ds})I_L$	$V_L = V_{in} - V_D - (r_L + r_d)I_L - V_o$
$V_o = V_C + r_c \cdot i_c$	$V_o = V_C + r_c \cdot i_c$
$i_c = -I_o$	$i_c = I_L - I_o$
$V_o = V_C - r_c I_o$	$V_o = V_C - r_c I_o + r_c I_L$
$V_{L1} = V_{in} - (r_L + r_{ds})I_L$	$V_{L2} = V_{in} - (r_L + r_d + r_c)I_L - V_D - V_C + r_c I_o$
$i_{c1} = -I_o$	$i_{c2} = I_L - I_o$
<i>The equations of the inductor voltage and the capacitor current may be used to define the amp-sec and volt-sec balances</i>	

Averaging
$Di_{c_1} + D'i_{c_2} = 0$ $D(-I_o) + D'(I_L - I_o) = 0$ $I_L = \frac{I_o}{D'}$ $DV_{L_1} + D'V_{L_2} = 0$ $V_{in} - D'V_D - D'V_C - (r_L + D'r_d + Dr_{ds} + DD'r_c)\frac{I_o}{D'} = 0$ $V_o = V_C = \frac{V_{in}}{D'} - V_D - (r_L + Dr_{ds} + D'r_d + DD'r_c)\frac{I_o}{D'^2}$

3.7. Modelling of DC-DC converters in Matlab/Simulink

The electrical circuit of the Boost converter used in this work is presented in *Figure 3.9*. However, the converter topology is modified slightly; namely a capacitor is added to the input. This is done in order to achieve a current fed topology, as it has been presented in [28]. The main reason for using a current fed boost converter is that the control system regulates the voltage. As discussed in Chapter 2, changes in irradiance have a relatively small effect on the output voltage, whereas the current produced by the PV system is very sensitive to the variations in irradiance, which means that the PV current's fluctuation is large in scale and fast. Therefore, control for such current would require fast dynamics and it might lead to controller's saturation. [29]

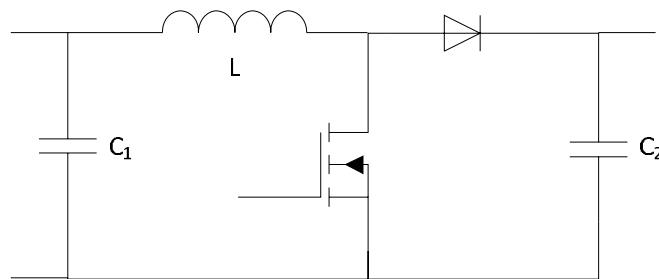


Figure 3.9. Converter topology used in the thesis.

There are several ways to implement model of the converter in Matlab/Simulink. The one which was implemented in this piece of research utilizes the SimPowerSystems toolbox, which is a supplement to the Simscape library. Modelling of the boost converter in Simulink is presented in *Figure 3.10*. SimPower systems libraries have all the basic components which are needed for the construction of converter models. One certain advantage of such an approach is that any necessary changes in the converter topology can be performed with minimum efforts and time, requiring only the addition of new blocks or changing the properties of existing blocks.

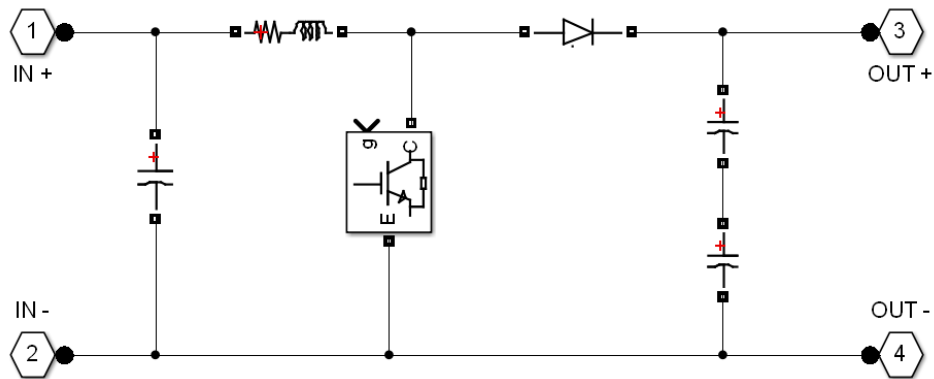


Figure 3.10. Modelling of the boost converter using SimPowerSystems library.

It is important to notice that the design of a physical model of a converter can also be achieved by means of the SimElectronics library. However there is a very important distinction to be drawn between the use of the SimElectronics and the SimPower components. Using the SimElectronics components results in a non-linear implementation. SimElectronics modelling is a very detailed SPICE type level simulation of the power electronic components, which includes temperature effects and microlevel nonlinearities of switching transistors. SimElectronics models at the microlevel, results in very detailed simulations, with a rather slow computational performance. On the other hand, SimPowerSystems uses piecewise linear approximation; instead of solving nonlinearities of switching devices, SimPower blocks use piecewise linear solutions [25]. The SimPower library enables the construction of fast-running electrical and electronic circuits. For instance, it has turned out to be very useful for building three-phase circuits of power distribution systems, for the purpose of performing transient and harmonic analyses.

Yet another, alternative, is to model the converter, using the mathematical equations presented in *Table 3.1*. Using the fundamental mathematical blocks from the Simulink library it is relatively easy to build the algebraic relationships. The Simulink implementation of the mathematical model is presented in *Figure 3.11*.

Mathematical modelling is an essential tool for analysing the behaviour of complex systems. It is useful for designing control systems, transfer function analysis, forecasting and optimizing system behaviour. Nevertheless, such a method has one associated drawback; any change in the converter topology would require the derivation of a new model, which would normally take a substantial amount of development time.

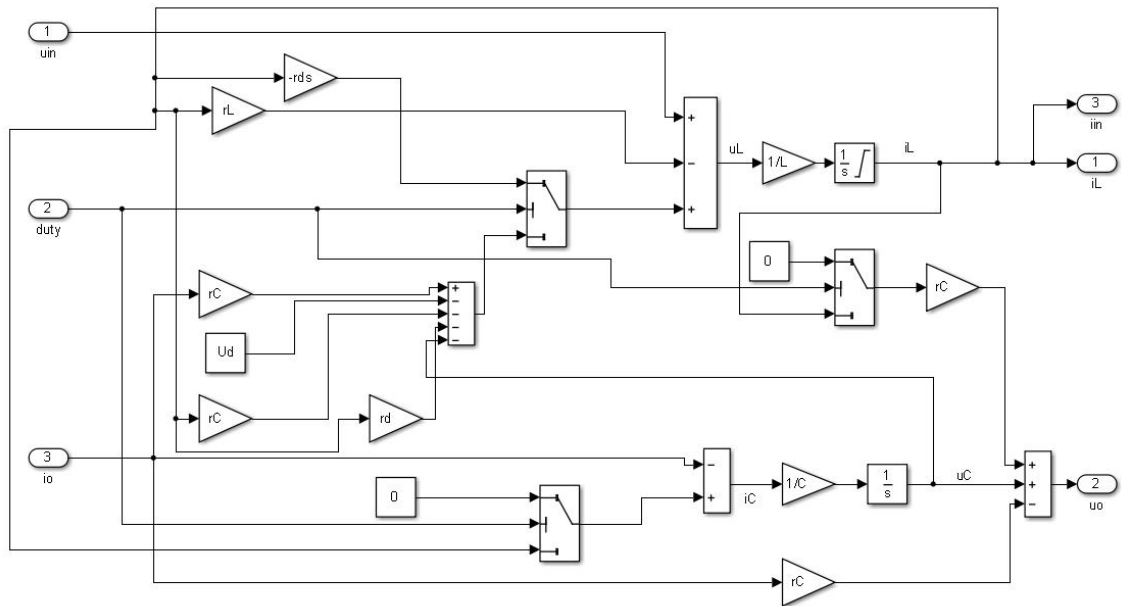


Figure 3.11. Mathematical representation of a voltage-fed voltage-output boost converter.

3.8. Summary

This chapter provided an overview of switched-mode DC-DC converters and introduced basic approaches of power converter modelling in the Matlab/Simulink environment. Based on the investigation presented in [28], [29] a current-fed current-output boost converter was designed in the Matlab/Simulink environment, as shown in *Figure 3.10*. It was decided to use the SimPowerSystems toolbox for the purpose of converter modelling due to the great simplicity and efficiency of such a tool.

4. MPPT TECHNIQUES

4.1. Introduction

Since the output power produced by a photovoltaic generator varies because of a changing irradiance and temperature, a key concern in the design of an efficient PV system is to track the maximum operating point; usually referred to as the maximum power point. The I-V and the P-V curves of the solar cell are non-linear, as illustrated in *Figure 4.1*. The basic idea behind the MPP tracking system is to be able to identify the maximum operating point taking accurate account of changes in operating conditions.

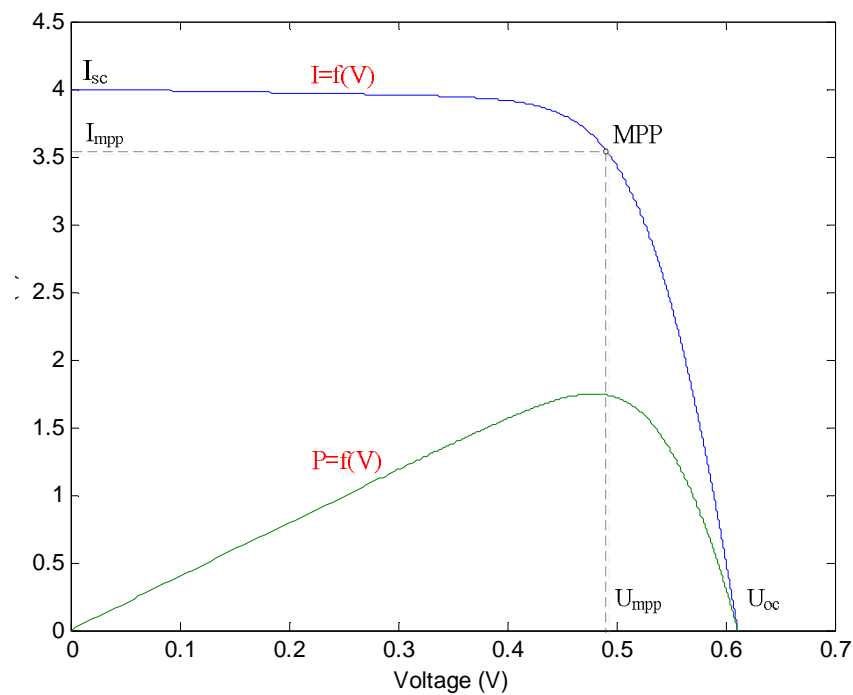


Figure 4.1. A current-voltage characteristic of a PV cell.

As discussed in previous chapters, power electronics is essential in the grid integration of a photovoltaic array. A power converter is needed to adjust the energy flow from the photovoltaic array to the load, which also has the vital function of tracking the point of maximum operating power. A typical flowchart of an MPPT algorithm is shown in *Figure 4.2*.

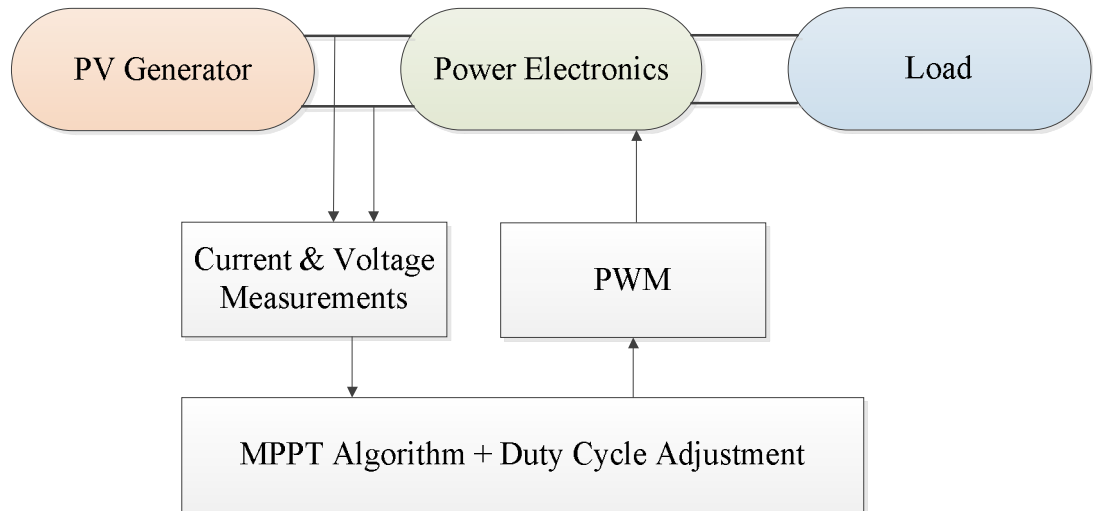


Figure 4.2. A high-level view of a power point tracking method.

The method relies on the continuous computation of power from measurements of current and voltage of the photovoltaic. The power signal is fed into the control algorithm, which in turns determines whether or not the system is operating at its maximum power point. This governs the required adjustment on the duty cycle to achieve maximum power.

There are at least 19 well-known MPPT techniques of varying performance [30]. In this chapter mainly two control algorithms are outlined, which are the ones implemented in the Simulink developments pursued in this work.

4.2. The perturb and observe method

The perturbation and observation method is widely used because of its simple implementation, few parameters and low computational cost compared to other methods. The basic idea behind the perturb and observe method is that the voltage derivative of the power is zero at the MPP.

The flowchart of the Perturb and Observe method is presented in *Figure 4.3*. The power of the photovoltaic system is calculated from the measured voltage and current values and is compared to the previous calculations of power, which are stored and available in memory. The control system operates by periodically incrementing or decrementing (perturbing) the PV voltage and current and by comparing the new and the old powers to increase or decrease the duty cycle. If the perturbation results in an increase of power then the direction of the perturbation pattern remains unchanged. In cases of power decrease the sign of the perturbation reverses. This loop is repeated until the point of maximum power is achieved which happens when $dP/dV=0$. One drawback of this method is that the control system does not stop perturbing when the maximum power point has been achieved and will keep oscillating which results in efficiency loss.

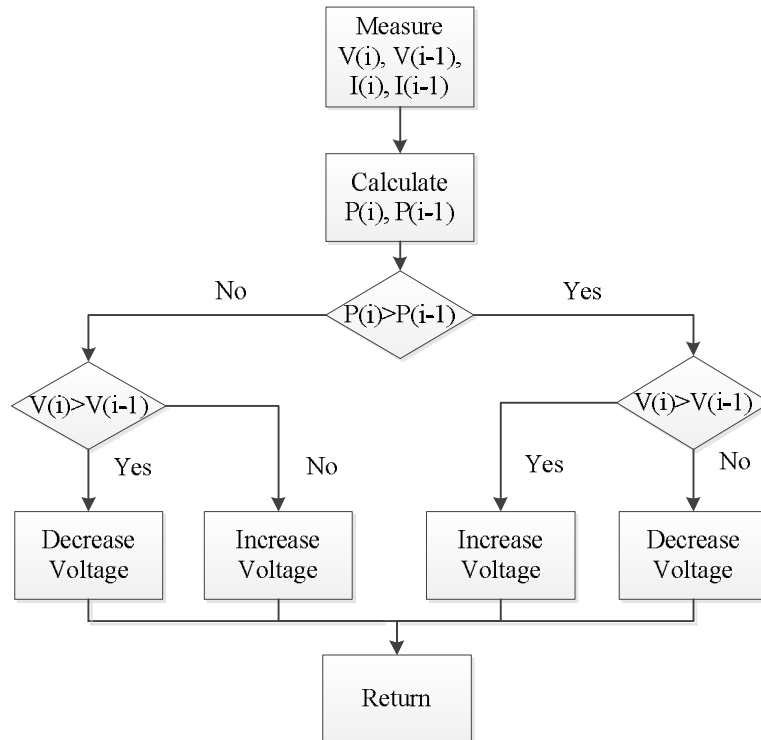


Figure 4.3. The perturbation and observation algorithm.

The implementation of the Perturb and Observe algorithm is quite straightforward. The approach used here relies on a Matlab function block, which allows bringing matlab code in to Simulink. The code is converted into C code and compiled while the simulation is running. The Matlab code is presented in Programme 4.1.

```

function D = PandO(Vpv,Ipv)
% MPPT controller based on the Perturb and Observe
% algorithm
persistent Dprev Pprev Vprev
if isempty(Dprev)
    Dprev=0.4;
    Vprev=0;
    Pprev=0;
end
Dmax = 0.7; % Optional value depending on the requirements
Dmin = 0.3; % Optional value depending on the requirements
deltaD = 0.0001;
Ppv = Vpv*Ipv;
if (Ppv-Pprev)~=0
    if (Ppv-Pprev)>0
        if (Vpv-Vprev)>0
            D=Dprev-deltaD;
        else
            D=Dprev+deltaD;
        end
    end
  
```

```

else
    if (Vpv-Vprev)>0
        D=Dprev+deltaD;
    else
        D=Dprev-deltaD;
    end
end
else
    D=Dprev;
end
if D >= Dmax | D <= Dmin
    D=Dprev;
end
Dprev = D;
Vprev = Vpv;
Pprev = Ppv;

```

Programme 4.1. *Perturb and Observe method.*

One of the advantages of using Matlab C code for the control system, as opposed to using the help of Simulink toolbox, is that it drastically reduces the simulation time. Computing gains might not be so obvious when using the code option for a single PV system, but it is definitely a major asset when applied to a full-scale power system with a large number of distributed generation units.

4.3. The incremental conductance plus integral regulator method

The incremental conductance method is based on measurements and comparison of the incremental conductance and the instantaneous conductance, with which changes in the voltage direction can be identified [30]. It is not difficult to see that it is a method based on the differentiation of the power vs. voltage curve, governed by the following equations:

$$\frac{\partial P}{\partial V} = \frac{\partial(VI)}{\partial V} = I \frac{\partial V}{\partial V} + V \frac{\partial I}{\partial V} = I + V \frac{\partial I}{\partial V} \quad (4.1)$$

$$\frac{\partial P}{\partial V} = 0 \quad (4.2)$$

$$I + V \frac{\partial I}{\partial V} = 0 \quad (4.3)$$

$$\frac{\partial I}{\partial V} = -\frac{I}{V} \quad (4.4)$$

where $\frac{I}{V}$ represents the instantaneous conductance of the PV array and $\frac{\partial I}{\partial V}$ is the instantaneous change in conductance. The comparison of these two quantities, given by (4.5),

defines whether or not the PV system is operating at maximum operating point or at which side from MPP the PV array is currently operating.

$$\begin{cases} \frac{\partial P}{\partial V} > 0, V < V_{mpp} \\ \frac{\partial P}{\partial V} = 0, V = V_{mpp} \\ \frac{\partial P}{\partial V} < 0, V > V_{mpp} \end{cases} \quad (4.5)$$

One of the main advantages of this method compared to the Perturb and Observe method is that after MPP is found, there is no need for further calculations of the incremental conductance, unless changes in the operating condition do occur again. An effective way to increase the performance of the incremental conductance algorithm is to include an integral regulator, which will minimize the error e , as shown in (4.6).

$$e = \frac{\partial I}{\partial V} + \frac{I}{V} \quad (4.6)$$

Such addition solves the problem of the PV system not being to operate exactly at the maximum operating point and the ensuing oscillations around it [31]. The flowchart of the Incremental conductance algorithm is presented in *Figure 4.4*.

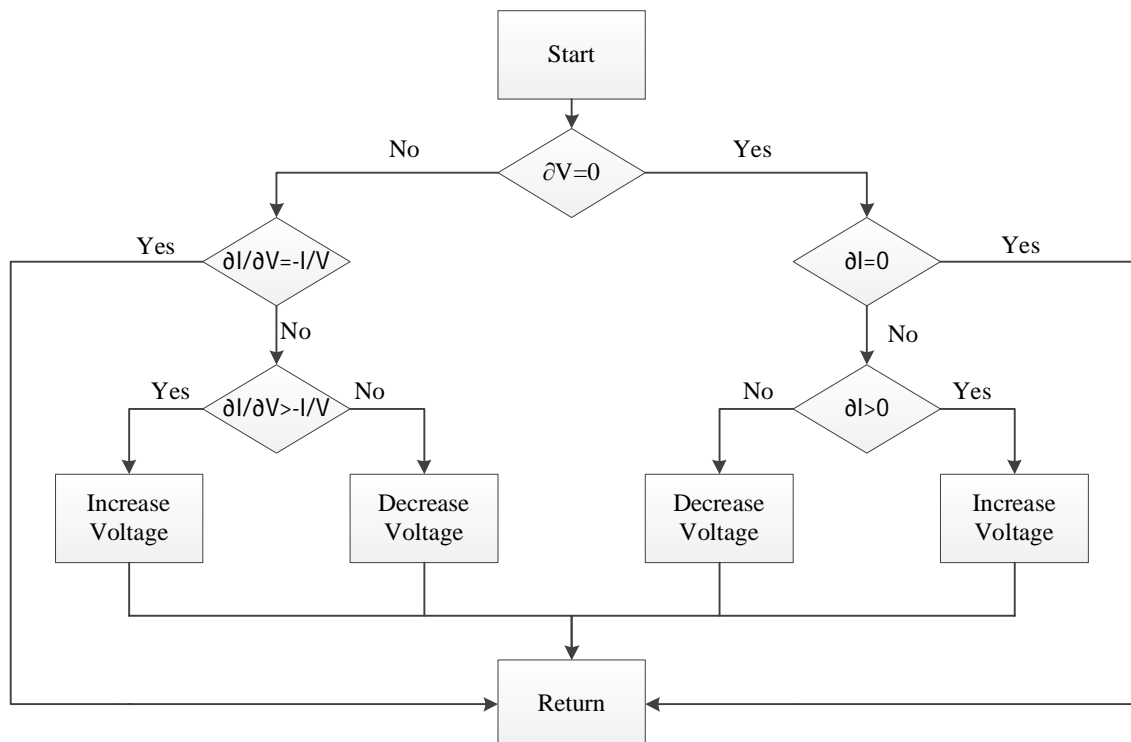


Figure 4.4. Flowchart of the incremental conductance algorithm.

Once the values for solar array voltage and current are measured; they are used to calculate ∂V and ∂I . If both are equal to zero then the PV system is operating at its maximum operating. The increase of irradiance will result in a rise of MPP voltage since $\partial I > 0$. In such a case the control system will have to raise the operating voltage in order to track down the maximum operating point. When a decrease in irradiance is observed, the MPPT decreases the system's operating voltage. When $\frac{\partial I}{\partial V} < -\frac{I}{V}$, the photovoltaic system is operating on the right-hand side of the MPP; therefore the voltage should decrease in order to reach the maximum operating point. On the contrary, when $\frac{\partial I}{\partial V} > -\frac{I}{V}$, the voltage raises in order to allow the array to operate at MPP. *Figure 4.5* shows the Matlab/Simulink implementation of the incremental conductance and the integral regulator algorithm where the controller's output will be corrected by the initial duty cycle. The model is based on the work reported in [31].

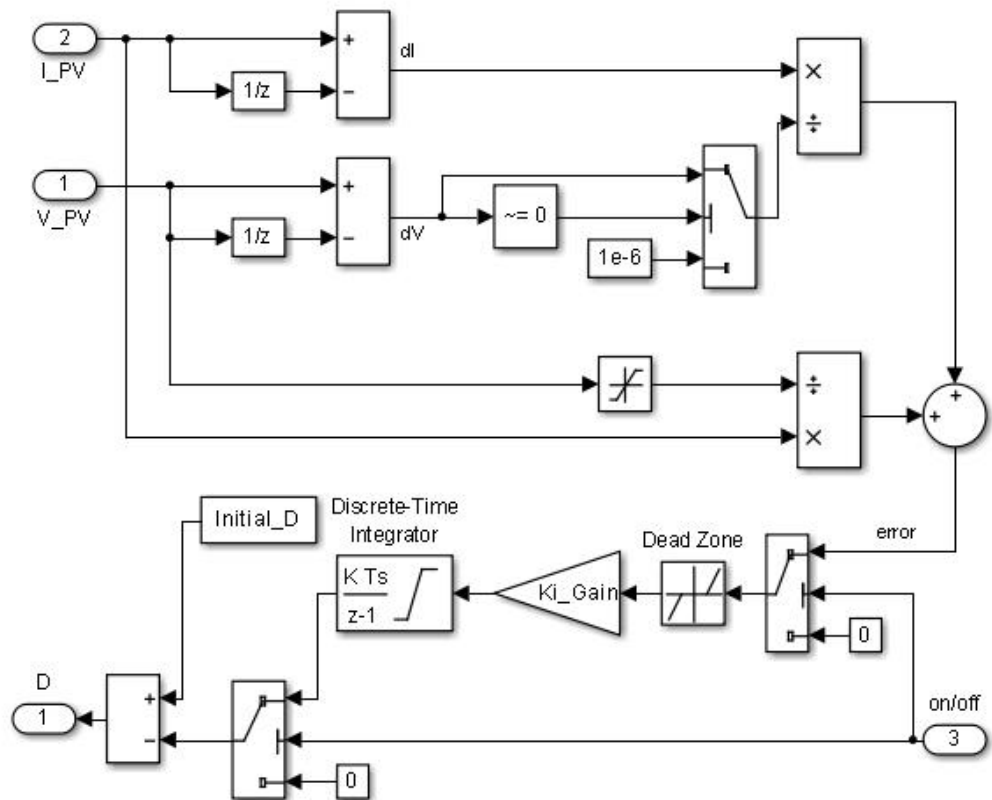


Figure 4.5. Matlab/Simulink implementation of the incremental conductance and internal regulator method.

4.4. General problems related to local MPP techniques

The MPPT algorithms presented above exhibit optimal performances when operating in conditions when there is only one maximum operating point. Unfortunately they do not operate properly when the I-V curve of a photovoltaic module exhibit several peaks,

which would be in PV panels being subjected to partial shading. According to Bruendlinger et. al. the power loss can be as much as 70% of its nominal value when using local MPP controllers [32]. Basically the presence of multiple peaks in the I-V curve reduces the performance index of local MPP techniques which assume the existence of only one maximum point. In such cases it is important to find out the global operating point in order to maximise the power output of the PV module. Typical examples of global MPPT algorithms are the two-stage power point tracking algorithm or the current sweep method [33].

4.5. Summary

This chapter provided an overview of the maximum power point tracking algorithms and introduced basic approaches of modelling MPPT in the Matlab/Simulink environment. The two most common algorithms were implemented: the Perturb and Observe method and the Incremental conductance plus integral regulator method. The Perturb and Observe method was designed by using C code which provides much better computational speed efficiency.

5. BASIC DC-AC INVERTERS

5.1. Grid connected renewable energy systems

To integrate photovoltaic generators into the AC power grid, the use of DC-AC inverter is mandatory. The fundamental role of any DC-AC inverter is the conversion of DC power into AC power. The layout of a grid-connected energy system is presented in *Figure 5.1*, where the aim is to inject maximum power in to the AC grid.

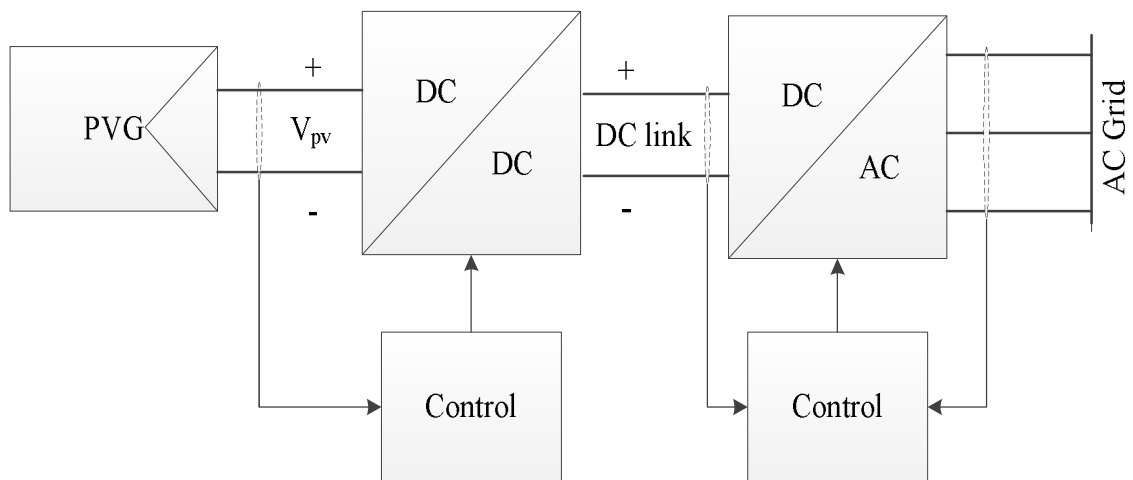


Figure 5.1. Diagram of a grid-connected PV generator.

The operation of such a system is defined as a grid-parallel operation, where the grid is an ideal voltage source. In such a case the inverter acts as a current source which has to be synchronised to the grid voltage. More often than not the operation of power network departs from its main intended function due to interruption of the main power supply, power consumption peaks or short-circuits in the grid. These events lead to grid voltage deviations and frequency fluctuations. In such cases, DC-AC inverters act as a voltage source and may even form microgrids with voltage levels and frequencies of their own. The output power is entirely dependent on the load connected to the renewable energy system. Such a mode of operation is known as grid-forming or islanded mode of operation.

5.2. Fundamentals of switched-mode inverters

This section discusses the basic principles of switched-mode inverter operation. *Figure 5.2* illustrates the output voltage and current characteristics of a typical single-phase inverter, where the load is of the inductive type [27]. The output signal is assumed to be sinusoidal. According to this diagram there are four modes of operation, as shown in *Figure 5.2*. Operation mode 1 comprises output voltage and current being of equal sign. The same also happens during operation mode 3. Such a regime corresponds to the inverter type of operation. Whereas in modes 2 and 4 the currents and voltages are of the opposite sign, which corresponds to the rectifier mode of operation.

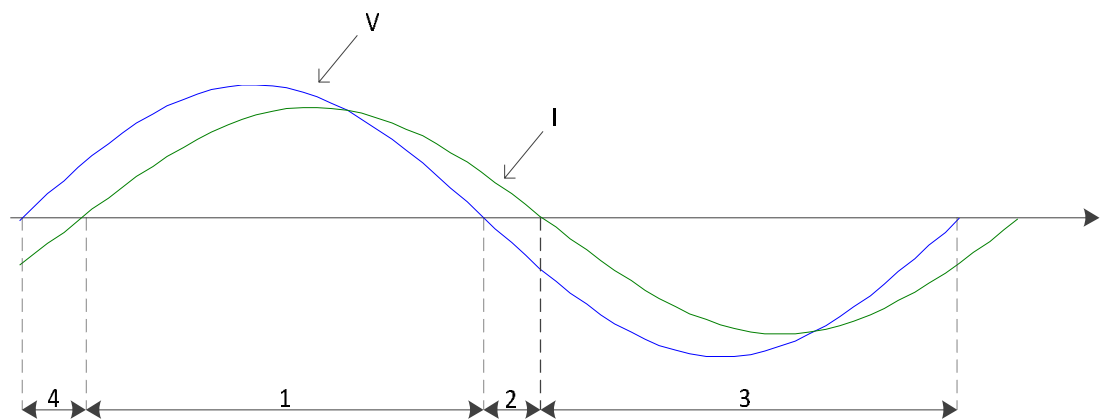


Figure 5.2. Output current and voltage characteristic of inverter.

In switched-mode inverters, the control signal is generated by means of pulse width modulators. The main idea behind the PWM control is that it helps to produce a sinusoidal-like output signal by comparing a control signal with a triangular waveform. The frequency of the triangular waveform defines the switching frequency and is usually kept constant. *Figure 5.3* illustrates this process, where V_{tri} is the triangular waveform, f_s is the switching frequency of the inverter switches and $V_{control}$ is the control signal which is used to modulate the duty ratio. It usually has its own frequency f_1 , called modulating frequency, which corresponds to the fundamental frequency of the output voltage [27].

There are two main parameters which are of vital importance for understanding the working of PWM control: amplitude modulation ratio m_a and frequency modulation ratio m_f . The amplitude modulation ratio is the ratio of $V_{control}/V_{tri}$ whereas frequency modulation ratio is determined as f_s/f_1 . The selection of frequency modulation ratio is of great importance, when considering the design of an inverter because it impacts greatly the overall system performance. It also affects the design of the output filter and current harmonic emissions injected to the grid.

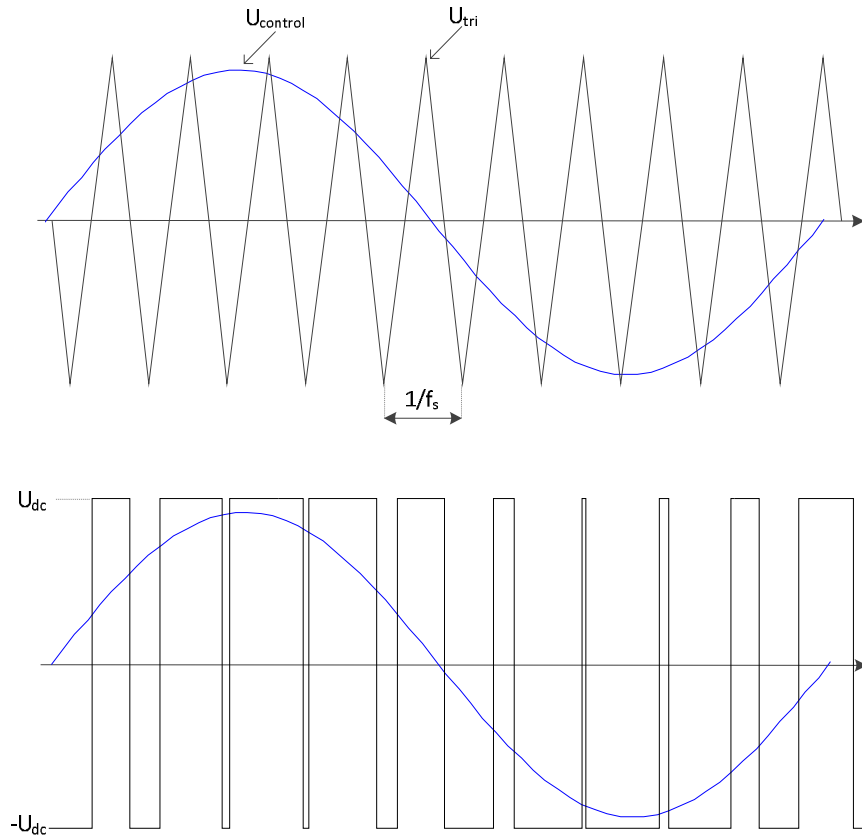


Figure 5.3. PWM behaviour.

The operation of inverter switches T_{A+} and T_{A-} is controlled by comparing two parameters, namely $V_{control}$ and V_{tri} . When $V_{control} > V_{tri}$ the the upper switch of the inverter legs T_{A+} is on. In the opposite scenario, T_{A-} is on. Due to the fact that T_{A+} and T_{A-} are never simultaneously on, the output voltage fluctuates between $\frac{V_{dc}}{2}$ and $-\frac{V_{dc}}{2}$. The output voltage, produced by a PWM inverter is a function of the modulation index. The peak amplitude of the fundamental voltage is equal to:

$$V_{AO} = m_a \frac{V_{dc}}{2} \quad (5.1)$$

5.3. Selection of the switching frequency and the frequency modulation ratio

Choosing the appropriate switching frequency and frequency modulation ratio is of vital importance in the design of DC-AC inverter because it relates to harmonics filtering. In principle, the higher the switching frequency, the easier it is to filter it but this comes with a price, because, higher switching frequencies result in higher switching losses. According to Mohan et. al. (2003) typical inverter switching frequency are either below 6 kHz or above 20 kHz [27]. The authors recommend using switching frequency above

20 kHz in cases when the design procedure suggests that the switching frequency falls in the range between 6 kHz to 20 kHz. The reason is that there is a major benefit in doing so on the grounds of audible noise reduction. It is stressed that the benefits acquired by noise reduction compare favourably with the disadvantages incurred by switching frequency increases. It is stated that the frequency modulation ratio of 21 is considered a borderline between a large and a small value. Further key design considerations are the following:

- For m_f smaller than 21 it is important that the control signal and the waveform are synchronised; therefore m_f should be an odd integer. There is a certain benefit in such a design as it prevents the presence of subharmonics which are highly undesirable.
- For m_f larger than 21 the value of subharmonics is not so significant and the control signal and waveform signal may not need to be synchronised. Nevertheless it should be noted that in AC motor applications even subharmonics which are close to zero values will result in large currents.

5.4. Typical inverter topologies

Arguably, the most popular VSC topologies are the half-bridge and the full-bridge, even though in renewable energy sources applications the inverter's input would be current. The main difference between the half-bridge and the full-bridge topologies is the voltage level of the DC link: the half-bridge inverter requires a voltage level at the DC link at least twice the peak grid voltage, whereas a full-bridge sub-topology can operate with the peak grid voltage level at the DC link. *Figure 5.4* illustrates a typical single-phase, three-level VSI inverter, more commonly known as three-level neutral point clamped inverter (NPC).

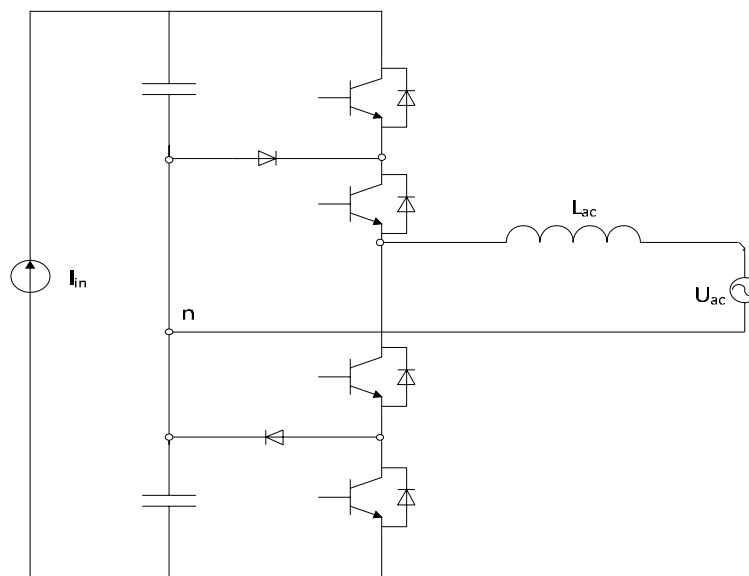


Figure 5.4. 3-level single phase NPC inverter.

The number of levels, usually two or three, reflects the number of different values the output voltage can take when referred to the middle point of the DC-link. For instance in the three-level NPC the possible voltage potentials are V_{in+} , V_{in-} and V_n . There is a number of technical advantages in using a three-level inverter over the two-level inverter [34]:

- The three-level inverter requires half the normal switching frequency then the two-level to achieve a clean output signal. This one is closely related to the topic of this thesis because there is a direct dependency between switching frequency and harmonic content.
- Lower rating IGBT modules in terms of voltage may be used.
- In cases when an output filter is used, this would be cheaper, due to the smaller size of components.
- Due to the smaller output voltage steps in the three-level inverter, it helps to resolve potential application problems such as those existing in motor supply when there are long cables between the inverter and the motor.
- The PV application efficiency improves because leakage currents are minimized

All these functional advantages make the NPC inverter suitable in grid-connected photovoltaic systems. Hence, the three-phase DC-AC inverter which is used in the thesis is a three-phase, three-level neutral-point-clamped inverter, shown schematically in *Figure 5.5*. It may be argued that such a topology may be equivalently modelled by substituting every stage of power inverter with a single phase NPC inverter.

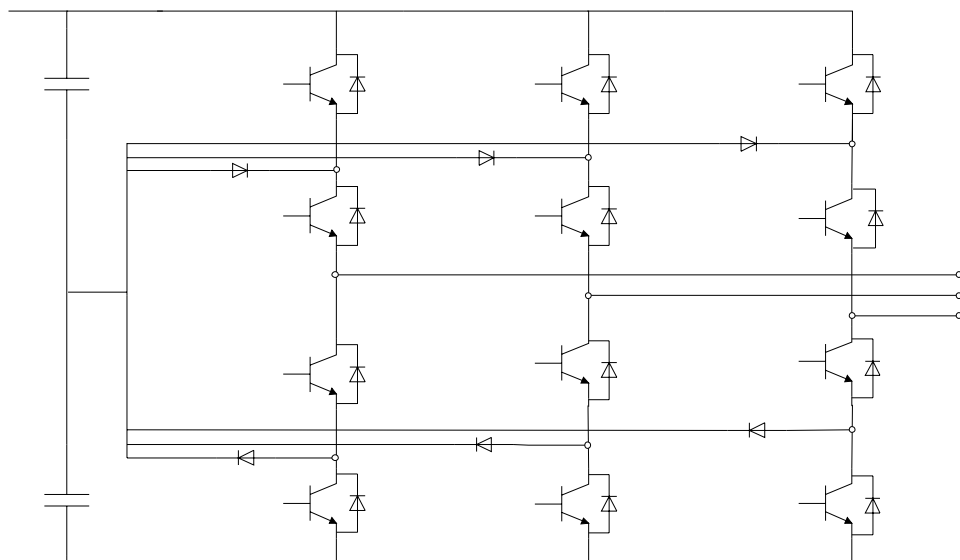


Figure 5.5. 3-level three phase NPC inverter.

5.5. Control of a grid-connected inverter

In renewable energy systems the main goal of the grid-connected inverter's control system is to enable maximum power output extraction. A block diagram for the inverter control system is depicted in *Figure 5.6*.

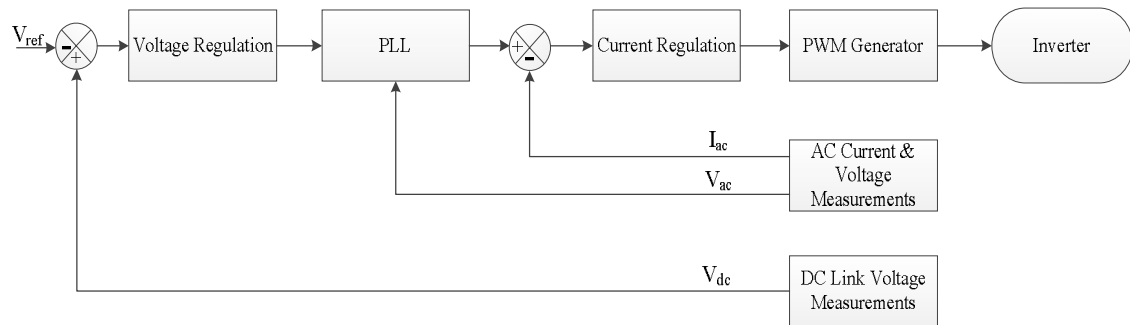


Figure 5.6. Control diagram for the inverter.

Due to the fact that the grid is operating at a particular voltage and frequency, it is important to synchronize the operation of the inverter to that of the grid. Therefore it is important to measure the grid voltage in *abc* coordinates at the PCC and to pass it through the phase lock loop, which generates a synchronized phase angle. In addition the input power losses should be minimized by regulating the DC-link voltage using feedback control. The current control regulation is designed in order to achieve maximum power injection into the grid.

The main challenge for the control of a three phase power system is that it is harder to manage the sampling and control of the three-phase sinusoidal signals. Such a process requires the use of suitable transformations to transform between reference frames. There are at least three different reference frames that can be used for grid-connected inverter controlling purposes, namely the natural frame, the stationary frame and the synchronous frame. The approach adopted in this thesis is the synchronous frame, also known as *dq0*-frame. For additional information on the control methods for grid-connected inverter please refer to [25], [35].

The natural or *abc* frame corresponds to the standard operation of the three-phase system. Transformation from the *abc* frame to the stationary *αβ0* frame, suggests that the three-phase system is transformed onto an orthogonal two-phase system, where *α* and *β* axes have an angle difference of ninety electrical degrees. The transformation to a rotating synchronous reference frame, also called Park's transformation, results in the *d* and *q* components which are akin to DC values in steady-state conditions. The *abc* to *dq0* Park's transformation in a rotating reference frame is presented in *Figure 5.7*.

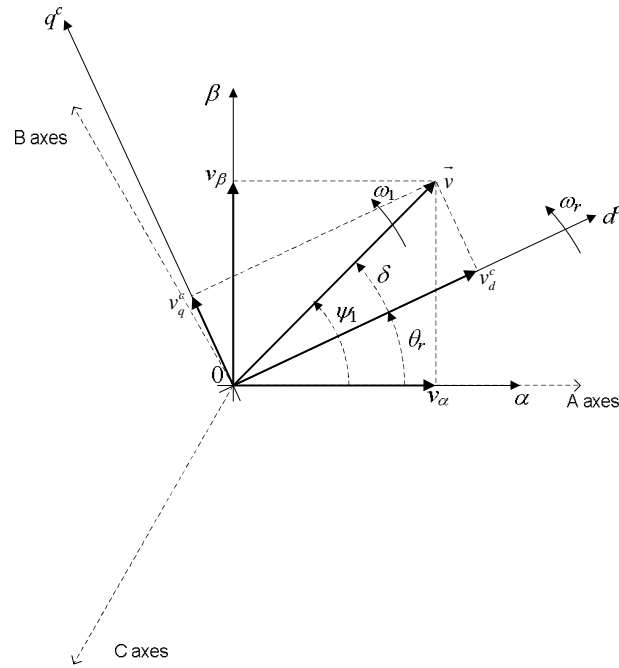


Figure 5.7. Reference frame transformation diagram.

A general synchronous reference control system for the inverter is shown in *Figure 5.8*. The control system performs a transformation from the natural frame to the synchronous frame and then it performs backward transformation to the natural reference frame, which can be fed into the PWM generator. As discussed previously the signals produced by the dq transformation are DC-like signals; therefore for regulating purposes, the PI controllers can be used. It is important to emphasize that any cross-coupling produced by dq transformations ought to be removed.

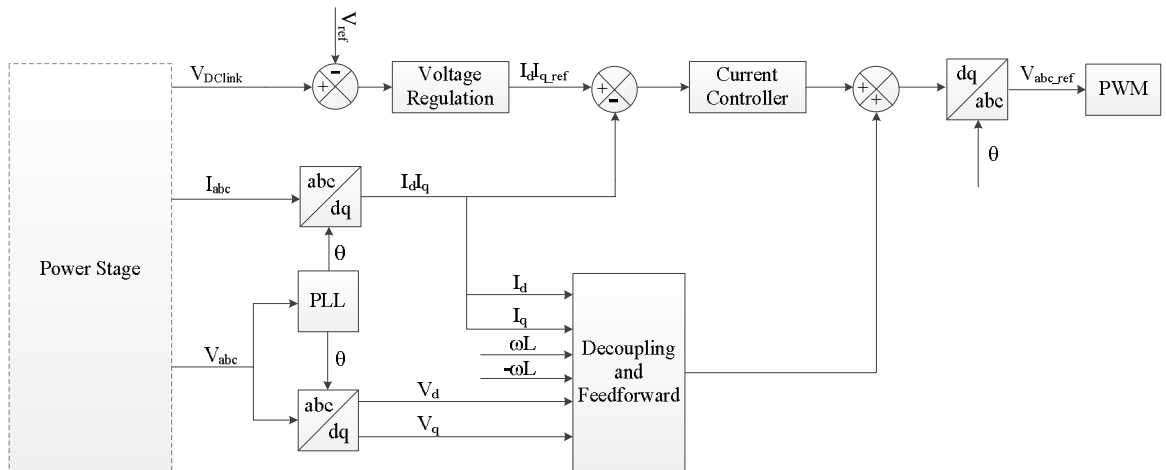


Figure 5.8. Control diagram using the synchronous reference frame.

5.6. Filter design considerations

This section presents the filter design guidelines for the grid-connected PV inverter simulated in this thesis. As discussed earlier the VSC and CSC is poised to become one of the main potential sources of harmonic distortion in the power grid. The filter at the AC side of the VSC and CSC is installed in order to minimise its current and voltage harmonic injections. Arguably, the most popular filter topologies are: L, LC and LCL. According to [36], [37], [38], LCL filters yield better harmonic filtering and ripple reduction owing to their third-order, low-pass filter characteristics. They also require smaller size components. Hence, the inverter filter topology which has been selected to use in the thesis is the LCL filter shown schematically in *Figure 5.9*. The main design rules regarding filter component selection is provided below; all this on the basis of the research findings presented in [39].

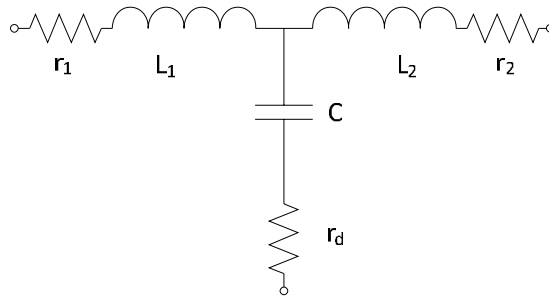


Figure 5.9. Single-phase model of the LCL filter.

5.6.1. Calculation of base values

In order to obtain the parameters for the LCL filter, the base values of the system should be specified. The calculation of per-unit values of impedance, inductance and capacitance are defined as:

$$Z_{base} = \frac{V_{base}^2}{S_{base}} = \frac{V_{base}}{\sqrt{3} \cdot I_{base}} \quad (5.2)$$

$$L_{base} = \frac{Z_{base}}{\omega_{base}} \quad (5.3)$$

$$C_{base} = \frac{1}{\omega_{base} \cdot Z_{base}} \quad (5.4)$$

where V_{base} is line-to-line RMS voltage, ω_{base} is the grid angular frequency, S_{base} is the nominal apparent power of the converter and I_{base} is the line-to-line RMS current.

5.6.2. Filter design rules and restrictions

Several key issues regarding filter design and component selection are considered below, such as:

- resonant frequency
- capacitor limitations
- value of inductances
- damping resistor selection

The resonant frequency of the LCL filter may significantly amplify the negative effect of harmonics in the power circuit and increase overshoots during transient responses. In order to eliminate the possible negative effect of resonances while keeping the controller design simple, the resonant frequency should be within the range [40]:

$$10 \cdot \omega_{base} \leq \omega_0 \leq \frac{\omega_{SW}}{2} \quad (5.5)$$

where ω_{base} is the fundamental angular frequency of the grid and ω_{SW} is the inverter angular switching frequency.

The capacitor value should not be too high because it might result in an overall decrease of filter impedance, which in turn will increase the magnitude of the current flowing through the inductance on the inverter side L_1 , with respect to the inductance at the network side L_2 . Such a phenomena will result in the increase of reactive power generation and a reduction of the active power that can be delivered by the PV-generation unit to the grid [41]. In order to avoid this problem the value of the capacitor must meet the following requirements:

$$C_0 \leq 0.1 \cdot C_{base} \quad (5.6)$$

The main consideration for the filter inductance design is that it should not be very high, because it may result in significant power losses and significant voltage drops. Also it is recommended to set the value of the network side inductance to be lower than the inverter side inductance in order to eliminate possible instabilities in the control system. Quite often PV inverters are connected to the AC grid through a step-up transformer. In such a case the leakage inductance of the transformer should be taken into account when selecting the grid-side inductance L_2 . The following restrictions should be observed when sizing L_1 and L_2 :

$$L_1 + L_2 \leq 0.3 \cdot L_{base} \quad (5.7)$$

$$L_1 = 1.5 \cdot L_2 \quad (5.8)$$

The value of the damping resistance should be high enough to eliminate the oscillations caused by filter resonances [42]. However, too high a value may increase the power losses. The damping resistance may be sized according to the requirement [43]:

$$R_d = \frac{1}{3\omega_0 \cdot C_0} \quad (5.9)$$

5.6.3. Filter design calculation

Table 5.1 describes the parameters of the grid-connected PV inverter, to be used in the test system in Chapter 6.

Table 5.1. Parameters for the grid-connected inverter.

Parameter	Value
Nominal power, S_{base}	235 kW
DC-link voltage, V_{dc}	580 V
Line to line rms voltage, V_{base}	300 V
Frequency of the system, f_1	60 Hz
Switching frequency, f_s	1980 Hz
Transformer leakage inductance, L_2	0.122 mH
Transformer leakage impedance, R_2	0.0015 Ω

As stated in the previous section, the leakage inductance and impedance of the transformer should be taken into account when selecting the parameters of the LCL filter. Hence, the transformer inductance is assumed to be the grid-side inductance L_2 of the filter. The parameters of the LCL filter are presented in Table 5.2:

Table 5.2. Parameters for the LCL filter.

LCL filter parameter	Value
Converter-side inductance, L_1	0.183 mH
Converter-side resistance, R_1	0.0023 Ω
Grid-side inductance, L_2	0.122 mH
Grid-side resistance, R_2	0.0019 Ω
Capacitance, C_o	677 μ F
Resonant frequency, f_0	715 Hz
Damping resistance, R_d	0.1083 Ω

Employing this configuration of LCL filter yields highly sinusoidal currents and voltages. The line current and the phase-to-phase voltage of the converter are presented in Figure 5.10. In this particular case the PV inverter is connected to the AC power grid through a step-up transformer; therefore the LCL filter was modelled in such a way that the transformer leakage inductance and resistance act as the grid-side inductance L_2 and the grid-side impedance R_2 . In addition the converter-side resistance R_1 is estimated by considering a quality factor Q section of 30, which is a realistic value.

$$Q = \frac{\omega_{base} \cdot L_1}{R_1} \quad (5.10)$$

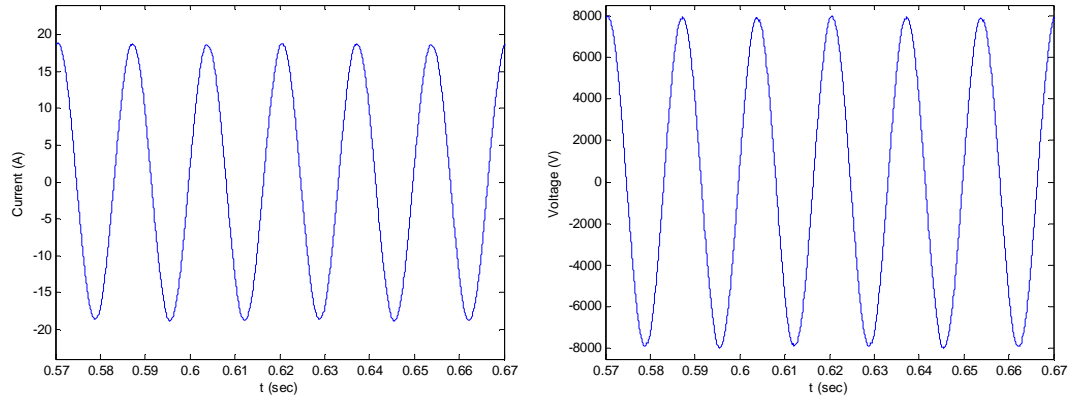


Figure 5.10. Line current and phase-to-phase voltage of a three-level NPC inverter.

The damping resistance is a rather important element of the LCL filter since it eliminates the oscillations caused by resonances in the filter. The bode diagram presented in *Figure 5.11* shows the effect of the damping resistance on the transfer function characteristic of the LCL filter. The corresponding transfer functions of the LCL filter without damping $G(S)_1$ and with damping $G(S)_2$ are given by (5.11) and (5.12), respectively.

$$G(S)_1 = \frac{1}{L_1 L_2 C_0 s^3 + C_0 (L_1 R_2 + L_2 R_1) s^2 + (L_1 + L_2 + R_1 R_2 C_0) s + R_1 + R_2} \quad (5.11)$$

$$G(S)_2 = \frac{1 + C_0 R_d S}{L_1 L_2 C_0 s^3 + C_0 (L_1 (R_2 + R_d) + L_2 (R_1 + R_d)) s^2 + (L_1 + L_2 + C_0 (R_1 R_2 + R_d (R_1 + R_2))) s + R_1 + R_2} \quad (5.12)$$

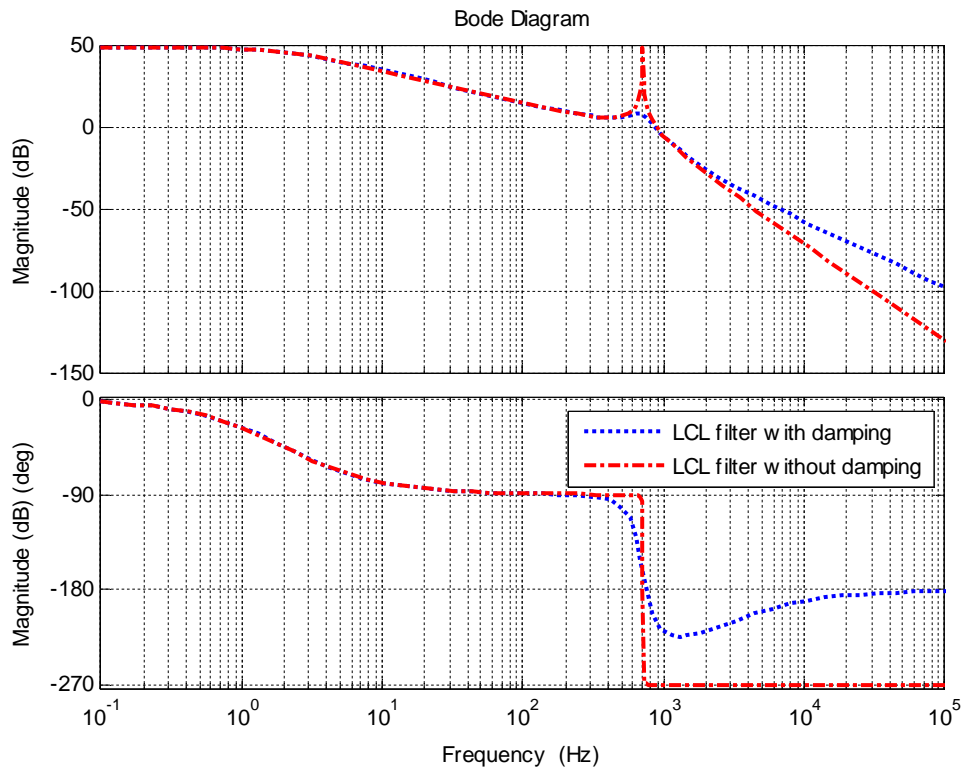


Figure 5.11. Transfer function of the LCL filter with and without damping.

5.7. Summary

This chapter provided an overview of switched-mode DC-AC inverters. The main focus was on the analysis of grid-connected PV inverters. Control methods of renewable energy systems were analysed with emphasis on grid-parallel mode of operation in a synchronous reference frame. In addition, simple and yet an effective design procedure for the inverter output filter was put forward. The analysis provides a parameter design method of the LCL filter, showing the resonance suppression method using damping resistors.

6. SIMULATION RESULTS

6.1. Distribution network model

The main aim of the research reported in this thesis is to investigate the impact of current harmonics generated by distributed photovoltaic systems connected to a medium-voltage network. The basis for this simulation is the distribution network shown on *Figure 6.1*. It is a typical distribution system of the kind found in the North of England. The transmission lines are in fact underground cables. For the purpose of the simulation studies, the reference is node 1 where the infeed transformer connects to, which is represented by a three-phase voltage source. Technical specifications for the cables as well as system loading data are given in Appendix A.

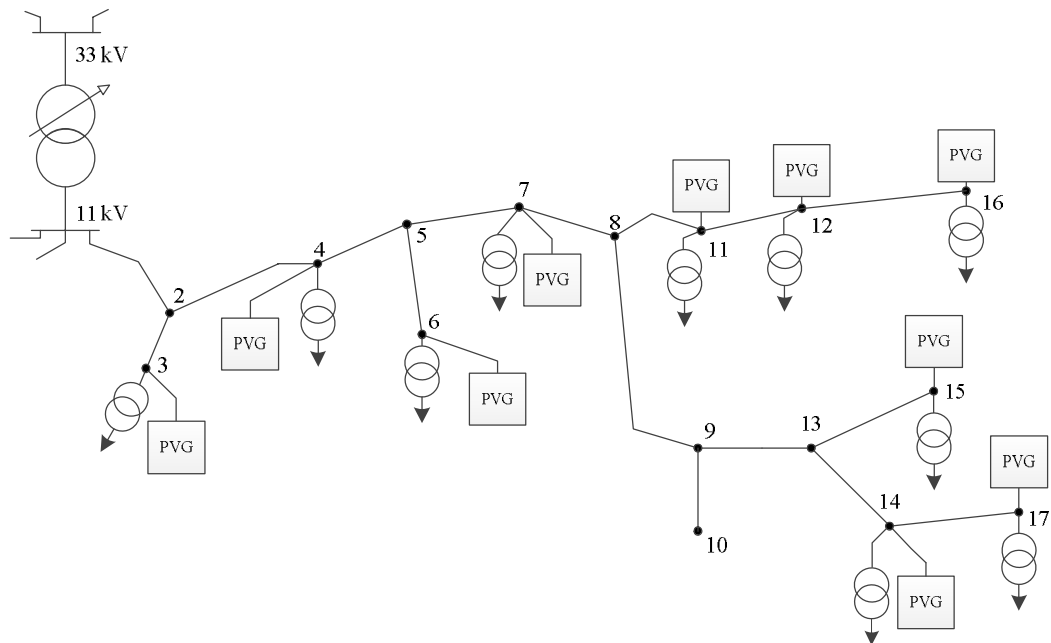


Figure 6.1. Distribution system.

The solar panel modules assumed to be connected to the various nodes of this distribution system for simulation purposes is the SUNPOWER SPR 220. The configuration of the PV generators together with the specifications of the solar modules for standard test conditions of 25°C temperature, spectrum of 1.5 air mass and irradiance of 1000 W/m², are given in Appendix B.

A photovoltaic generator or PV energy conversion system includes solar panels connected in a series/parallel array, a DC-DC switched-mode converter, a DC-AC inverter and LCL filters. It is connected to the grid via a step-up transformer. The topolo-

gy of the DC-DC converter is of the boost type with an MPPT controller, namely, Perturb and Observe controller. Two simulations were conducted, using a single PV system so that the Perturb and Observe control method and the Incremental Conductance plus Integral regulator could be compared. The results show that current harmonic emissions were the same in both cases, therefore, the Perturb and Observe method was chosen for the purpose of this research since it carries less computational burden than the Incremental Conductance plus Integral regulator method. The DC-AC inverter is designed to operate in a grid-parallel mode, thus enabling maximum power injection and synchronization to the power grid operating voltage and frequency, where the grid-current is the inner loop and the DC-link voltage provides the feedback for the grid-current loop as shown in *Figure 5.8*. In addition, it is important to mention that the results presented in the thesis are only valid for irradiance levels up to 1000 W/m². The design of the system may require some parameter tuning for irradiance levels higher than the nominal.

6.2. Simulation results of a single PV array

The Fast Fourier Transform (FFT) algorithm is used in this chapter to extract the harmonic content from the PV voltage and current waveforms. This facility is readily available within the Powergui environment block for SimPowerSystems models. It is important to notice that in this work the FFT is set to calculate the frequencies at every 1 Hz, hence, the ensuing frequency spectrums will show not only the harmonic terms but also all the interharmonic terms. The first part of the simulations concentrates on the analysis of a single PV system feeding into a load point via a connecting transformer. The main motivation behind this experiment is to gain insight into the different factors that affect the harmonic generation of a single PV array. The configuration setup of the PV generator is directly taken from the PV generator connected to node 11 of the power grid presented in *Figure 6.1*. The factors taken into account are changes in irradiance, changes in the inverter switching frequency, load unbalances, resonances in RLC-type loads, single-phase open-circuit faults in LCL filters and LCL filter deterioration. The simulation results under normal operating conditions, i.e. irradiance of 1000 W/m², temperature of 25°C, inverter switching frequency of 1980 Hz (33rd harmonic) and the associated filters in good working order, show quite a low level of THD, producing an almost sinusoidal output current signal as shown in *Figure 6.2*. Additional results regarding the harmonic spectrum at different stages of the PV system, such as harmonic spectrums at the output of the PV panel and DC-DC converter, are presented in Appendix C. The harmonic analysis at the output of the PV panel shows the presence of harmonics at 5000 Hz which is the switching frequency of the DC-DC converter. In addition, some small harmonics are present at near the fundamental frequency. The harmonic spectrum at the output of the DC-DC converter shows a more prominent harmonic emission happening at multiples of the switching frequency of the converter with intervals of 20 harmonics.

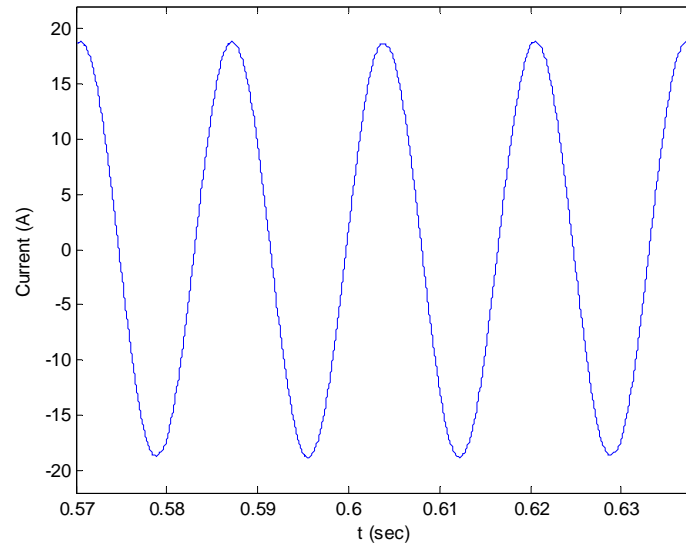


Figure 6.2. Single phase output current at the PCC.

Table 6.1. Harmonic analysis of a single PVG under normal operating conditions.

Harmonic order	Current magnitude (%)
3 rd	0.09
5 th	0.18
7 th	0.12
9 th	0.06
11 th	0.14
13 th	0.09
15 th	0.02
17 th	0.10
19 th	0.08
21 st	0.00
23 rd	0.10
25 th	0.13
27 th	0.00
29 th	0.42
31 st	0.15
33 rd	0.01
35 th	0.10
37 th	0.21
Total THD	0.81

The data presented in *Table 6.1* shows that the total harmonic emissions produced by a single PV array are much lower than the limits set by the IEEE 929 standard. The THD carries a value of 0.81%. However individual high order harmonic are of some concern, especially the 29th, 31st, 35th and 37th. Therefore these high order harmonics

will be analyzed in further experiments in order to investigate whether or not changes in operating conditions can cause these high order harmonics to exceed the limits set by IEEE standards.

The reason for the existence of these high order harmonics is due to the fundamental properties of the operation of DC-AC inverters. According to Mohan et. al. (2003) the harmonics produced by the inverter appear as multiples of the switching frequency and appear as sidebands [27]. It is stated that the harmonic order at which these harmonic appear obey the formula:

$$h = j(m_f) \pm k \quad (6.1)$$

where h is the harmonic order, k is the sideband of j times the frequency modulation ratio. It should be noted that when j is an even value, harmonics exist only for odd value of k . Conversely, when j is an odd value, harmonics exist only for even value of k . The frequency f_h at which harmonic appears can be computed as:

$$f_h = (jm_f \pm k)f_1 \quad (6.2)$$

Such a characteristic of the switched-mode DC-AC inverters is further investigated by looking at the impact of different switching frequencies on the current harmonic emissions. *Table 6.2* presents evidence that selection of the switching frequency is an important factor in designing PV inverters, since the switching frequency is directly proportional to current harmonic generation.

Table 6.2. Simulation results under different inverter switching frequency.

Inverter switching frequency	Current THD (%)	Highest harmonics (%)			
		41 st	43 rd	47 th	49 th
2700 Hz	0.78	0.15	0.06	0.04	0.09
		0.24	0.09	0.06	0.13
2340 Hz	1.20	0.42	0.15	0.10	0.21
		0.82	0.27	0.17	0.34
1980 Hz	0.81	1.83	0.52	0.32	0.62
		3.65	0.81	0.51	1.29
1620 Hz	1.23	1.7 th	19 th	23 rd	25 th
		29 th	31 st	35 th	37 th
1260 Hz	2.41	11 th	13 th	17 th	19 th
		23 rd	25 th	29 th	31 st
900 Hz	4.57	0.82	0.27	0.17	0.34
		0.42	0.15	0.10	0.21

Moreover, unsuitable selection of the switching frequency may yield interharmonic generation close to the fundamental frequency, which will result in THD increases. Data

on the interharmonic generation is shown in *Table 6.3*. The appearance of interharmonics is an intriguing problem which ought to be investigated. Aiming at gaining some insight the switching frequency of the inverter is set to be equal to the switching frequency of the switched-mode DC-DC converter. It is noticed that this action reduces the presence of the interharmonics very considerable but that there is no total elimination of these frequency terms. It calls to attention these very low value of a wide range of frequencies throughout the spectrum shown and one wonders at this stage if these maybe actual frequency terms or only numerical noise incurred by the FFT algorithm available within the Powergui. This matter is investigated further in the following section. Nevertheless and beyond the persistence of these low values of interharmonic it is important to notice that the intermodulation of the two different switching frequencies employed in the DC-DC and DC-AC converters play a major role in amplifying the low frequency interharmonic terms. However, it should be remarked that such a high switching frequency for the DC/AC power inverter is not practical because of high switching losses accrued and this exercise was carried out more as a matter of some academic interest.

Table 6.3. Value of interharmonics at different switching frequencies.

Harmonic content	Inverter switching frequency (Hz)					
	5000	2700	2340	1980	1620	900
20 Hz	0.01	0.13	0.04	0.05	0.09	0.29
100 Hz	0.03	0.08	0.16	0.01	0.06	0.08
140 Hz	0.00	0.07	0.07	0.04	0.04	0.12
220 Hz	0.01	0.00	0.05	0.04	0.01	0.04
260 Hz	0.01	0.01	0.07	0.02	0.04	0.08
340 Hz	0.00	0.03	0.03	0.00	0.02	0.06
380 Hz	0.01	0.03	0.04	0.03	0.05	0.10
Total interharmonic value	0.15	0.46	0.54	0.33	0.44	1.05

Note: Values for interharmonics are provided in amperes (A)

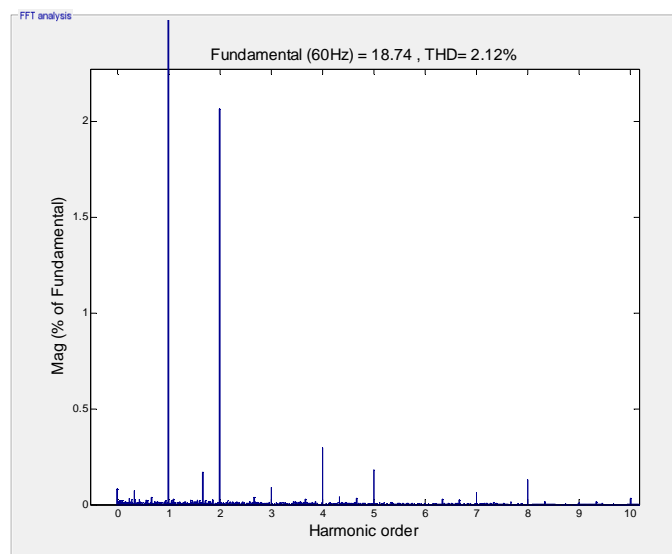


Figure 6.3. Harmonic spectrum of the PV generator when $f_s = 5000$ Hz.

6.2.1. Analysis of the Powergui FFT tool

The results presented in Section 6.2 point out the existence of interharmonics incurred by the operation of power electronics converters. It was stated that at first thought it was difficult to assess whether or not these terms were in fact very low values of interharmonics or only numerical noise incurred by the FFT algorithm available within the Powergui. In order to investigate this matter further an experiment was conducted using a three-phase controllable voltage source available within the Simscape environment. This block allows the selection of two harmonic terms to be superimposed on to the fundamental voltage, i.e. a programmable voltage source with any two selected harmonics. The selected frequencies were the 180 Hz 300 Hz with magnitudes of 0.15 pu and 0.20 pu, respectively. The source is connected to a three-phase RL load. The resulting harmonic spectrum of the system is shown in *Figure 6.4*.

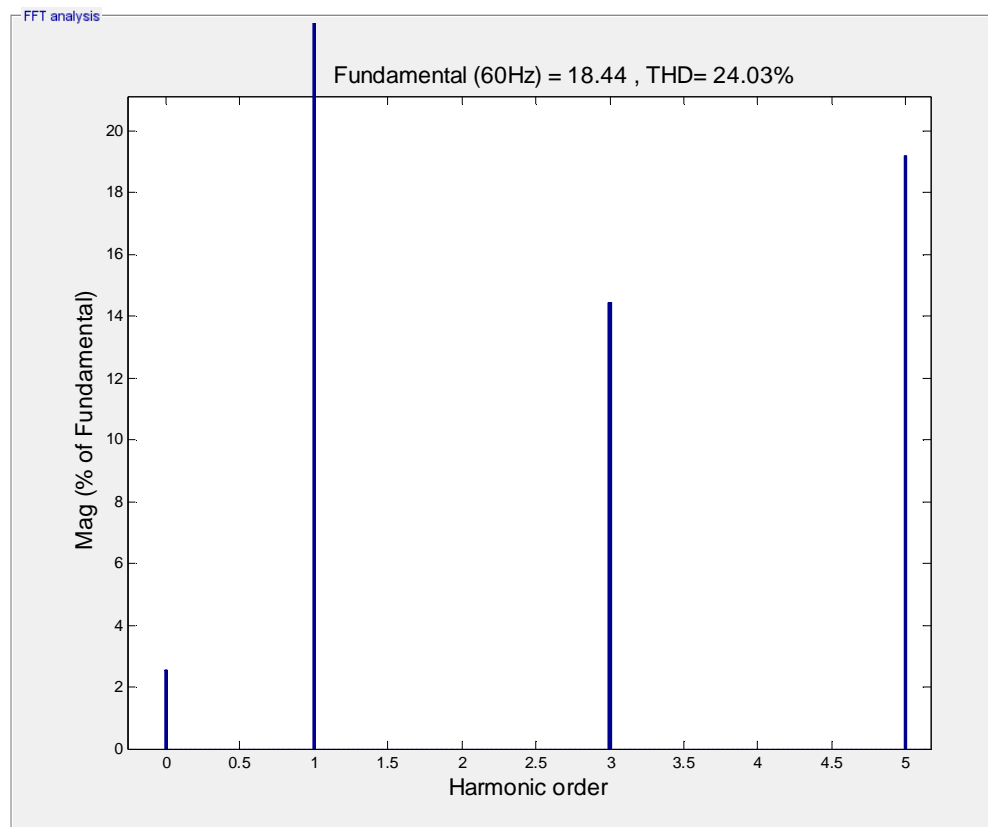


Figure 6.4. Harmonic spectrum of the test system.

Apart from a 2.5% value of DC term owing to the fact that the waveform is not yet at its true periodic steady-state, the resulting harmonic spectrum shows that the Powergui FFT tool does not produce noise, a fact that it is reassuring in itself but leaves with the difficult task to define the origin of the small interharmonics presented in *Figure 6.3*. It should be pointed out that other researchers have observed the similar problems [44].

6.2.2. Effect of irradiance levels on the THD

The experimental results provided in this section present the impact of solar irradiance conditions on the harmonic generation of the PV system. It is important to mention that no partial shading phenomena is considered as a part of this research. *Table 6.4* gives values of harmonics for different irradiances reaching the surface of the PV panel. It can be seen that irradiance decreases result in THD increases but they are kept always below the 5% limit set by the IEEE 929 standard. Also, individual harmonic terms increase with low levels of solar irradiance and some of these terms go above the limits set by the standard.

Table 6.4. Simulation results under different irradiance levels.

<i>Different irradiance levels</i>	Current THD (%)	29 th (%)	31 st (%)	35 th (%)	37 th (%)
1000 W/m ²	0.81	0.42	0.15	0.10	0.21
500 W/m ²	1.48	0.77	0.47	0.33	0.37
200 W/m ²	3.65	1.82	1.50	1.04	0.87

Such anomalous power quality indexes may be explained partly because of the definition available for the calculation of current THD (1.5) as presented in *Table 6.5*. It can be observed that the harmonic values remains fairly constant throughout the simulations but the fundamental component decreases significantly with decreasing irradiance levels. As stated in Chapter 1, there is at present no specific guidelines provided by IEEE concerning interharmonics but it may be seen from the analysis that their levels remain fairly constant throughout the various irradiance levels.

Table 6.5. Harmonic analysis under different irradiance levels.

<i>Irradiance levels</i>	Fundamental component	Harmonic values excluding fundamental component and interharmonics	Interharmonics value
1000 W/m ²	18.77 A	0.40 A	0.33 A
500 W/m ²	9.637 A	0.41 A	0.31 A
200 W/m ²	3.864 A	0.41 A	0.25 A

High harmonics generation at low irradiance levels have also been reported in [45]. The authors state that THD in three-phase VSC and CSC can be represented as a function of the modulation index M , as shown in *Figure 6.5*.

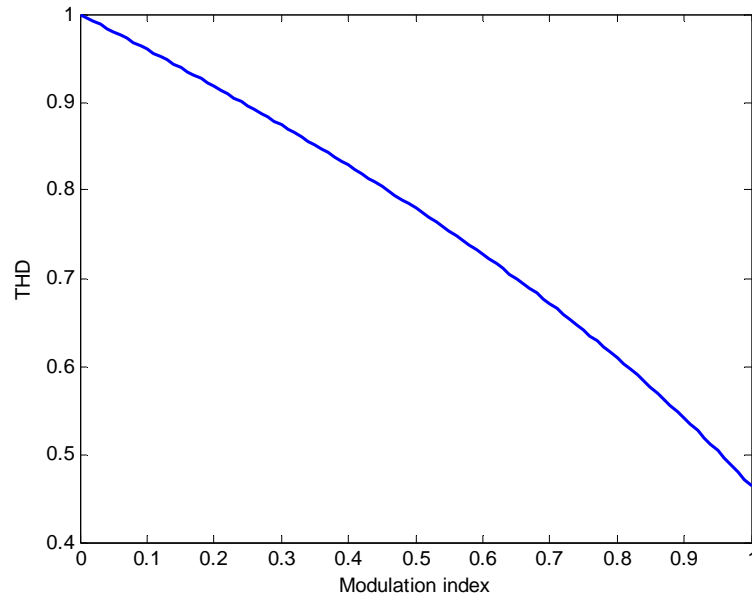


Figure 6.5. THD for a VSC and CSC as a function of modulation index (adapted from 45).

6.2.3. Impact of the operating conditions of LCL filters

In real-life situations it is quite often the case that filters are not operating properly due to incipient faults of various degrees of severity, as a result of aging filter components. Therefore this part of the simulations concentrates on the analysis of the impact of components deterioration of LCL filters. The simulation results are shown in *Table 6.6*.

Table 6.6. Simulation results under different operating conditions of LCL filter.

<i>Deterioration of LCL filter</i>	Current THD (%)	29 th (%)	31 st (%)	35 th (%)	37 th (%)
10% deterioration in converter side inductance L_1	0.96	0.47	0.17	0.12	0.23
10% deterioration in C filter	0.86	0.48	0.17	0.12	0.23
Overall 10% deterioration of filter components	1.00	0.54	0.20	0.14	0.26

It is concluded that in cases of suitable filter designs, filter component deterioration of the kind investigated in the section, do not have a significant adverse impact on harmonic emissions. To put these results in context, *Figure 6.6* shows the harmonic spectrum of the PV generator at PCC without filtering system at the switching frequency of 1980 Hz and 5000 Hz. It is clearly seen that the absence of the output filter yields an exceedingly high THD, where interharmonics and high frequency harmonics are clearly visible. In contrast, harmonic spectrum presented in *Figure 6.7* shows the reduction of

interharmonic terms when the switching frequency of inverter and DC-DC converter is the same.

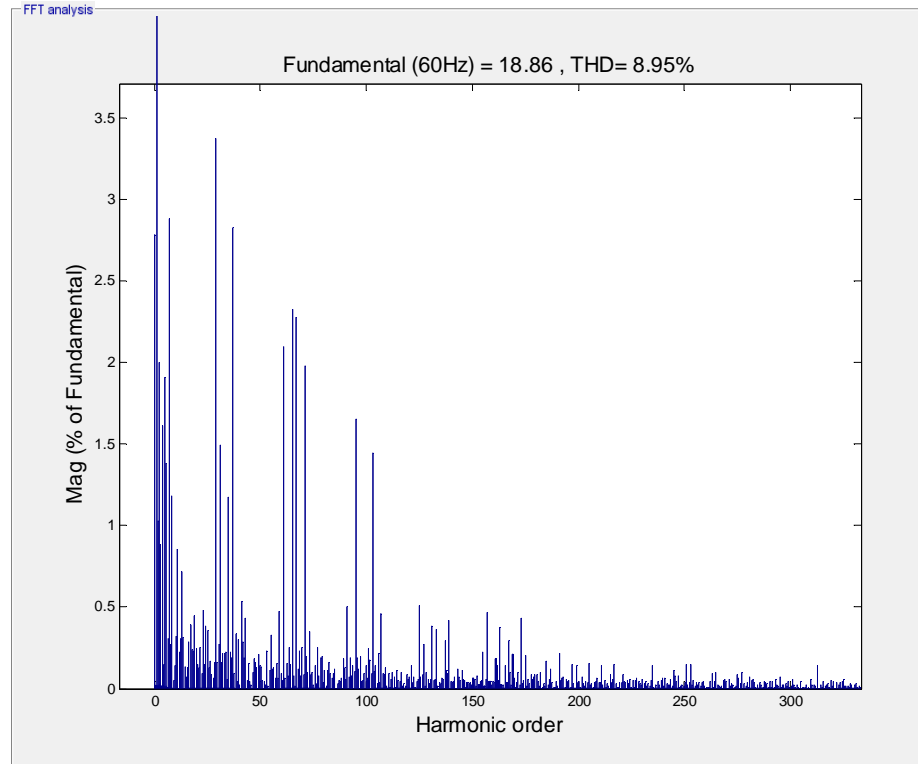


Figure 6.6. Harmonic spectrum of the PV generator without LCL filter ($f_s=1980$ Hz).

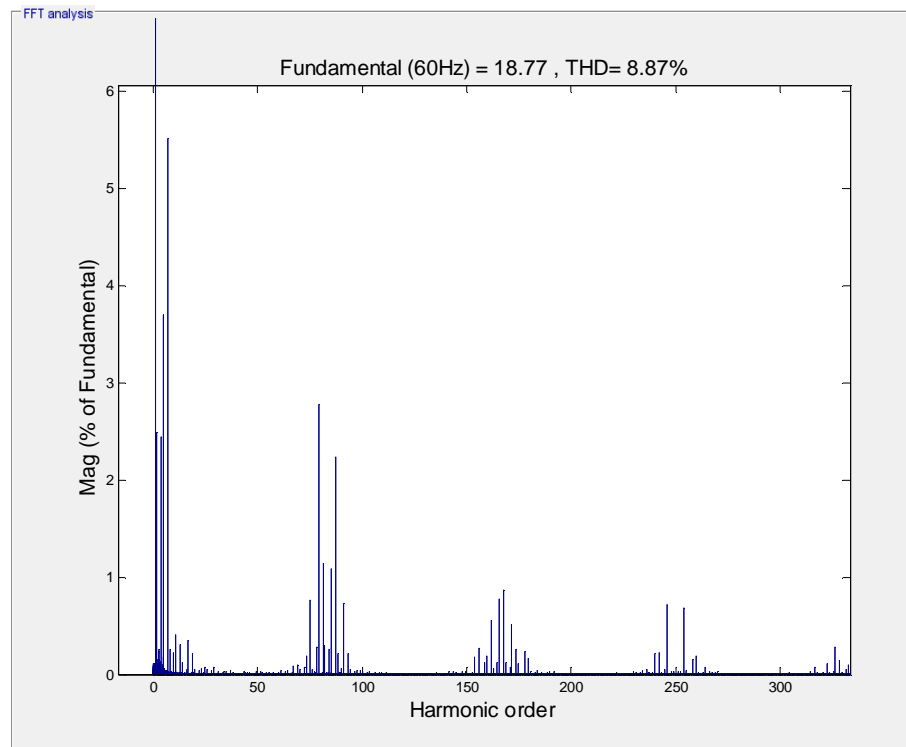


Figure 6.7. Harmonic spectrum of the PV generator without LCL filter ($f_s=5000$ Hz).

6.2.4. Impact of the open-circuit conditions of LCL filters

The set of simulations conducted in this part of the research is aimed at investigating the consequences of open-circuit conditions in components of the LCL filter. The results are presented in *Table 6.7*. It provides results on current harmonics for case of single-phase open-circuit faults in the LCL filter. It may be concluded that one phase open in an LCL filter does not result in a high THD. Three-phase voltage and current waveforms of both experiments are presented in *Figures 6.8-6.11*. As expected the results indicate that the opening of one phase of the series inductor-resistor yields rather unbalanced voltage and current waveforms, therefore, deteriorating the power quality of the distribution grid. On the other hand, the opening of one phase of the series shunt capacitor and damping resistor of the filter does not yield such an unbalanced situation but rather it causes some high frequency ripple in the waveforms.

Table 6.7. Impact of the open-circuit condition of LCL filter.

<i>Fault applied to LCL filter</i>	Current THD (%)	29 th (%)	31 st (%)	35 th (%)	37 th (%)
One phase fault in L ₁ filter	1.71	0.30	0.32	0.22	0.15
One phase fault in C filter	2.38	0.98	0.45	0.32	1.03

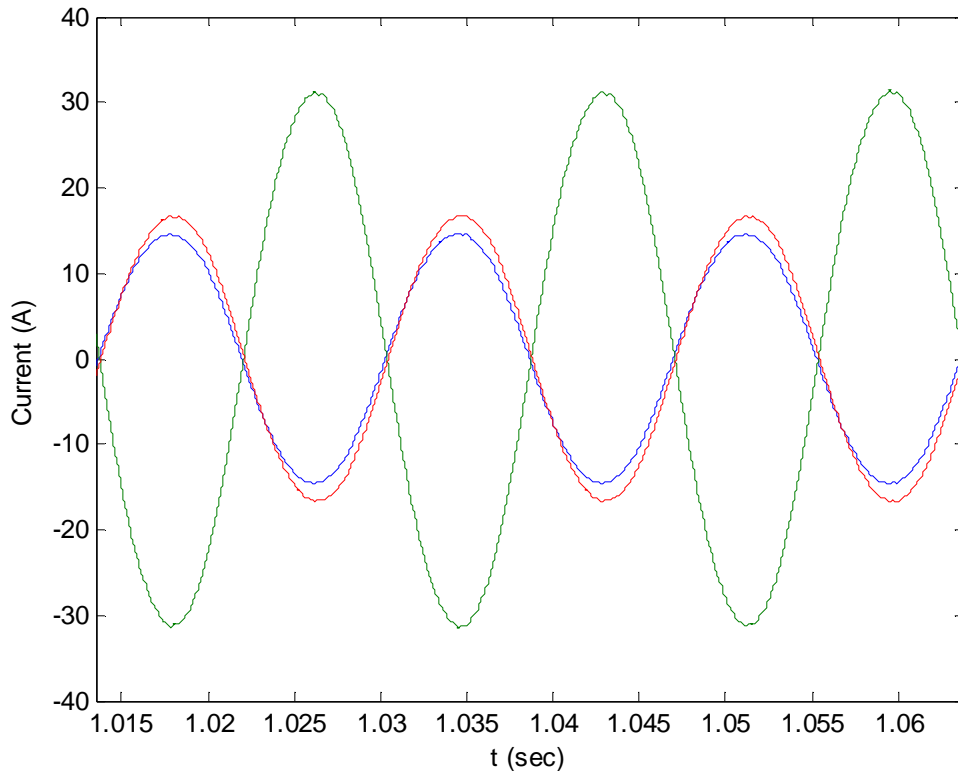


Figure 6.8. Three-phase current at the PCC in case of open-circuit condition of L filter.

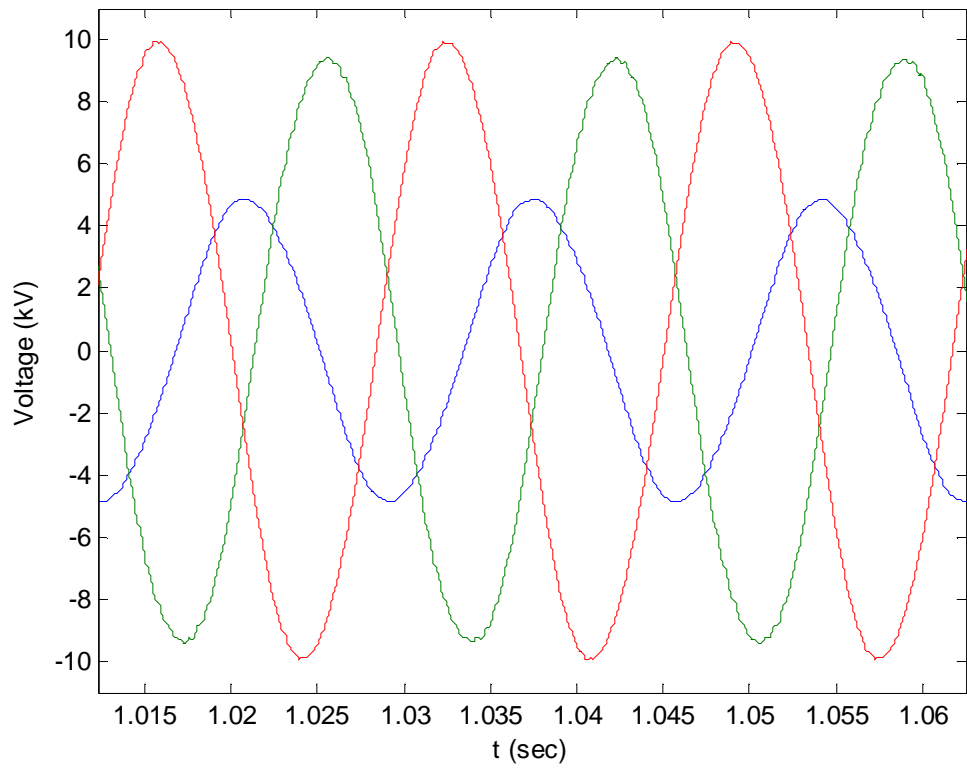


Figure 6.9. Three-phase voltage at the PCC in case of open-circuit condition of L filter.

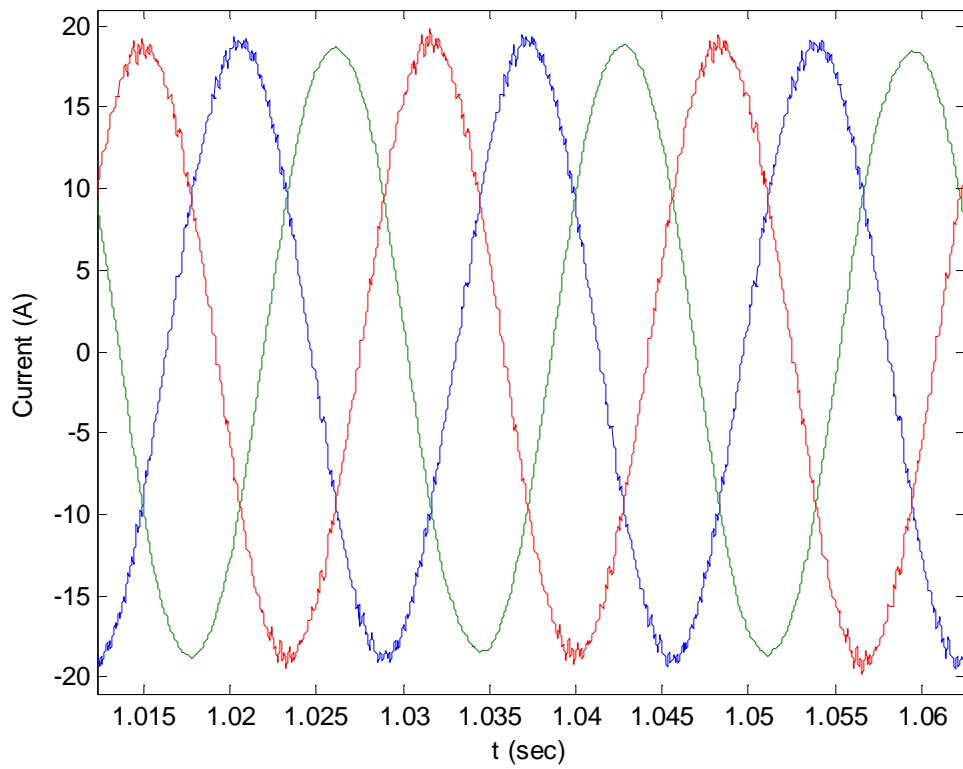


Figure 6.10. Three-phase current at the PCC in case of open-circuit condition of C filter.

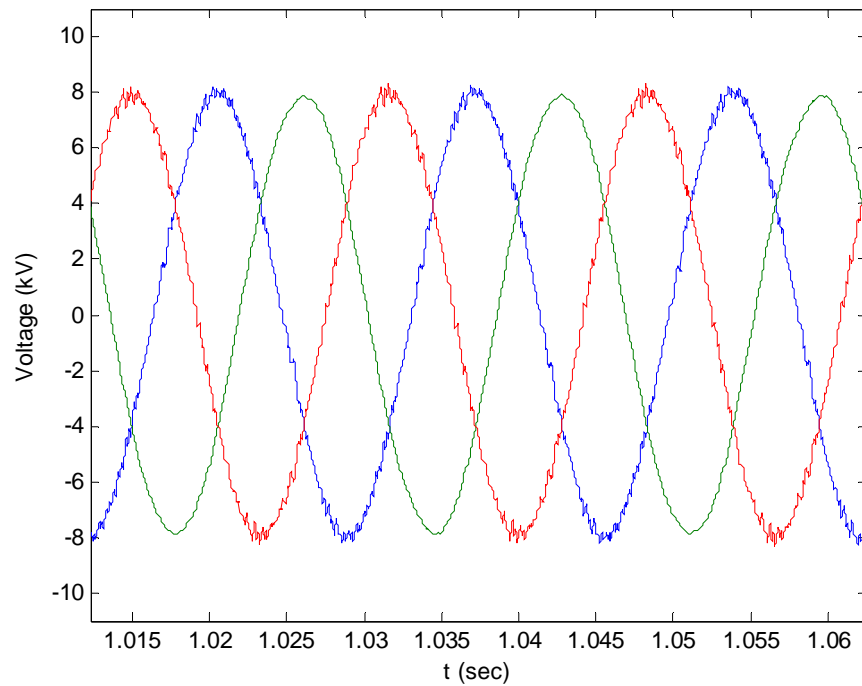


Figure 6.11. Three-phase voltage at the PCC in case of open-circuit condition of C filter.

6.2.5. Impact of the loading type and load unbalance on the THD

Actual power systems are three-phase and they do not have perfectly balanced loads. *Table 6.8* provides results on the impact of unbalanced load on the current harmonic generation of a single PV generator. According to the data provided, it can be concluded that unbalanced loading results in the increase of harmonic distortion, however, it does not exceed the limits stated by IEEE standards. In addition unbalances in the load do not have a significant impact on the individual harmonics. The increase of the THD is mainly due to the increase of low frequency harmonics and inter-harmonics.

Table 6.8. Effect of the unbalanced load on the THD.

Harmonic content	Type of unbalance in RL load			
	normal conditions	20% increase in one phase	20% decrease in one phase	20% increase in one phase and 20% decrease in one phase
20 Hz (%)	0.15	0.17	0.37	0.30
100 Hz (%)	0.14	0.20	0.47	0.15
3 rd (%)	0.09	0.67	1.14	1.64
29 th (%)	0.42	0.42	0.41	0.42
31 st (%)	0.15	0.18	0.11	0.12
35 th (%)	0.10	0.12	0.08	0.09
37 th (%)	0.21	0.20	0.20	0.20
THD (%)	0.81	1.04	1.41	1.82

6.2.6. Impact of resonance conditions on the THD

The results in this section relate to the case when the PV system feeds into a point of the network which exhibits a resonance at, say, the second harmonic. This is achieved by modelling the load point as an equivalent RLC branch as opposed to only RL, with appropriate values of R, L and C parameters. This part of the research investigates the cumulative effect of solar insolation levels and resonance conditions. The results are shown in *Table 6.9*, with the corresponding harmonic spectrums and current waveforms presented in *Figures 6.12-6.17*. It can be concluded that the existence of a resonance at a particular frequency induces a very significant increase of the harmonic magnitude at that frequency, causing large distortions in the current waveform. Moreover, at lower insolation levels due to the increased existence of low-order interharmonics; resonance shifts to other frequency occur as a result of frequency interaction. This is seen in *Figure 6.12, 6.14 and 6.16* where the gradual decrease of irradiance levels have the effect of increasing the values of interharmonics and, hence, with the interaction of interharmonics and the second harmonic, results in an overall spread of the frequency spectrum.

Table 6.9. Effect of the resonance in RLC load and irradiance on the THD

Different irradiance levels	Current THD (%)
1000 W/m ²	13.05
500 W/m ²	21.13
200 W/m ²	58.16

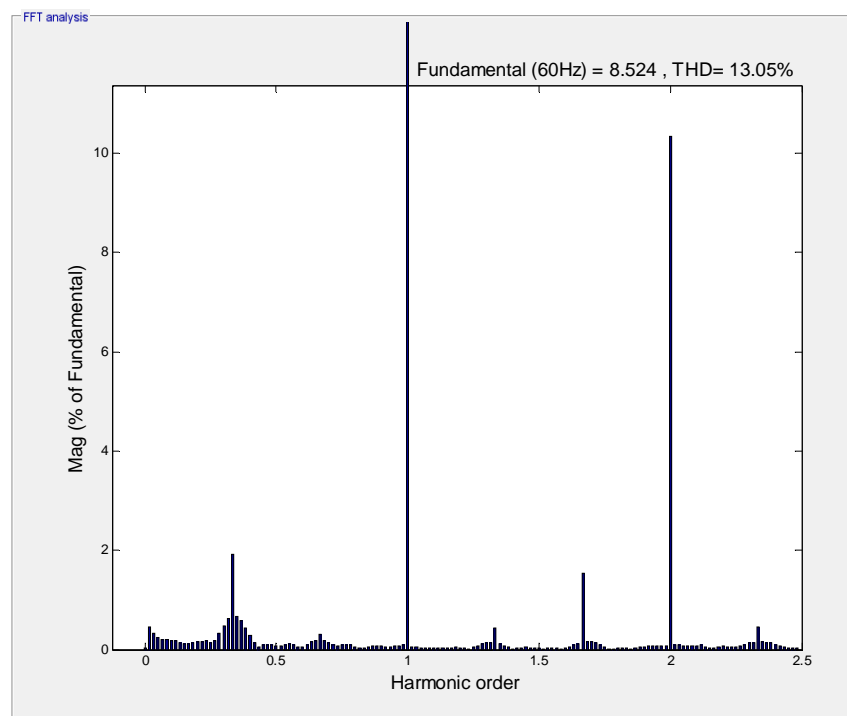


Figure 6.12. Harmonic spectrum of the current at PCC at 1000 W/m² irradiance.

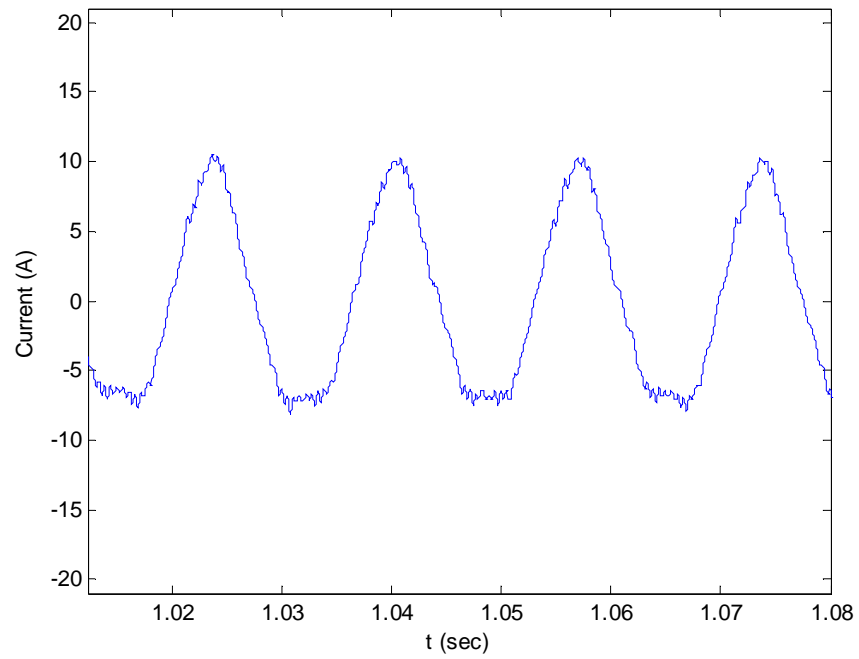


Figure 6.13. Single phase output current at the PCC at 1000 W/m^2 irradiance.

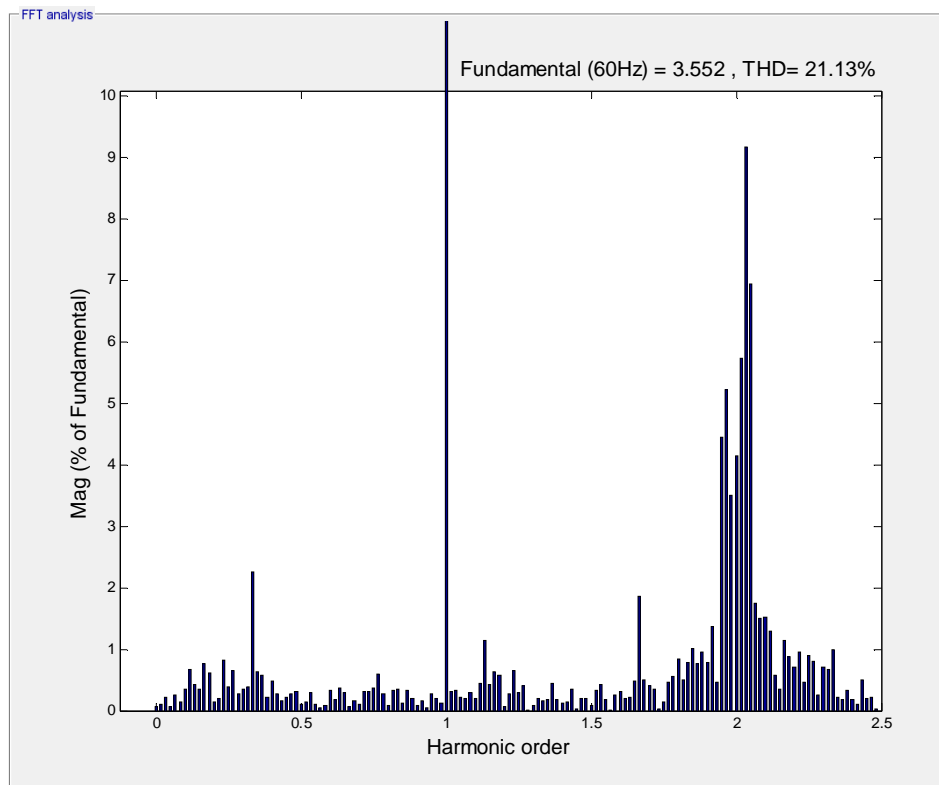


Figure 6.14. Harmonic spectrum of the current at PCC at 500 W/m^2 irradiance.

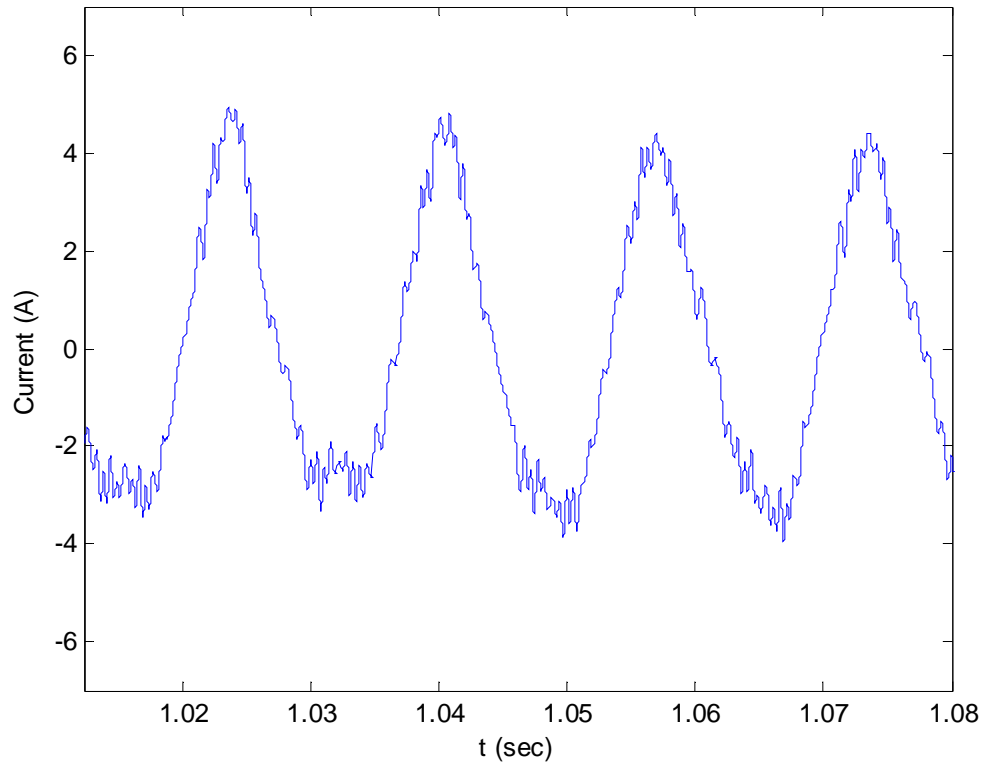


Figure 6.15. Single phase output current at the PCC at 500 W/m^2 irradiance.

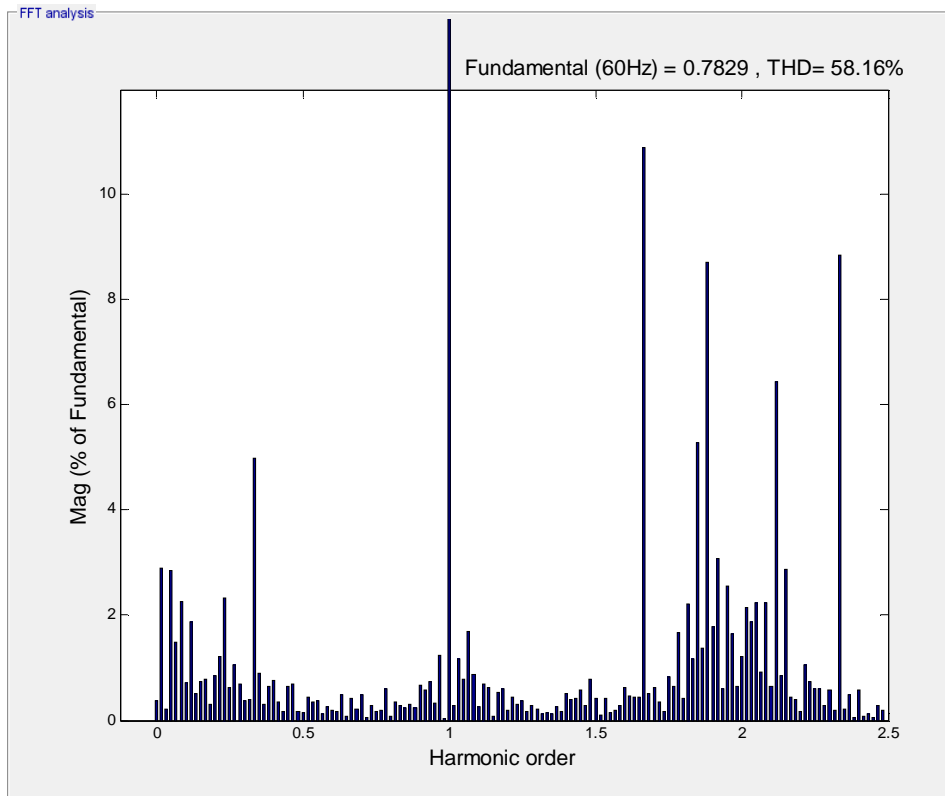


Figure 6.16. Harmonic spectrum of the current at PCC at 500 W/m^2 irradiance.

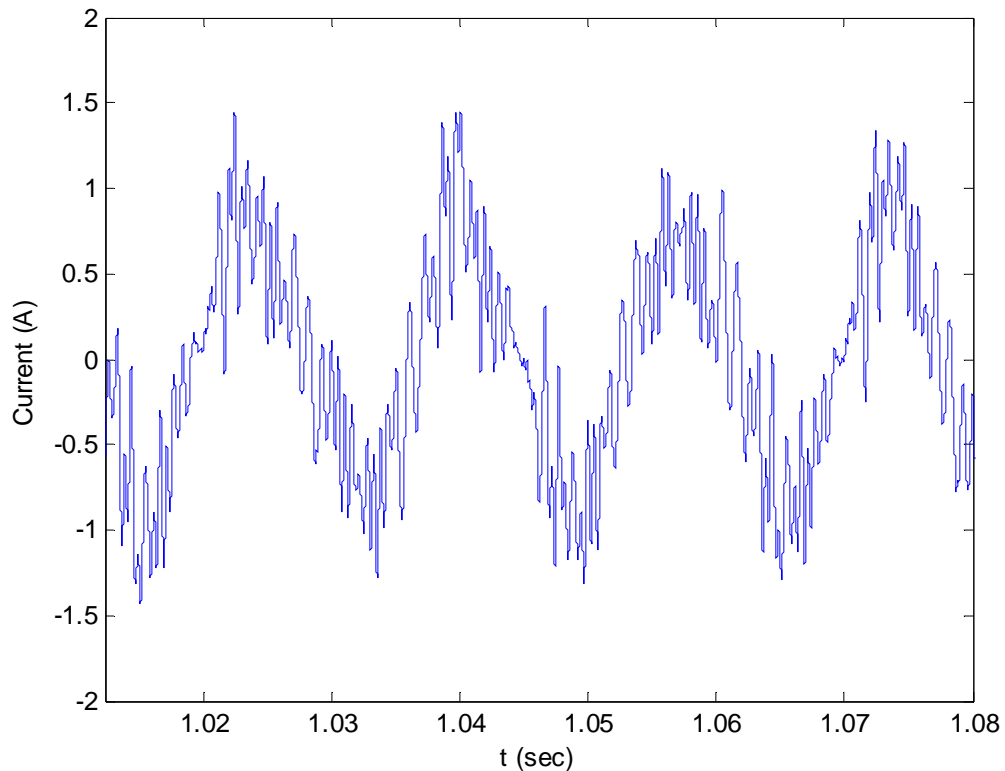


Figure 6.17. Single phase output current at the PCC at 200 W/m² irradiance.

6.3. Harmonic emissions caused by multiple PVGs in the network

This section investigates the impact of multiple PV generators connected to the distribution grid shown in *Figure 6.1*. The kinds of simulations carried out are:

- Analysis of the grid operating under normal operating conditions.
- Investigating the overall effect of varying solar insolation in the PV systems of the test grid.
- Investigating the impact of components deterioration of LCL filters in the PV systems of the grid.

The first set of simulations is presented in *Table 6.10*. It is observed that the current THD levels do not exceed the levels specified by IEEE standard. It may also be concluded that there is not so much of a difference between the THD levels of different points of the distribution grid. As expected, the total harmonic emissions in a multi-power PV would increase as well as the individual high order harmonics, comparing to the case of one PVG. One possible reason for the increase of harmonics is the presence of underground cables in the network, which are modelled as distributed RLC elements. However, the increase of harmonics may be considered only marginal.

Table 6.10. Simulation results under normal operating conditions.

Node	Current THD (%)	29 th (%)	31 st (%)	35 th (%)	37 th (%)
3	1.05	0.55	0.39	0.23	0.20
4	1.05	0.56	0.39	0.23	0.20
6	1.06	0.55	0.39	0.24	0.20
7	1.05	0.56	0.39	0.23	0.20
11	1.15	0.57	0.40	0.24	0.21
12	1.15	0.59	0.42	0.26	0.27
14	1.08	0.56	0.39	0.24	0.20
15	1.15	0.56	0.39	0.24	0.21
16	1.03	0.55	0.39	0.23	0.20
17	1.08	0.56	0.39	0.24	0.20

The second set of simulations, presented in *Table 6.11* shows the impact of solar irradiance applied to multiple PV inverters. This particular case was modelled in such a way that PVGs at nodes 3, 4, 6 and 7 have insolation level of 200 W/m² and PV systems at nodes 11, 12, 14, 15, 16 and 17 have irradiance of 800 W/m². It is seen from this table that low irradiance levels yield very high harmonic distortion and also that the moderate value of irradiance yield harmonic terms that already surpass the IEEE recommendation, i.e., 0.3% above the 33rd harmonic term. It is observed that irradiance tends to have a local effect, i.e., the adverse impact that low irradiance levels have, is confined to the area where this environmental condition applies in the network. The area where the irradiance is 800 W/m² does not seem to be affected much by the area of low irradiance.

Table 6.11. Impact of low level irradiance on the THD.

Node	Irradiance (W/m ²)	Current THD (%)	29 th (%)	31 st (%)	35 th (%)	37 th (%)
3	200	10.29	3.26	3.64	2.22	1.21
4	200	12.28	4.76	5.38	3.29	1.77
6	200	9.73	3.05	3.40	2.07	1.13
7	200	12.14	4.75	5.39	3.29	1.77
11	800	1.23	0.58	0.57	0.35	0.22
12	800	1.24	0.60	0.60	0.37	0.23
14	800	1.06	0.57	0.56	0.34	0.21
15	800	1.20	0.57	0.56	0.34	0.22
16	800	1.05	0.56	0.55	0.33	0.21
17	800	1.06	0.57	0.56	0.34	0.21

One further scenario is investigated relating the irradiance of 400 W/m² is applied to the PVGs at nodes 3, 4, 6 and 7. It can be observed that the surge of THD is not as high as in previous case. Nevertheless, some increases are beginning to appear compared to the case when irradiances are set at 1000 W/m².

Table 6.12. *Impact of middle level irradiance on the THD.*

Node	Irradiance (W/m ²)	Current THD (%)	29 th (%)	31 st (%)	35 th (%)	37 th (%)
3	400	2.80	1.23	1.20	0.73	0.45
4	400	2.82	1.23	1.21	0.74	0.45
6	400	2.80	1.23	1.22	0.74	0.45
7	400	2.83	1.23	1.22	0.74	0.45
11	800	1.31	0.64	0.57	0.35	0.24
12	800	1.22	0.66	0.60	0.37	0.24
14	800	1.22	0.63	0.56	0.34	0.23
15	800	1.34	0.63	0.56	0.34	0.23
16	800	1.19	0.62	0.55	0.34	0.23
17	800	1.22	0.63	0.56	0.34	0.23

An experiment is carried out now for the case when there is a 10% LCL filter components deterioration in all PV systems. The simulation results are presented in *Table 6.13*. It is observed that ageing of filter components does impact THD negatively, mainly at high frequency harmonics. It is noticed that the 29th and 35th harmonic terms surpass the IEEE recommended values of 0.6% and 0.3%, respectively, at all the PCCs. It should be emphasized that all the DC to AC inverters in these test cases are made to switch at 1980 Hz (i.e., 33rd harmonic).

Table 6.13. *Impact of filter deterioration on the THD.*

Node	Current THD (%)	29 th (%)	31 st (%)	35 th (%)	37 th (%)
3	1.31	0.73	0.51	0.31	0.26
4	1.31	0.73	0.52	0.31	0.26
6	1.33	0.73	0.52	0.31	0.26
7	1.31	0.73	0.52	0.31	0.26
11	1.40	0.75	0.53	0.31	0.27
12	1.45	0.77	0.56	0.34	0.27
14	1.33	0.73	0.52	0.31	0.26
15	1.37	0.74	0.52	0.31	0.26
16	1.29	0.72	0.51	0.30	0.25
17	1.33	0.73	0.52	0.31	0.26

6.4. Summary

This chapter researched into the harmonic production capability of PVGs and their ability to distort the voltage and current waveforms at PCC. In particular, the impact of irradiance, imperfect conditions of the filtering system, loading imbalances, selection of inverter switching frequency, the presence of resonance conditions and the choice of MPPT controller; were all comprehensively investigated. The research relied on simulations using the Matlab/Simulink environment.

It may be concluded that irradiance is the vital factor influencing THD and that at low PV power outputs, harmonic emissions may exceed harmonic distortion limits, particularly when the network present resonances. It is well-understood that an appropriate filter design is the key to achieving effective harmonic filtering. But what it is interesting to have emerged is that realistic imbalances in load and imperfect conditions of filtering system do not have a significant deteriorating impact on harmonic indexes, such as THD. All this, of course, refers to the case when the connecting grid is represented in a rather simplified form, namely, as an equivalent load at PCC, with no capacitive effects. In some of the experiments high frequency harmonics are observed to exceed the recommended limits found in IEEE standards but the THD is within the accepted limits. The effect of two different operating principles of MPPT controller is investigated and it is concluded that it does not impact significantly the THD. The impact of the inverter switching frequency selection was also investigated. Low switching frequencies result in high harmonic emissions, whereas high switching frequencies make for a more effective harmonic filtering. The intermodulation of two different switching frequencies was investigated and this was found to be a source of interharmonics. These correspond to the switching frequencies of the DC-DC and DC-AC converters. The impact of multiple PV arrays on the THD is investigated. The analysis shows that irradiance is also the primary factor influencing the THD and the individual harmonic terms, however, the results are slightly increased comparing to the case of one PVG. In addition, resulting THD values are sufficient to overcome the maximum IEEE recommended values. This is due to presence of the underground cables in the network, which are modelled as distributed RLC elements with full frequency dependency.

7. CONCLUSIONS

The research reported in this thesis has made inroads into the little studied field of grid-connected PVG harmonics. Indeed the seeming presence of inter-harmonics leaves more questions open than answers at this stage of the research. From the outset, the decision was made to concentrate on the two-stage PV generator topology and to use the Matlab/Simulink environment as computing and simulation engine. This was based, respectively, on the basis of a comprehensive literature survey relating to the grid-connected PV technology and the popularity of the Matlab/Simulink environment within the department as well as its large number of power electronics in-built models.

The model of a “grid-connected” PV generator was assembled and connected to a three-phase voltage source. The aim was to have the simplest of a “realistic” grid-connected PVG system as possible, in order to gain insight into the main factors that cause waveform distortion in such installations. Further to the PV module, the DC-DC step-up converter, the DC-AC three-phase inverter, the other essential elements are the interfacing transformer, the filtering system and the power load. It is concluded that solar irradiance is the primary factor affecting THD. It is also concluded that load imbalances and a realistic degree of harmonic filter deterioration do not have a significant adverse impact on harmonic levels, provided the power electronics conversion stage and harmonic filters are well designed. The only exception found was the case when the power load exhibited a resonant point at a rather low harmonic order – the second harmonic. Overall, it may be concluded that the key to achieving low THD factors at PCC is to have well designed filtering systems and suitable selections of switching frequencies.

The intriguing existence, at this point in time, of the so-called inter-harmonics was present to varying degrees in all these experiments. It was observed that low-frequency inter-harmonics and the actual harmonic terms remained largely independent of irradiance level. However, the overall result was an increase in THD at PCC; a fact compounded by the persistence of harmonics and inter-harmonics and a decrease of the fundamental frequency component. Aiming at investigating the root-cause of the appearance of interharmonics, a simple but insightful experiment was carried out: the switching frequency of the DC-AC inverter was set at the switching frequency of the DC-DC converter; the overall result was a drastic reduction in the level of inter-harmonics but there was no total elimination. Of course, in practice it is not advisable to select such high values of switching frequencies for the DC-AC power inverter on grounds of the excessive power losses incurred. It should also be pointed out that the very practical issue of partial shading of PV panels was not covered in this research and that this is

likely to affect adversely the inter-harmonic performance of the PV installations since this will induce low values of irradiance at a portion of the PV panel. This is an interesting research problem that goes into the area of future research.

To investigate the timely issue of distributed PVGs, as a major second stage of the current research, the full model of the PVG was placed at various locations of a power distribution network model. It should be remarked that the power distribution network topology and parameters, used in this experiment, is representative of the underground power networks used in the North of England. On the basis of the comprehensive simulation results carried out, it may be concluded that irradiance is also in this case the primary factor that influences harmonic and interharmonic generation. However, a sustained increase in the level of harmonics is noted as a result mainly, of the network of underground cables that make up the power distribution network and the increased number of PVG used in the test case. In this distribution network, no resonances were apparent but, even in cases of standard environmental conditions and realistic *LCL* filter deterioration, some of the harmonic terms around the switching frequency surpass the limits given by the IEEE 929 standard. This situation worsens with low and even moderate values of solar irradiance. It may be argued that further research is required concerning the modelling of this power distribution network. For instance, a more detailed representation of the system load may be required but it is anticipated that this is not expected to change current results significantly owing to the lack of capacitive effects in the system load. It is surmised that what would impact current findings would be an expansion of the power distribution network where the incorporation of additional underground cables might bring the undesirable harmonic resonances closer to the range of frequencies that might be excited by a PVG installation.

7.1. Suggestions for future research

The research carried out as part of this thesis represents, in many ways, only a starting point and a great deal of additional work is required to investigate further the preliminary findings here reported in the area of harmonic performance of grid-connected PGV. It is envisaged that the issues here raised will grow in importance as the deployment of PV installations takes place in earnest in Europe and in the rest of the world. In particular, when Smart Grids become the norm; with their underground means of transporting the electrical energy which will be produced by the great many PVGs distributed over a large geographical area.

It is in this context that a comprehensive programme of harmonics and interharmonics measurements is recommended, in an actual grid-connected PV installation, in order to verify the accuracy of the current research findings. It is also recommended that research be carried out into the modelling of partial shading and the incorporation of Battery Energy Storage Systems (BESS). The former is a very practical issue in the operation of PVGs and the latter will bring much added functionality and acceptance of PV panels as a general and “continuous” source of electrical energy. It may be surmised

that both issues are poised to exacerbate the generation of harmonics and interharmonics in the power distribution system. It then becomes of paramount importance to investigate all the options available for harmonic suppression at source, even before these reach the filtering system. It is well understood that filtering design and specification is a technical-economic issue and to this effects an accurate quantification of energy losses become a matter of great significance. This implies researching thoroughly on algorithms of harmonic cancelation by the inverter control system, such as harmonic flux reinjection. If successful this technique may be applicable to harmonic and interharmonic cancellations thus reducing on the size of the filtering system requirements.

REFERENCES

- [1] U.S Energy Information Administration 2013. International Energy Outlook. Available in: <http://www.eia.gov/forecasts/ieo/index.cfm>.
- [2] European Commission 2013. The EU climate and energy package. Available in: http://ec.europa.eu/clima/policies/package/index_en.htm.
- [3] Renewable Energy Policy Network for the 21st Century 2012. Global status report. Renewables 2012.
- [4] Observ'ER 2012. Worldwide electricity production from renewable energy resources. Fourteenth inventory 2012 edition.
- [5] Valkealahti, S., Bergman, J.-P., Karhumaki T., Keikko, T., Komulainen, R., Tuomo, K., Lakila, M., Lehtinen, H., Partanen, J., Poikonen, P., Rinne, P., Venta, O., Wahlstrom, B. 2006. Hajautetun energiantuotannon tulevaisuusskenaariot ja vaikutukset liiketoimintamalleihin. Lappeenrannan teknillinen yliopisto ISSN 1459-2614.
- [6] EnergyLogix Solutions Inc. 2013. Harmonics and IEEE 519. Available in: http://energylogix.ca/harmonics_and_ieee.pdf.
- [7] Ellis, R 2001. Power system harmonics. A reference guide to causes, effects and corrective measures. Available: http://literature.rockwellautomation.com/idc/groups/literature/documents/wp/mvb-wp011_en-p.pdf.
- [8] IEEE Interharmonics task force, Cigre/CIREN CC02. 1997. Interharmonics in power systems. Available in: <http://grouper.ieee.org/groups/harmonic/iharm/ihfinal.pdf>.
- [9] Li, C., Xu, W., Tayjasanant, T. 2003. Interharmonics: basic concept and techniques for their detection and measurement. Department of Electrical and Computer Engineering, University of Alberta. Electric power system research, volume 66, issue 1, pp. 39-48. Available in: <http://www.sciencedirect.com/science/article/pii/S0378779603000701#>.
- [10] Arrillaga, J., Watson, N. 2003. Power system harmonics. John Wiley & Sons Ltd, ISBN 0-470-85129-5.
- [11] Francisco, R. 2006. Harmonics and power systems. Distribution control systems, Inc., CRC Press ISBN 0-8493-3016-5.

- [12] Arseneau, R. 2003. Application of IEEE standard 1459-2000 for revenue meters. Power Engineering Society General Meeting, volume 1, pp. 87-91.
- [13] Jih-Sheng, L. 1997. Effectiveness of harmonic mitigation equipment for commercial office buildings. IEEE Transaction on Industry Application, volume 33, issue 4, pp. 1104-1110.
- [14] Victor, A. 1999. Treating harmonics in electrical distribution systems. Computer Power & Consulting Corporation. Available in:
<http://www.cpccorp.com/harmonic.htm#How%20do%20harmonics%20affect%20my%20site%20or%20facility?>.
- [15] Zhou, K., Qiu, Z., Yang, Y. 2012. Current harmonics suppression of single-phase PWM rectifiers, in Proc. of PEDG'12, pp. 55-57.
- [16] IEEE. 2000. IEEE recommended practice for utility interface of photovoltaic systems. ISBN 0-7381-1935-0 SS94811.
- [17] Zhao, X., Liu, S. 2012. A research of harmonics for multiple PV inverters in grid-connected. Power and Energy Engineering Conference (APPEEC), pp. 1-4.
- [18] Benhabib, M., Myrzik, M., Duarte, J. 2007. Harmonic effect caused by large scale PV installations in LV network. Electrical Power Quality and Utilization, 9th International Conference, pp. 1-6.
- [19] Rawa, M., Thomas, D., Sumner, M. 2013. Modelling and simulation of a 3kW residential photovoltaic for harmonic analysis, 15th International Conference on Computer modelling and simulation (UKSim), pp. 563-568.
- [20] Xiao-Ming, H., Wen-Bing, L. 2013. Photovoltaic grid simulation and harmonic analysis. International conference on quality, reliability, risk, maintenance and safety engineering, pp. 2014-2017.
- [21] Wang, Y., Yazdanpanahi, H., Xu, W. 2013. Harmonic impact of LED lamps and PV panels. 26th IEEE Canadian Conference of Electrical and Computer Engineering, pp. 1-4.
- [22] Ortega, M., Hernandez, J., Garcia, O. 2013. Measurement and assessment of power quality characteristics for photovoltaic systems: harmonics, flicker, unbalance and slow voltage variations. Electric power system research, vol. 96, pp. 23-35.

- [23] Yang, Y., Zhou, K., Blaabjerg, F. 2013. Harmonics suppression for single-phase grid-connected PV systems in different operation modes. Applied power electronics conference and exposition, pp. 889-896.
- [24] Reddy, P. 2010. Science and Technology of Photovoltaics, 2nd edition, CRC Press, Leiden.
- [25] Osorio, C. 2011. MathWorks. Modelling and simulation of PV solar power inverters. Available in: www.mathworks.com.
- [26] MathWorks 2013. Mathematical modeling. Available in: <http://www.mathworks.se/mathematical-modeling/building-models-data-scientific-principles.html>.
- [27] Mohan, N., Undeland, T., Robbins, W. 2003. Power Electronics. Converters, Applications and Design. John Wiley and Sons, Inc.
- [28] Suntio, T., Leppaaho, J., Nousiainen, L., Puukko, J., Huusari, J. 2010. Implementing current-fed converters by adding an input capacitor at the input of voltage-fed converter for interfacing solar generator. 14th Int. Power Electronics and Motion Control Conference (EPE/PEMC), pp. T12-81 T12-88.
- [29] Xiao, W., Ozog, N., Dunford, W. 2007. Topology study of photovoltaic interface for maximum power point tracking. IEEE Transactions on Industrial Electronics, vol. 54, no. 3, pp. 1694-1704.
- [30] Esram, T. and Chapman, P. 2007. Comparison of photovoltaic array maximum power point tracking techniques. IEEE Trans. Energy Conver., vol. 22, pp. 439-449.
- [31] Abdulkadir, M., Samosir, A., Yatim, A. 2012. Modelling and simulation of Maximum Power Point Tracking of Photovoltaic System in Simulink model. IEEE international Conference on Power and Energy (PECon), pp. 325-330.
- [32] Bruendlinger, R., Bletterie, B., Milde, M. and Oldenkamp, H. 2006. Maximum power point tracking performance under partially shaded PV array conditions. Proc. 21st EUPVSEC, Dresden, Germany, pp. 2157-2160.
- [33] Maki, A. 2009. Topology of a silicon-based grid-connected photovoltaic generator. Master Thesis. Tampere University of Technology.

- [34] Mitsubishi Electric Power Semiconductors 2009. Introduction to TLI technology. POWEREX. Available in: <http://www.pwr.com/pwr/app/TLI%20Series%20Application%20Note.pdf>.
- [35] Shuitao, Y., Qin, L. 2011. A robust control scheme for grid-connected voltage-source inverters. *IEEE Transactions on Industrial Electronics*, vol. 58, no. 1, pp. 202-212.
- [36] Tang, Y., Chiang, P., Wang, P., Choo, F., Gao, F. 2012. Exploring inherent damping characteristic of LCL-Filters for three-phase grid-connected voltage source inverters. *IEEE transaction on power electronics*, vol. 27, issue 3, pp. 1433-1443.
- [37] Zou, Z., Wang, Z., Cheng, M. 2013. Modelling, analysis and design of multi-function grid-interfaced inverters with output LCL filter. *IEEE transaction on power electronics*, issue 99, p. 224-229.
- [38] Liserre, M., Blaabjerg, F., Dell Aquila, D. 2004. Step-by-step design procedure for a grid-connected three-phase PWM voltage source converter. *International Journal of Electronics*, vol. 91, no. 8, pp 445-460.
- [39] Bueno, E. 2005. Optimizacion del comportamiento de un convertidor de tres niveles NPC conectado a la red electrica. Doctoral thesis. Universidad de Alcala. Available in: dspace.uah.es/dspace/bitstream/handle/10017/239/Tesis.pdf.
- [40] Liserre, M., Blaabjerg, F., Hansen, S. 2001. Design and control of an LCL-filter based Three-Phase Active Rectifier. *Industry Applications Conference, 36th IAS Annual Meeting*.
- [41] Paquete 1.1. desarrollo de inversores para CPV. Estudio comparativo de diversas tecnicas de control de corriente en el inversor para el control de las potencias activa y reactiva. July, 2013.
- [42] Blasko, V., Kaura, V. 1997. A novel control to actively damp resonance in input LC filter of a three-phase voltage source converter. *IEEE Transactions on Industry Applications*, vol. 33, issue 2, pp. 542-550.
- [43] Lettl, J., Bauer, J., Linhart, L. 2011. Comparison of different filter Types for Grid Connected Inverter. Department of Electrical Drives and Traction, Czech Technical University in Prague.

[44] Seyed, R., Dian, G., Lang, Q. 2005. Harmonics and interharmonics generation in general VSI/CSI inverters: a new approach. The 7th International Power Engineering Conference, vol. 2, pp. 1165-1170.

[45] Bierhoff, M., Fuchs, F. 2005. Analytical evaluation of the total harmonic current in three phase voltage and current source converters. European Conference on Power Electronics and Applications, pp. 10.

APPENDIX A: DATA FOR THE POWER DISTRIBUTION SYSTEM

Table A.1. Impedance parameters of the underground cables.

Positive- and zero-sequence resistance (Ohms/km)	[0.16428 0.31211]
Positive- and zero sequence inductance (H/km)	[6.8715e-4 3.393e-3]
Positive- and zero sequence capacitance (F/km)	[0.247e-6 0.247e-6]

Table A.2. Cable connectivity and length.

Node	Length (m)
1-2	1297
2-3	304
2-4	626
4-5	391
5-6	738
5-7	492
7-8	583
8-9	1000
9-10	539
9-13	1154
13-15	583
13-14	652
14-17	791
8-11	1110
11-12	539
12-16	1253

Table A.3. System loading data.

Bus	P (kW)	Q (kVAR)
3	238	71
4	159	48
6	340	102
7	178	53
10	0	0
11	458	137
12	221	66
13	221	66
14	97	29
15	386	116
16	161	48
17	64	19

APPENDIX B: DATA OF PV PANELS

Table B.1. Parameters of the PV panel SUNPOWER SPR-220.

Rated power	220W
Current at maximum power	5.56 A
Voltage at maximum power	40.03V
Short-circuit current	5.988A
Open-circuit voltage	48.53V
Total number of cells in series	72
Total number of cells in parallel	1

Table B.2. PV generators connected in the power distribution system.

Node	Modules in series	Modules in parallel	Pmax (kW)
3	8	90	160
4	8	60	107
6	8	96	171
7	8	60	107
11	8	132	235
12	8	63	121
14	8	30	53
15	8	120	214
16	8	60	107
17	8	30	53

APPENDIX C: HARMONIC SPECTRUM AT DIFFERENT SIDES OF THE DC-DC CONVERTER

Selection of the switching frequency of the DC-DC converter seems to rely largely on experimentation. The final value selected for the simulation experiments carried out in this thesis is 5 kHz; a selection based on the minimum THD at PCC, which is 0.9%. Other switching frequencies were investigated in the quest for an improved value of THD but to little effect. For instance, the THD for a switching frequency of 1 kHz is 10.71%. The current and voltage frequency spectrums shown in *Figure C.1* and *C.2*, respectively, show, in addition to the DC component, the frequency component at the switching frequency, i.e. 5 kHz. Further to that, there is a range of low frequency terms, close to the DC term, which are difficult to explain but an expansion of this region of the spectrum indicates that these frequency terms appear at intervals of 40 Hz. These frequency terms are of very low magnitude to be of any practical significance in this particular experiment.

At the terminal of the DC-DC converter that connects with the DC-AC inverter, the band of frequency components that lie next to the DC voltage term follows the same pattern as the spectrum at the other side of the DC-DC converter, as shown in *Figure C.3*. However and as expected, the current frequency spectrum at both sides of the DC-DC converter are very different from each other owing to the two very different equivalent impedances seen by the voltage source that the converter represents, as shown in *Figure C.4*. The large third harmonic current shown in the frequency spectrum to the right of the converter is quite noticeable.

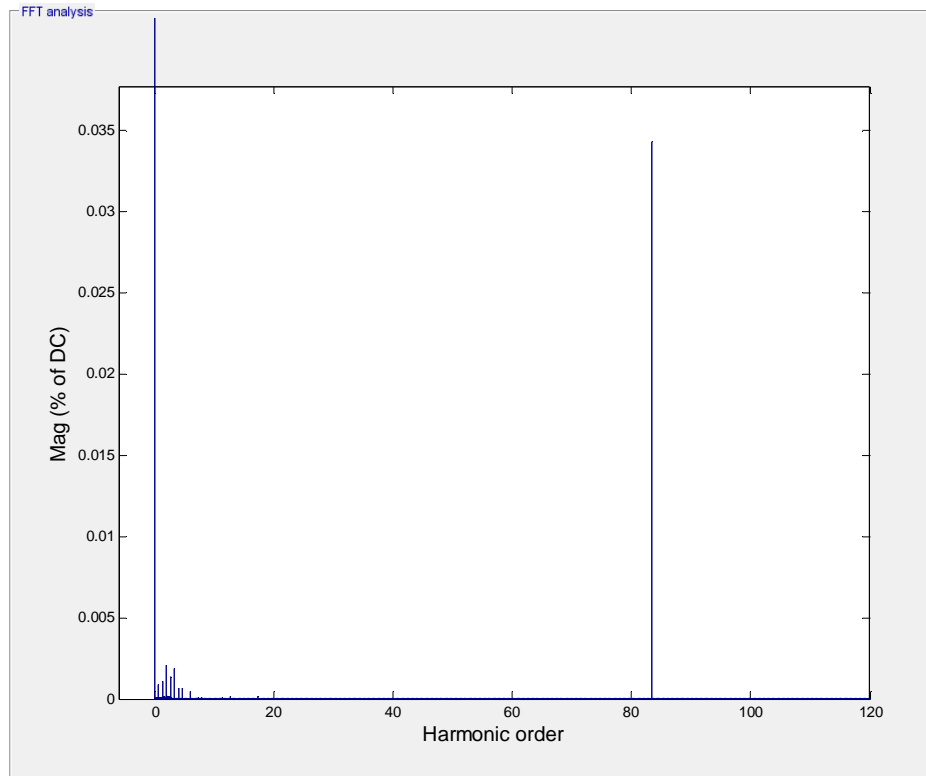


Figure C.1. Harmonic spectrum of the current at the output of the PV panel.

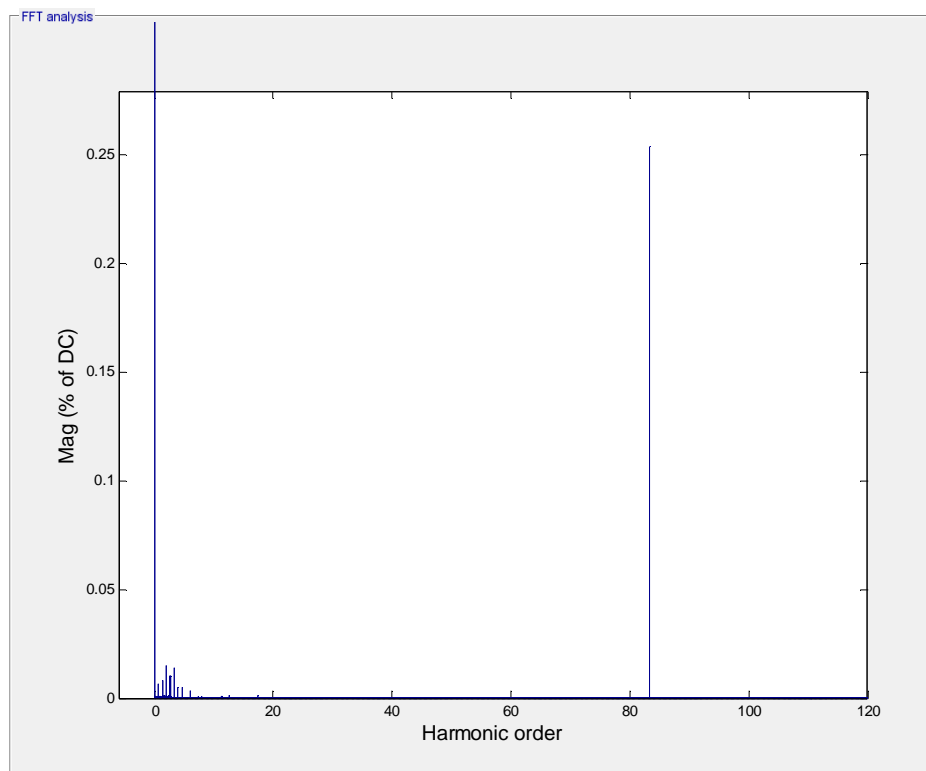


Figure C.2. Harmonic spectrum of the voltage at the output of the PV panel.

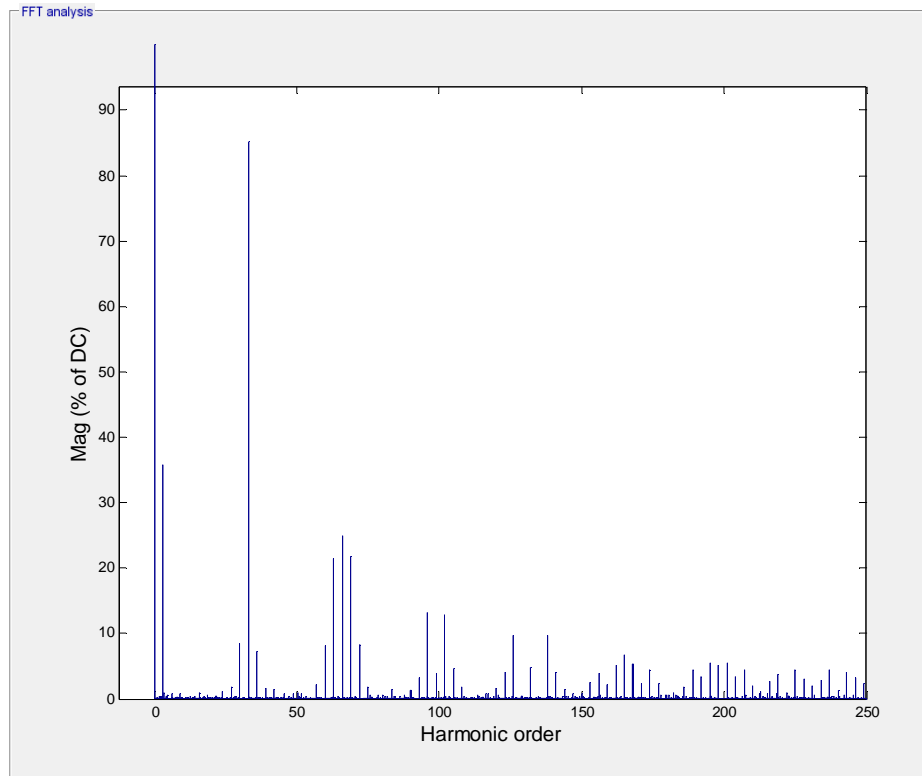


Figure C.3. Harmonic spectrum of the current at the output of the boost converter.

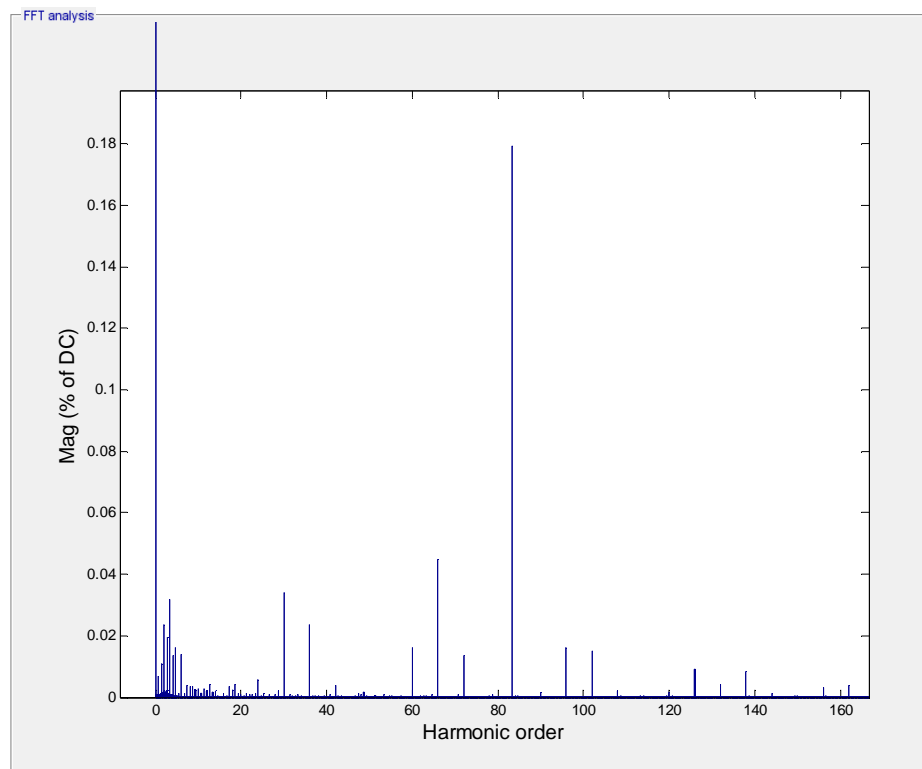


Figure C.4. Harmonic spectrum of the voltage at the output of the boost converter.

APPENDIX D: HARMONIC ASSESSMENT OF ELECTRIC POWER DISTRIBUTION GRIDS WITH DISTRIBUTED PV SYSTEMS

On 2nd June 2014, the journal paper: “Harmonic assessment of electric power distribution grids with distributed PV systems” was submitted with a view to publication in The Scientific World Journal.

Harmonic Assessment of Electrical Power Distribution Grids with Distributed PV Systems

Andrii Pazynych¹, Enrique Acha¹ and Xavier del Toro²

¹Department of Electrical Engineering, Tampere University of Technology, 33720 Tampere, Finland

²School of Industrial Engineering, University of Castilla-La Mancha, 33071 Ciudad Real, Spain

Abstract: The paper reports on an investigation of key factors that impact adversely the quality of the current and voltage waveforms in a power distribution network with distributed photovoltaic (PV) installations. These factors include irradiance levels, imperfect conditions of the filtering system, resonant conditions and inverter's switching frequency. A comprehensive model of a PV system is developed to assess the quality of the current and voltage harmonic injections under a wide range of credible scenarios, and the presence of interharmonics is detected. The study indicates that irradiance is the primary factor influencing total harmonic distortion (THD) and that at low PV power outputs the THD index and some of the individual harmonic terms exceed the recommended harmonic distortion limits set by current Standards. The use of well-designed filters is the key to keeping harmonics emissions low. Nonetheless, perfect filtering does not exist in actual installations and the study investigates the impact of imperfect filtering parameters on the voltage and current waveforms at the various points of common coupling with the distribution network. In this case too, the harmonic currents around the switching frequency surpass the limits set by current standard.

Key words: photovoltaic generators, distributed generation, harmonics, interharmonics, IEEE 929 Standard.

1 INTRODUCTION

A PV system transforms solar radiation into electrical energy in DC form. Connection of the PV system to the utility AC power system requires a power electronic interface. However, an undesirable characteristic of the use of the power electronic equipment is that the current and voltage waveforms at the point of common coupling (PCC) with the power grid contain a degree of harmonic distortion which, in some instances, may exceed the levels recommended by existing standards [1], [2].

The two available options to connect a photovoltaic energy system into the AC power grid are to use either a two-stage or a single stage power electronic topology. In the former case a DC-DC converter and a DC-AC inverter are used in tandem whereas in the latter case only the DC-AC inverter is used. The two-stage PV generator topology is illustrated schematically in Fig. 1.

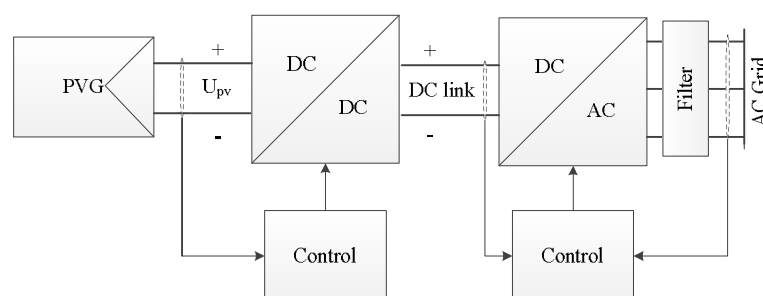


Fig. 1. Two-stage PV system

The two-stage topology enables maximum power extraction for a given amount of solar irradiance and temperature, and it is the most popular option. However, there are some performance-related issues which remain unsolved and require investigation. One such issue is the control performance of PV generators under conditions of partial shading and another is the subject of this paper, namely, the current and voltage harmonic distortion that the PV generators incur and the ensuing interaction with the power grid. Nevertheless, some progress has been made and various researchers have presented their findings regarding the factors that influence the generation of harmonic currents and voltages of PV generators, some of which are reviewed below.

Zhao and Liu [3] investigated the impact of environmental factors and pulse width modulation (PWM) control methods on the harmonic current injection at the PCC produced by one PV generator and two PV generators. The main finding of the study is that irradiance is the primary factor influencing the level of current harmonic distortion, especially THD, which deteriorates at low irradiance levels. They also conclude that harmonic levels are PWM control-dependent and that two photovoltaic systems may yield less current harmonic distortion at the PCC, than a single one. The latter point is a debatable one and it is contrary to what we have observed using a realistic model of a power distribution system. The research conducted by Benhabib, Myrzik and Duarte [4] suggests that the presence of non-linear loads, particularly *RC*-type loads, may result in an increased THD. This is an expected result owing to the presence of potential resonances at the load point. Rawa, Thomas and Sumner [5] investigated possible aspects of modelling simplifications in a Simulink[®] model. For such a purpose, two models were used: one model with the full PV cell model, the power converter and the inverter; in the second model the PV module and the DC-DC converter are substituted by a simple voltage source. The aim of the research was to show that in normal operating conditions, the PV cell and the DC-DC converter do not play any significant role in harmonics injection. This is a most debatable point since it is the explicit representation of the DC-DC converter that reveals the presence of interharmonics.

The investigation presented in [6] shows the advantage of using *LCL* filters over *L* filters (i.e., single inductance) in terms of minimizing current harmonic distortion. It is elaborated that this is due to the third-order, low-pass filter characteristics of the *LCL* filters. Our experience indicates that *L* filters do keep the THD below 5% but some of the high-order harmonic terms exhibit values of 1% or higher. The research conducted in [7] concludes that the harmonics produced by PV installations depend on the actual operating conditions and that the lower the PV power output, the higher the THD. A similar conclusion is reached in [8], stating that at low power outputs the harmonic current emissions would exceed the maximum levels set in the IEEE 929 and IEC 61727 standards [1], [2]. This is commensurate with our findings but what we have observed is that the individual harmonic and interharmonic terms tend to remain largely constant regardless of irradiance levels. Of course, the THD deteriorates at low irradiance levels due to the lower value of the fundamental frequency current. In this case, the Total Demand Distortion (TDD) may be a more realistic index to use. The impact of different operating modes on the harmonic current is presented in [9]. The emphasis of the work is on assessing different control methods, namely, proportional resonant controllers, multi-resonant controllers and repetitive current controllers. It is concluded that different control methods have different impact on current harmonic emission with proportional resonant plus repetitive current control method achieving the lowest distortion.

The research presented in this paper assesses the impact of environmental and operational conditions on PV generators, concerning their ability to produce periodic, non-sinusoidal voltage and current waveforms at the PCC. In particular, the impact of irradiance, imperfect conditions of the filtering system, selection of inverter switching frequency, and the presence of resonance conditions were all comprehensively investigated. An assessment of the simulation packages available to carry out this kind of research was conducted and it was concluded that substantial difference existed between Simulink[®] and PSCAD[™]. It was decided to use the former package because its wider user base in our research group.

The research casts additional light into the heretofore little researched problem of interharmonics produced by PV generators. It indicates what are the main equipment and operational factors responsible for the generation of interharmonics. The research demonstrates that using a well-designed *LCL* filtering system, as opposed to an *L* filter, is of paramount importance to maintaining the operational integrity of the PV plant under a wide range of non-ideal but credible operating and environmental conditions. However, in cases where the AC equivalent circuit at the PCC exhibits an excitable resonance, the *LCL* filtering system is not able to overcome the ensuing large harmonic distortion on its own and additional measures would be required, perhaps in the form of shunt filters tuned at the appropriate resonant frequencies. The impact of dispersed photovoltaic generators is assessed using the model of a realistic distribution system comprising a network of underground cables. The results show that the harmonic currents around the switching frequency (i.e., 33rd) surpass the limits set by the IEEE 929 standard. It should be mentioned that no saturation of the magnetizing branch of the transformer has been assumed in all our studies.

2 THE PHOTOVOLTAIC GENERATOR

2.1 Photovoltaic power cell

For most practical purposes a PV cell circuit model may be seen to comprise an ideal current source and one or two diodes in parallel [10]; representing the dark saturation currents due to electrons recombination in the quasi-neutral and the depletion regions. In addition the actual photovoltaic cell also has parasitic elements in the form of a shunt resistance and a series resistance. The main origin of the parasitic series resistance is the metal contacts and the transverse flow of current. The reason behind the parasitic shunt resistance is the p-n junction and impurities near the junction. The *I-V* characteristic of the PV cell is normally expressed as [11]:

$$I = I_{ph} - I_o \left(e^{\frac{(U+IR_s)}{AU_t}} - 1 \right) - \frac{U+IR_s}{R_{sh}} \quad (1)$$

where I_{ph} is the photo-current, U_t is the thermal voltage and I_o is the diode saturation current, T is the temperature, k is the Boltzmann constant, q is the electron charge, U is the output voltage of the PV cell, R_{sh} is the parasitic shunt resistance and R_s is the parasitic series resistance and an ideality factor A .

2.2 DC-DC converter

The DC-DC converter in Fig. 1 is a boost-type converter with a capacitor added to the input in order to achieve a current fed topology [12]. The main reason for using a current fed boost converter is that the control system regulates the voltage. The current produced by the PV system is very sensitive to irradiance variations, which means that the PV current's fluctuations are large in scale and fast. The control for such currents would require fast dynamics and it might lead to the controller saturation [13]. It is said that changes in irradiance have relatively little effect on output voltage [10].

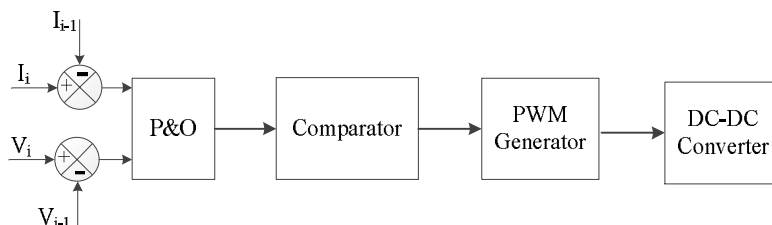


Fig. 2. Control diagram for the DC-DC boost converter.

The DC-DC converter is fitted with a Perturb and Observe controller in order to achieve MPPT. This control method carries low computational burden and lower costs compared to alternative MPPT methods [14].

The power is computed from the measured voltage and current values and compared to previous values of power, which are stored in memory. The control system operates by incrementing or decrementing (perturbing) the PV voltage and by comparing the new and the old powers to increase or decrease the duty cycle. If the perturbation results in an increase of power then the direction of the perturbation pattern remains unchanged. In case of power decreases the sign of the perturbation reverses. This cycle is repeated until the MPPT is achieved, which happens when $dP/dV=0$.

2.3 Inverter model

The DC-AC inverter is a three-level neutral-point-diode-clamped. It is designed to enable maximum power injection and synchronization to the power grid operating voltage and frequency. The grid-current is the inner loop and the DC-link voltage provides the feedback for the grid-current loop, as shown in Fig. 3.

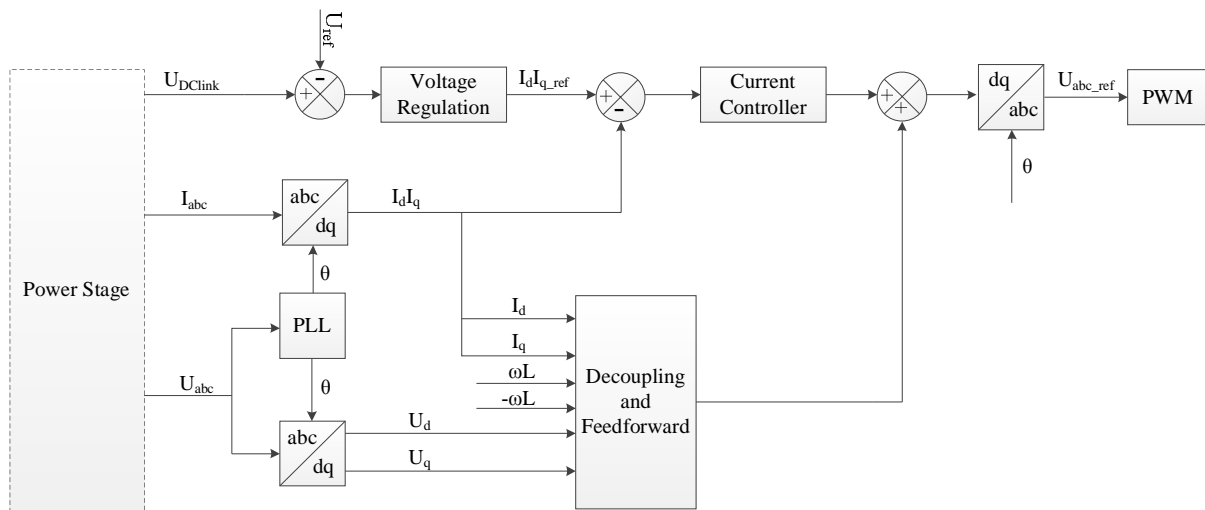


Fig. 3. Control diagram using the synchronous reference frame

The inverter incorporates at its output an *LCL* filter, which yields low harmonic and ripple cancellation using small size components [15]-[17]. This design criterion is detailed in Appendix I.

Notice that the control is carried out using the synchronous reference frame. The control system performs a transformation from the natural reference frame onto the synchronous frame and it then performs a backward transformation onto the natural reference frame, ready to be fed into the PWM generator. The signals produced by the *dq* transformation are DC-like signals; therefore for regulating purposes, PI controllers may be used.

3 SIMULATION RESULTS

3.1 Harmonic emissions produced by a single PV generator

This section deals with the analysis of waveform distortion produced by a single PV system feeding into a three-phase voltage source via a connecting transformer. An *RL* shunt load sits between the three-phase voltage source and the transformer. The motivation behind this experiment is to gain some fundamental insight into the main factors responsible for distorting the waveform in grid-connected PV systems. The environmental, design and operational factors considered are the following: solar irradiance, converter switching frequency, resonances in *RLC*-type loads, *LCL* filter deterioration and the capacitive nature of a realistic distribution system comprising a network of underground cables.

The solar panel module taken as a reference in this research is the SUNPOWER SPR 220, with the technical specifications given in Appendix II. The FFT algorithm available within the SimPowerSystems block set is used to extract the harmonic content from the PV voltage and current waveforms. All FFT calculations are based on a 60 cycles, 1e-6 sampling time and rectangular-type window. Notice that the FFT is set to calculate frequencies at every 1 Hz, hence, the ensuing frequency spectrums will show not only the harmonic terms but also all the interharmonic terms. Two power quality indices were used to assess harmonic distortion, namely, the Total Harmonic Distortion (THD) and the Total Demand Distortion (TDD). Because of the way the sampling is carried out, these indices will include both the interharmonic and the harmonic terms. The current THD and TDD values may be computed using the following expressions:

$$THD = \frac{\sqrt{I_{RMS}^2 - I_{RMS(1)}^2}}{I_{RMS(1)}} \cdot 100\% \quad (2)$$

$$TDD = \frac{\sqrt{I_{RMS}^2 - I_{RMS(1)}^2}}{I_{RMS(L)}} \cdot 100\% \quad (3)$$

where $I_{RMS(1)}$ is the fundamental component of the current waveform, I_{RMS} is the sum of all the harmonic components of current including the fundamental and $I_{RMS(L)}$ is the nominal or rated current.

The simulation results below correspond to normal environmental and operating conditions, i.e. irradiance of 1000 W/m², temperature of 25°C, DC-DC converters switching at 5 kHz, DC to AC inverter switching at the 33rd harmonic (1980 Hz) and the associated filters in good working order. The fundamental frequency of the grid is 60 Hz.

The results presented in Fig. 4 show that the harmonic emissions of a single PV array are lower than the limits set by IEEE 929 which sets a maximum THD limit of 5%. In this case the THD carries a value of 0.81%.

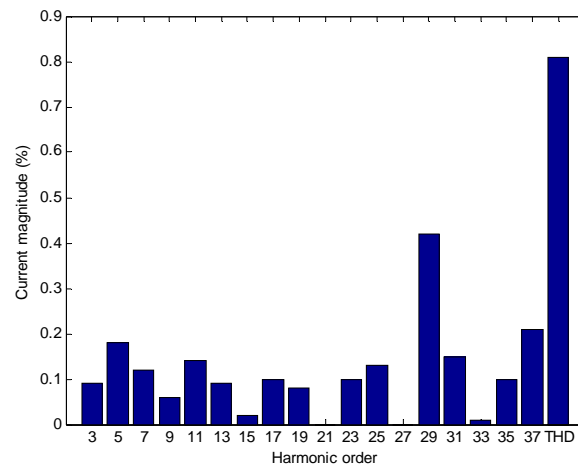


Fig. 4. Harmonic content of the PVG under nominal operating conditions

However, some individual harmonics cause some concern, especially the 29th, 31st, 35th and 37th, for which values of 0.6% are set for harmonics 23rd-33rd and 0.3% for harmonics above the 33rd. Further experiments are carried out in order to assess whether or not changes in operating conditions may cause some harmonics to exceed the limits set by IEEE 529 [1].

3.2 The impact of switching frequencies on harmonic emissions

These harmonics are caused by the DC-AC inverters [18]. Hence, the effect of different switching frequencies on the current harmonic emissions of the PV plant is investigated. Table I shows that selection of the switching frequency is a key factor in PV inverter design since, in general, higher switching frequencies result in smaller THD values.

TABLE I. IMPACT OF INVERTER SWITCHING FREQUENCY ON THD (1000 W/M²).

Inverter switching frequency	Current THD (%)	Highest harmonics (%)			
		41 st	43 rd	47 th	49 th
2700 Hz	0.78	0.15	0.06	0.04	0.09
		0.24	0.09	0.06	0.13
2340 Hz	1.20	0.29 th	31 st	35 th	37 th
		0.42	0.15	0.10	0.21
1620 Hz	1.23	23 rd	25 th	29 th	31 st
		0.82	0.27	0.17	0.34
1260 Hz	2.41	17 th	19 th	23 rd	25 th
		1.83	0.52	0.32	0.62
900 Hz	4.57	11 th	13 th	17 th	19 th
		3.65	0.81	0.51	1.29

3.3 The impact of switching frequencies on interharmonic emissions

It is noticed that interharmonic generation has a degree of switching frequency-dependency and that an unsuitable selection of switching frequency tends to increase the THD. Aiming at gaining some insight into the phenomenon of interharmonic generation in the PV application, the switching frequency of the inverter is set to be equal to the switching frequency of the DC-DC converter (i.e. 5 kHz). It is seen from the results in Table II that this reduces the presence of the interharmonic terms very considerably. However, it is also noted that such an action yields 2% of second harmonic and that the THD increases to 2.12%. This contrasts to the 0.81% when the inverter is made to switch at 1980 Hz.

Even though the interharmonic terms are not completely eliminated in Fig. 5, it is appreciated that the intermodulation of the two different switching frequencies used in the DC-DC and DC-AC converters is the main culprit for the generation of interharmonics. However, it should be said that such a high switching frequency for the DC-AC power inverter is not practical since switching power losses are likely to be very high. Such an exercise was carried out more as a matter of academic interest.

TABLE II. VALUE OF INTERHARMONIC AT DIFFERENT SWITCHING FREQUENCIES (1000 W/M²).

Harmonic content	Inverter switching frequency (Hz)					
	5000	2700	2340	1980	1620	900
20 Hz	0.01	0.13	0.04	0.05	0.09	0.29
100 Hz	0.03	0.08	0.16	0.01	0.06	0.08
140 Hz	0.00	0.07	0.07	0.04	0.04	0.12
220 Hz	0.01	0.00	0.05	0.04	0.01	0.04
260 Hz	0.01	0.01	0.07	0.02	0.04	0.08
340 Hz	0.00	0.03	0.03	0.00	0.02	0.06
380 Hz	0.01	0.03	0.04	0.03	0.05	0.10
Total interharmonic value	0.15	0.46	0.54	0.33	0.44	1.05
Note: Values are provided in amperes (A)						

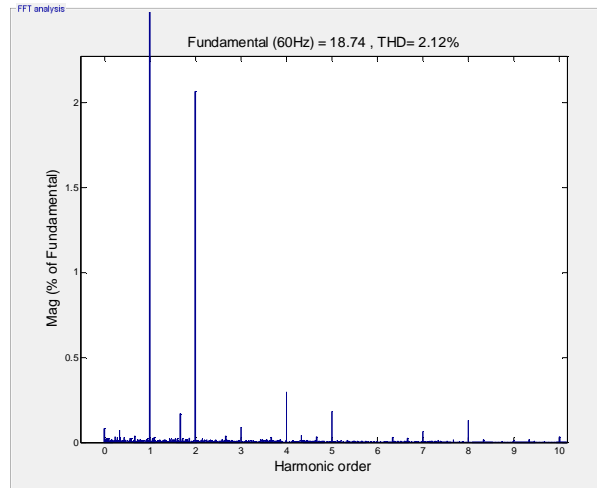


Fig. 5. Harmonic spectrum with inverter switching at 5 kHz (1000 W/m^2)

3.4 The impact of solar irradiance on harmonic emissions

Table III gives values of individual harmonics and THD for different irradiances reaching the surface of the PV panel. It can be seen that irradiance decreases result in THD increases but they are kept always below the 5% limit set by the IEEE 929 standard. Also, individual harmonic terms increase with low levels of solar irradiance and some of these terms go above the limits set by the standard. However, it should be noted that the THD as given by equation (2) and the individual harmonic terms are expressed as a fraction of the fundamental frequency and that this too reduces with decreasing irradiance values. In contrast, the TDD values as given by equation (3) and presented in Table IV tend to be largely independent of changes in irradiance levels.

TABLE III. IMPACT OF IRRADIANCE LEVELS ON THD

Irradiance levels	Current THD (%)	29 th (%)	31 st (%)	35 th (%)	37 th (%)
1000 W/m^2	0.81	0.42	0.15	0.10	0.21
500 W/m^2	1.48	0.77	0.47	0.33	0.37
200 W/m^2	3.65	1.82	1.50	1.04	0.87

TABLE IV. IMPACT OF IRRADIANCE LEVELS ON TDD

Irradiance levels	Current TDD (%)
1000 W/m^2	1.321
500 W/m^2	1.156
200 W/m^2	1.128

As shown in Figs. 6 and 7, the harmonic and interharmonic terms remain within narrow values from each other but the fundamental component decreases significantly with decreasing values of irradiance. It should be noted that there is at present no guidelines given by IEEE on interharmonics but it is seen from this analysis that their levels remain lower than the harmonic terms for the various irradiance levels.

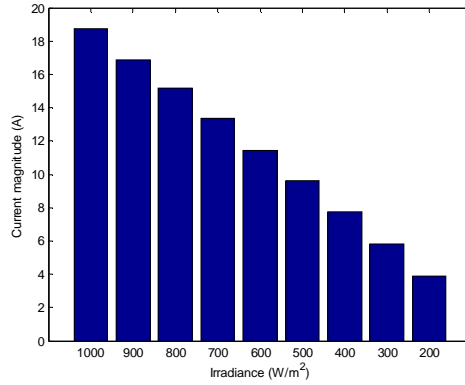


Fig. 6. Fundamental component of PVG at different irradiance levels

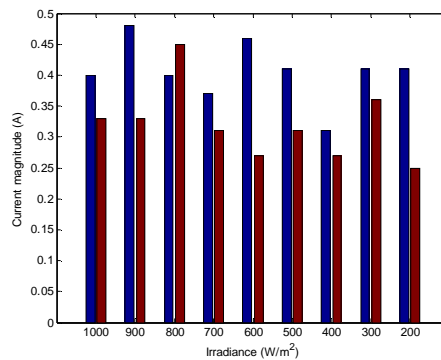


Fig. 7. Values of harmonics and interharmonics at different irradiance levels

3.5 The impact of imperfect filter conditions on harmonic emissions

In real-life situations it is quite often the case that filters do not operate exactly as intended due to incipient faults of various degrees of severity, may be due to aging of filter components and ambient conditions. To explore this point, some changes are introduced in the components of the *LCL* filters to signify deterioration of the original filter design. The simulation results are shown in Table V.

TABLE V. IMPACT OF *LCL* FILTER DETERIORATION ON THE THD (1000 W/m²)

Detuning of <i>LCL</i> filter	Current THD (%)	29 th (%)	31 st (%)	35 th (%)	37 th (%)
10% detuning in converter side inductance L_1	0.96	0.47	0.17	0.12	0.23
10% detuning in C filter	0.86	0.48	0.17	0.12	0.23
Overall 10% detuning of filter components	1.00	0.54	0.20	0.14	0.26

It may be said that when a suitable filter design is in place, filter component deterioration, of the kinds investigated in this paper, do not seem to play a significant adverse role on harmonic emissions.

To put these results in context, Fig. 8 shows the harmonic spectrum of the PV generator at PCC, with no filtering system. The absence of the output filter yields exceedingly high distortion. In contrast, the harmonic spectrum shown in Fig. 9 illustrates the reduction in interharmonic terms when the DC-AC inverter and the DC-DC converter are made to switch at the same frequency.

As mentioned earlier, this result may not be practical at the present time, with current valve technology, because of the very high switching losses that the inverter may incur. However, from the academic perspective, this result does indicate that intermodulation between two converters operating at different switching frequencies is largely responsible for the generation of interharmonics.

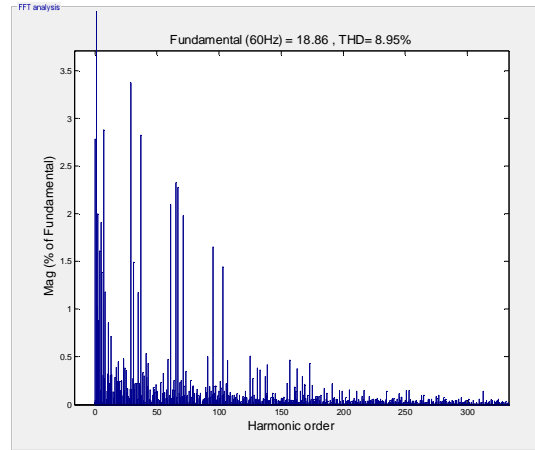


Fig. 8. Harmonic spectrum of the PVG with no LCL filter ($f_s=1980$ Hz, 1000 W/m²)

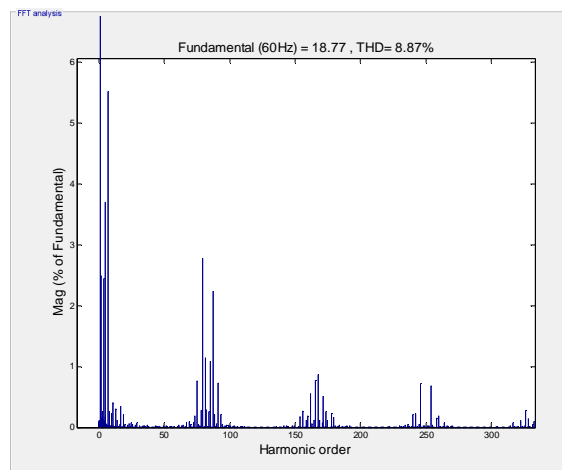


Fig. 9. Harmonic spectrum of the PVG with no LCL filter ($f_s=5000$ Hz, 1000 W/m²)

3.6 The impact of resonance conditions on THD

This section exemplifies the case when the PV system feeds into a load point that exhibits a shunt resonance at the second harmonic. The resonance results from representing the load as an equivalent RLC branch, as opposed to only RL , with appropriate values of R , L and C parameters. This is commensurate with the research reported in [4] concerning increased THD values when RC -type loads are considered. It is seen from Figs. 10-12 that the existence of the resonant point induces large values of harmonic distortion which increase, in a non-linear fashion, with decreasing values of solar irradiance. Moreover, at lower radiation levels, due to the increased values of low-order interharmonics, resonance shifts to other frequencies do take place. This is seen in Figs. 11 and 12.

TABLE VI. EFFECT OF RESONANCE IN RLC LOAD AND IRRADIANCE.

Irradiance levels	Current THD (%)
1000 W/m ²	13.05
500 W/m ²	21.13
200 W/m ²	58.16

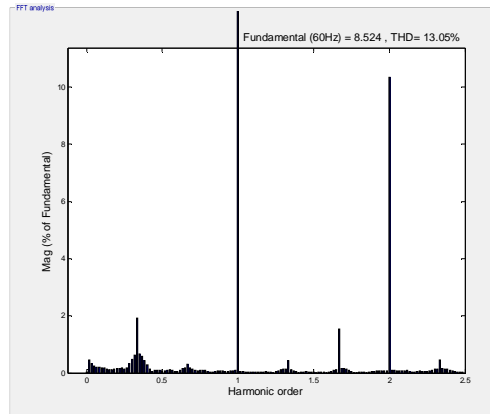


Fig. 10. Harmonic spectrum at PCC at 1000 W/m²

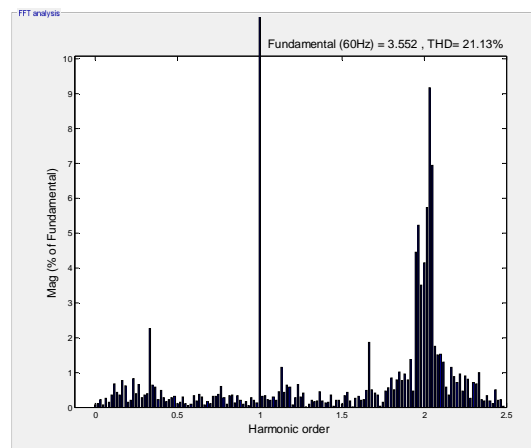


Fig. 11. Harmonic spectrum at PCC at 500 W/m²

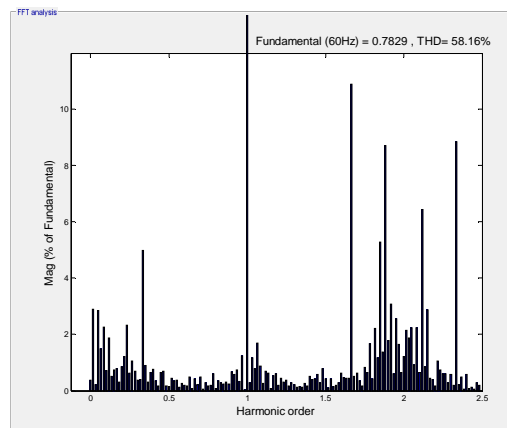


Fig. 12. Harmonic spectrum at PCC at 200 W/m²

3.7 Harmonic emissions from distributed PV generators

The power distribution network shown in Fig. 13 is used to carry out the assessment of distributed PV generators. It is a typical distribution system of the kind found in the North of England, with underground cables and the parameters given in Appendix III. Data for the PV generators' topologies and power ratings are given in Appendix IV.

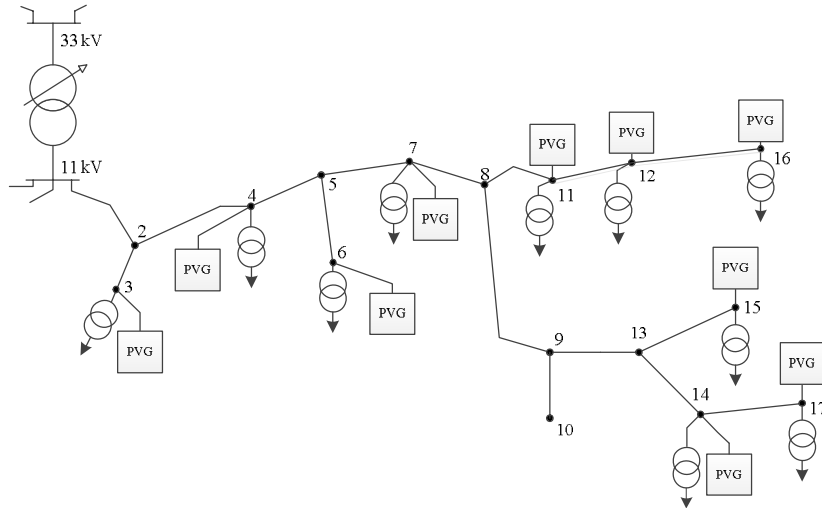


Fig. 13. Distribution network model

A rather comprehensive set of environmental and operational scenarios were investigated using this power distribution network with distributed PV generation, namely: (i) power grid operating under normal environmental and operating conditions; (ii) assessing the impact of varying solar radiation in the PV systems; (iii) assessing the impact of components deterioration in the *LCL* filters.

It is observed from the results presented in Table VII that the current THD levels do not exceed the levels specified by the IEEE standard by any means and that the THD levels of different points of the distribution grid are very similar in value. However, the THD and the individual harmonic terms increase slightly, compared to the case of one PVG. This is an expected result owing to the presence of underground cables in the network, which are modelled as distributed *RLC* elements with full frequency dependency.

TABLE VII. SIMULATION DATA UNDER NOMINAL OPERATING CONDITIONS

Node	Current THD (%)	29 th (%)	31 st (%)	35 th (%)	37 th (%)
3	1.05	0.55	0.39	0.23	0.20
4	1.05	0.56	0.39	0.23	0.20
6	1.06	0.55	0.39	0.24	0.20
7	1.05	0.56	0.39	0.23	0.20
11	1.15	0.57	0.40	0.24	0.21
12	1.15	0.59	0.42	0.26	0.27
14	1.08	0.56	0.39	0.24	0.20
15	1.15	0.56	0.39	0.24	0.21
16	1.03	0.55	0.39	0.23	0.20
17	1.08	0.56	0.39	0.24	0.20

The results in Table VIII show the solar irradiance's impact. It is assumed that the PVGs at nodes 3, 4, 6 and 7 receive an irradiance level of 200 W/m² and that the PV systems at nodes 11, 12, 14, 15, 16 and 17 receive an irradiance of 800 W/m². It is seen from this table that low irradiance levels yield very high harmonic distortion and also that the moderate value of irradiance yield harmonic terms that already surpass the IEEE recommendation, i.e., 0.3% above the 33rd harmonic term. It is observed that irradiance tends to have a local effect, i.e., the adverse impact that low irradiance levels have, is confined to the area where this environmental condition applies in the network. The area where the irradiance is 800 W/m² does not seem to be affected much by the area of low irradiance.

TABLE VIII. IMPACT OF LOW IRRADIANCE

Node	Irradiance (W/m ²)	Current THD (%)	29 th (%)	31 st (%)	35 th (%)	37 th (%)
3	200	10.29	3.52	3.94	2.40	1.31
4	200	12.28	4.78	5.43	3.31	1.78
6	200	9.73	3.17	3.55	2.16	1.18
7	200	12.14	4.77	5.42	3.31	1.78
11	800	1.23	0.58	0.57	0.35	0.22
12	800	1.24	0.60	0.60	0.37	0.23
14	800	1.06	0.57	0.56	0.34	0.21
15	800	1.20	0.57	0.56	0.34	0.22
16	800	1.05	0.56	0.55	0.33	0.21
17	800	1.06	0.57	0.56	0.34	0.21

The simulation results for the case when a 10% detuning is assumed in all the *LCL* filter components indicate that the THD tends to be affected negatively, mainly at the higher harmonic frequencies. The simulation results are presented in Table IX. It is noticed that the 29th and 35th harmonic terms surpass the IEEE recommended values of 0.6% and 0.3%, respectively, at all the PCCs. It should be emphasized that all the DC to AC inverters in these test cases are made to switch at 1980 Hz (i.e., 33rd harmonic).

TABLE IX. IMPACT OF FILTER DETUNING (1000 W/M²)

Node	Current THD (%)	29 th (%)	31 st (%)	35 th (%)	37 th (%)
3	1.31	0.73	0.51	0.31	0.26
4	1.31	0.73	0.52	0.31	0.26
6	1.33	0.73	0.52	0.31	0.26
7	1.31	0.73	0.52	0.31	0.26
11	1.40	0.75	0.53	0.31	0.27
12	1.45	0.77	0.56	0.34	0.27
14	1.33	0.73	0.52	0.31	0.26
15	1.37	0.74	0.52	0.31	0.26
16	1.29	0.72	0.51	0.30	0.25
17	1.33	0.73	0.52	0.31	0.26

4 CONCLUSIONS

A comprehensive model of a PVG was built using the Simulink[®] environment. The PVG model was made to feed into a PCC and it is concluded that a good *LCL* filter design is key to preventing the PV installation from injecting excessive harmonic currents at the PCC. In line with recent findings, it is concluded that solar irradiance is the primary factor affecting THD. However, in all cases the THD is well below the 5% threshold value set by the IEEE 929 standard, except when the PCC exhibited a resonant condition. On the other hand, it is observed that the individual harmonic terms around the switching frequency have larger values than the rest but that they are still below the limits set by the standard. Also in the case of one PVG, a realistic degree of harmonic filter deterioration does not seem to have a significant adverse impact on THD. It was noted that interharmonics were present in all the experiments, irrespective of irradiance levels. With the aim of investigating the root-cause of interharmonics, an experiment was carried out: the switching frequency of the DC-AC inverter was set at the switching frequency of the DC-DC converter; the overall result was a drastic reduction in the level of interharmonics but their total elimination did not occur.

The full model of the PVG was placed at various locations in a realistic distribution network model. On the basis of the comprehensive simulation results carried out, it was also concluded that in this case, irradiance is the primary factor that influences harmonic and interharmonic generation. It was observed that, from the harmonic distortion viewpoint, irradiance tends to be a local effect and that it is accompanied by a sustained harmonic level increase, compared to the case of one PVG. This is

mainly due the network of underground cables that make up the power network and the increased number of PVGs. In this distribution network, no resonances were apparent but, even in cases of standard environmental conditions and realistic *LCL* filter deterioration, some of the harmonic terms around the switching frequency surpass the limits given by the IEEE 929 standard. This situation worsens with low and even moderate values of solar irradiance.

CONFLICT OF INTEREST

The authors declare that they have no conflicts of interest with regards to this manuscript

REFERENCES

- [1] IEEE 929, "Recommended practice for utility interface of photovoltaic systems", ISBN 0-7381-1935-0 SS94811, 2000.
- [2] IEC 61727, "Photovoltaic systems – characteristics of the utility interface", 2004.
- [3] X. Zhao and S. Liu, "A research of harmonics for multiple PV inverters in grid-connected", Power and Energy Engineering Conference (APPEEC), pp. 1-4, 2012.
- [4] M. Benhabib, M. Myrzik, J. Duarte, "Harmonic effect caused by large scale PV installations in LV network", Electrical Power Quality and Utilization, 9th International Conference, pp. 1-6, 2007.
- [5] M. Rawa, D. Thomas, M. Sumner, "Modelling and simulation of a 3kW residential photovoltaic for harmonic analysis", 15th International Conference on Computer modelling and simulation (UKSim), pp. 563-568, 2013.
- [6] H. Xiao-Ming and L. Wen-Bing, "Photovoltaic grid simulation and harmonic analysis", International conference on quality, reliability, risk, maintenance and safety engineering, pp. 2014-2017, 2013.
- [7] Y. Wang, H. Yazdanpanahi and W. Xu, "Harmonic impact of LED lamps and PV panels", 26th IEEE Canadian Conference of Electrical and Computer Engineering, pp. 1-4, 2013.
- [8] M. Ortega, J. Hernandez and O. Garcia, "Measurement and assessment of power quality characteristics for photovoltaic systems: harmonics, flicker, unbalance and slow voltage variations", Electric power system research, vol. 96, pp. 23-35, 2013.
- [9] Y. Yang, K. Zhou and F. Blaabjerg, "Harmonics suppression for single-phase grid-connected PV systems in different operation modes", Applied power electronics conference and exposition, pp. 889-896, 2013.
- [10] D. T. Lobera, "Measuring actual operating conditions of a photovoltaic power generator", MSc thesis, Tampere University of Technology, 2010.
- [11] H. Haberlin, "Photovoltaics. System design and practice", John Wiley & Sons, Ltd, 2012.
- [12] T. Suntio, J. Leppaaho, L. Nousiainen, J. Puukko and J. Huusari, "Implementing current-fed converters by adding an input capacitor at the input of voltage-fed converter for interfacing solar generator", 14th Int. Power Electronics and Motion Control Conference (EPE/PEMC), pp. T12-81 T12-88, 2010.
- [13] W. Xiao, N. Ozog, W. Dunford, "Topology study of photovoltaic interface for maximum power point tracking", IEEE Transactions on Industrial Electronics, vol. 54, no. 3, pp. 1694-1704, 2007.
- [14] T. Esram and P. Chapman, "Comparison of photovoltaic array maximum power point tracking techniques", IEEE Transactions on energy conversion, vol. 22, pp. 439-449, 2007.
- [15] Y. Tang, P. Chiang, P. Wang, F. Choo and F. Gao, "Exploring inherent damping characteristic of LCL-Filters for three-phase grid-connected voltage source inverters", IEEE transaction on power electronics, vol. 27, issue 3, pp. 1433-1443, 2012.
- [16] Z. Zou, Z. Wang, M. Cheng, "Modelling, Analysis and Design of Multi-Function grid-interfaced inverters with output LCL filter", IEEE transaction on power electronics, issue 99, pp. 224-229, 2013.
- [17] E.J. Bueno, "Optimizing the performance of a three-level NPC grid-connected converter", PhD thesis, University of Alcalá, Spain, 2005.
- [18] N. Mohan, T. Undeland and W. Robbins, "Power Electronics. Converters, Applications and Design", John Wiley & Sons, Inc., 2003.

APPENDIX I: LCL FILTER DESIGN GUIDELINES

Per-unit value of impedance	$Z_{base} = \frac{V_{base}^2}{S_{base}}$
Per-unit value of inductance	$L_{base} = \frac{Z_{base}}{\omega_{base}}$
Per-unit value of capacitance	$C_{base} = \frac{1}{\omega_{base} \cdot Z_{base}}$
Grid angular frequency	$\omega_{base} = 2\pi f$
Resonant frequency range	$10 \cdot \omega_{base} \leq \omega_0 \leq \frac{\omega_{SW}}{2}$
Capacitor range	$C_0 \leq 0.1 \cdot C_{base}$
Inductors range	$L_1 + L_2 \leq 0.3 \cdot L_{base}$ $L_1 = 1.5 \cdot L_2$
Damping resistor selection	$R_d = \frac{1}{3\omega_0 \cdot C_0}$

APPENDIX II: PARAMETERS OF THE SUNPOWER-SPR 220 PV PANEL

Rated power	220W
Current at maximum power	5.56 A
Voltage at maximum power	40.03V
Short-circuit current	5.988A
Open-circuit voltage	48.53V
Total number of cells in series	72
Total number of cells in parallel	1
Modules in series	8
Modules in parallel	132

APPENDIX III: IMPEDANCE PARAMETERS OF THE UNDERGROUND CABLES

Positive- and zero-sequence resistance (Ohms/km)	[0.16428 ; 0.31211]
Positive- and zero sequence inductance (mH/km)	[0.68715 ; 3.393]
Positive- and zero sequence capacitance (μ F/km)	[0.247 ; 0.247]

Note. These parameters were calculated with an underground cable parameter calculation computer program, which takes full frequency dependent effects into account as well as sheath and ground effects. These values are fed as basic parameters into the Simulink model of the power distribution network shown in Fig. 13.

Cables' connectivity and length System loading data

Connecting nodes	Length (m)	Node	P (kW)	Q (kVAR)
1-2	1297	3	238	71
2-3	304	4	159	48
2-4	626	6	340	102
4-5	391	7	178	53
5-6	738	10	0	0
5-7	492	11	458	137
7-8	583	12	221	66
8-9	1000	13	221	66
9-10	539	14	97	29
9-13	1154	15	386	116
13-15	583	16	161	48
13-14	652	17	64	19
14-17	791			
8-11	1110			
11-12	539			
12-16	1253			

APPENDIX IV: CONFIGURATION OF PV GENERATORS AND CONNECTING NODES

Node	Modules in series	Modules in parallel	Pmax
3	8	90	160
4	8	60	107
6	8	96	171
7	8	60	107
11	8	132	235
12	8	63	121
14	8	30	53
15	8	120	214
16	8	60	107
17	8	30	53